Order Number 9118021

# Sodium channel activation mechanisms: Insights from deuterium oxide and delta-9-tetrahydrocannabinol substitution

Alicata, Daniel Andrew, Ph.D.

University of Hawaii, 1990



U·M·I
300 N. Zeeb Rd.
Ann Arbor, MI 48106

# SODIUM CHANNEL ACTIVATION MECHANISMS: INSIGHTS FROM DEUTERIUM OXIDE AND DELTA-9-TETRAHYDROCANNABINOL SUBSTITUTION

A DISSERTATION SUBMITTED TO THE GRADUATE DIVISION OF THE UNIVERSITY OF HAWAII IN PARTIAL FULFILLMENT OF THE REQUIREMENTS FOR THE DEGREE OF

DOCTOR OF PHILOSOPHY

IN BIOMEDICAL SCIENCES (PHYSIOLOGY)

DECEMBER 1990

By

Daniel Andrew Alicata

Dissertation Committee:

Martin D. Rayner, Chairman
John G. Starkus
Nancy K. Lind
Peter C. Ruben
Robert E. Kane
Ian M. Cooke

# DEDICATION

To my mother and father,

for their ceaseless love, encouragement and support.

To Christine, who was my wife and best friend,

for giving me the courage to dream.

# ACKNOWLEDGMENTS

I wish to acknowledge my appreciation for the guidance I received from my research advisors: Dr. Martin D. Rayner, Dr. John G. Starkus, and Dr. Peter C. Ruben. I will be forever grateful to Dr. Rayner and Dr. Starkus for giving me the chance to flourish in research and science, and to Dr. Ruben who kept me focused during times of great difficulty. Over the past five years, they have tutored me in the theoretical and technical aspects of membrane physiology, and the conclusions presented here are the product of long hours of rich investigation, discussion and contemplation. I am grateful to them for having had the opportunity to participate in the extraordinary dynamics and excitement characteristic of this field of scientific exploration, and I am fortunate to have them as friends.

In addition, I wish to thank the other members of my committee: Dr. Ian M. Cooke, Dr. Nancy K. Lind and Dr. Robert E. Kane.

# ABSTRACT

Schauf and Bullock (1979, 1982) demonstrated that solvent substitution with deuterium oxide ($D_2O$) significantly affects both sodium channel activation and inactivation kinetics without corresponding changes in gating current or tail current rates. They concluded, (a) no significant component of gating current derives from the final channel opening step and, (b) channels must deactivate (during tail currents) by a different pathway from that used in channel opening. By contrast, Oxford (1981) found in squid axons that, when a depolarizing pulse is interrupted by a brief return to holding potential, subsequent reactivation is very rapid and shows almost monoexponential kinetics. Increasing the interpulse interval resulted in secondary activation rate returning towards control, sigmoid kinetics. He concluded that channels open and close via the same pathway.

I have repeated both sets of observations, confirming the results obtained in both previous studies, despite the apparently contradictory conclusions reached by these authors. However, I find that secondary activation following a brief interpulse interval is insensitive to $D_2O$, although reactivation following longer interpulse intervals returns towards a $D_2O$-sensitivity similar to that of primary activation. I conclude that $D_2O$-sensitive primary activation and $D_2O$-insensitive tail current deactivation involve separate pathways. However, $D_2O$-insensitive secondary activation involves reversal of the $D_2O$-insensitive deactivation step.

Strichartz et al. (1978) were the first to investigate the effects of delta-9-tetrahydrocannabinol (THC) on sodium channel conductance mechanisms under voltage-clamp conditions. The authors reported that THC modified channel conductance by slowing the activation kinetics of $I_{Na}$ and suppressing ionic conductance ($g_{Na}$) in a voltage-dependent manner. They also noted that channel inactivation processes were not affected by THC action. The authors concluded that the lengthening of $t_p$ and the shift in the voltage-dependence of peak $g_{Na}$ are both related to the relative kinetics of sodium activation and inactivation, and since inactivation was unaffected by THC, alterations of activation alone account for these observed changes.

I have repeated the above observations, but I can confirm only one of the three results obtained in the previous studies. I find that THC affects both activation and inactivation kinetics. However, I find that the normalized $F(V_m)$ curves are almost identical indicating no significant shift in surface charge following THC treatment.

# TABLE OF CONTENTS

# LIST OF TABLES

# LIST OF FIGURES

# CHAPTER 1

# GENERAL INTRODUCTION

## Activation of sodium conductance

In the early 1950s Hodgkin et al. (1952) and Hodgkin and Huxley (1952b) noted that the voltage- and time-dependent behavior of the observed sodium (and potassium) conductance could be effectively simulated using four independent first-order reactions. The authors measured voltage-clamp currents in squid axon in normal ($I_{Na} + I_K$) and sodium-free ($I_K$) solutions. $I_{Na}$ was calculated as the difference between the two conditions.

Pharmacological studies confirmed the independence of potassium and sodium conductances. Tetrodotoxin (TTX) (Narahashi et al., 1964; Moore and Narahashi, 1967) and saxitoxin (STX), paralytic natural toxins, are specific blockers of sodium channels in nanomolar concentrations. Tetraethylammonium ion (TEA) is a simple quaternary ammonium compound and was first used experimentally to block potassium channels by Hagiwara and Saito (1959); and Armstrong and Binstock (1965). The list of useful blockers for potassium channels includes the inorganic cations $Cs^+$ and $Ba^{2+}$, and the organic cations 4-aminopyridine (4-AP), TEA, and many related small molecules with quaternary or protonated nitrogen atoms (Hille, 1984).

The concept of the ion-selective channel was refined, and through the techniques of electrophysiological investigation, the characteristic permeability sequences were established for sodium, potassium and calcium channels. The four first order reactions initially proposed by Hodgkin and Huxley increasingly came to be regarded as independent, identical and charged "gates" physically controlling the electrical excitability of sodium ion channels. Thus, three separate "m-gates" were hypothesized to control sodium channel activation, while a single parallel "h-gate" regulated inactivation. Therefore, sodium channel conductance ($g_{Na}$) was described as, $g_{Na} = g_{\overline{Na}}\ m^3 h$, where $g_{\overline{Na}}$ is a scaling factor which provides appropriate dimensions to the equation.

The molecular events that regulate opening and closing of sodium channels in the axon membrane are driven by rearrangement of charged gating structures in response to a change of membrane potential. The charged elements of the channel macromolecule which are sensitive to voltage and responsible for the control mechanism underlying channel conductance are also called "gating particles" or the "voltage sensor." Since the channel opens after membrane depolarization, the gating event controlling channel opening must involve movement of positive charge in the outward direction or movement of negative charge in the inward direction (although both conditions would produce outward directed current). Hodgkin and Huxley (1952d) predicted that movement of these charged structures within the membrane should produce a small electric current that would precede the onset of ionic currents. However, in the early 1950's the technical state of voltage clamp recording and analysis of channel macroscopic current did not allow the resolution of the predicted gating current. In the early

1970's, significant technical development allowed multiple data traces to be digitized and signal-averaged. This experimental technique substantially improved the signal to noise ratio of the data, and the small "gating currents" or "asymmetry currents" were soon detected and measured in skeletal muscle (Schneider and Chandler, 1973) and squid giant axon (Armstrong and Bezanilla, 1973, 1974; Keynes and Rojas, 1973, 1974; Meves, 1974). Gating current is a nonlinear (asymmetric) component of the membrane capacitance, and is isolated from the capacity current at depolarized test potentials (see Methods).

During a step depolarization sodium channel conductance activates rapidly and decays by closure of the inactivation "h-gate." Hodgkin and Huxley (1952b,c) modeled the inactivation process as a simple first order and independently voltage-sensitive process occurring in parallel with the more complex activation mechanism. In the Hodgkin and Huxley analysis, activation is the rapid process that opens sodium channels during a depolarization. A quick reversal of activation (deactivation) accounts for the rapid closing of channels ("m-gate" closure) after a brief depolarizing pulse is terminated and the membrane is repolarized to the holding potential.

The steep voltage dependence of peak sodium conductance ($g_{Na}$) presumably arises from a correspondingly steep voltage dependence of activation (Almers, 1978). Hodgkin and Huxley measured peak $g_{Na}$ during depolarizing voltage steps under voltage clamp conditions. The investigators normalized their data to 1.0 at large depolarizations and plotted the results on a logarithmic scale as a function of the membrane potential of the test pulse [$g_{Na}(V_{test})$]. An alternative method of interpreting this data is

to plot the results as a fraction of the total channel population open at saturating depolarizing test potentials. Therefore, the data be can be presented as an $F(V_m)$ curve where $V_o$ represents the depolarizing potential at which 50% of the total channel population are open. A line drawn through the first 5 data points (near threshold potential ~-50 mV to -70 mV) represents the limiting equivalent voltage sensitivity of ~4 mV per *e*-fold increase of $g_{Na}$ for small depolarizations. Limiting slope analysis for total channel valence is determined at threshold potentials because here there is the greatest probability that channel opening involves the movement of all three "m-gates." Hodgkin and Huxley determined from their "limiting slope" analysis that the total gating charge necessary (valence) for opening a sodium channel is equivalent to about 6 elementary charges (6*e*). The results of Hodgkin and Huxley have been carefully confirmed by other investigators (Oxford, 1981; Stimers et al., 1985). Furthermore, Almers (1978) suggests that the two (or possibly three) different slopes characterizing the $g_{Na}(V_{test})$ curve indicate a complex multi-state (and possibly multi-particle) activation mechanism, consistent with the observed sigmoid onset of sodium currents during depolarizing voltage steps.

## Inactivation

In the early 1970s additional electrophysiological evidence shed further light on the basic Hodgkin and Huxley assumptions describing sodium channel behavior. Armstrong et al. (1973) demonstrated that the sodium channel inactivation could be

removed by internal perfusion with the proteolytic enzyme pronase. These experiments suggested that the inactivation "h-gate" was a separate distinct physical mechanism from the sodium channel activation "m-gate," as Hodgkin and Huxley had proposed. However, evidence from macroscopic currents (Armstrong and Bezanilla, 1977; Bezanilla and Armstrong, 1977; Meves and Vogel, 1977a,b; Goldman and Kenyon, 1982), and single channel studies (Aldrich and Stevens, 1984; Cota and Armstrong, 1989) suggested that inactivation may not be independently voltage sensitive, and that it derives its voltage sensitivity from tight coupling to the activation process. Hille (1984) pointed out that the possibility that inactivation was completely independent of activation is unsatisfying on a conceptual level because it is hard to imagine, on a molecular scale, how two separate voltage-dependent processes can occur completely independently of one another in a single channel. Thus the inactivation "h-gate" proposed by Hodgkin and Huxley was confirmed to involve a separate gating mechanism from detailed studies of axonal preparations, but these studies could not confirm its independent voltage sensitivity.

An important physical interpretation of Hodgkin and Huxley's description of the activation process proposes that the sodium channel becomes conducting only after all three subunits, "m-gates," have made independent first-order transitions from the resting to the activating (depolarizing favored) position. The channel closes as soon as the first "m-particle" has reverted to its resting (hyperpolarizing favored) position. Since the Hodgkin and Huxley model assumes that sodium channel activation derives its voltage dependence entirely from the charged "m-gates", all gating current should be due

to their movement. The Hodgkin and Huxley model predicted that a channel should close as soon as the first "m-gate" reverted to its resting position, but continue to generate gating current until all three "m-gates" have returned to their closed states. Therefore, OFF gating current (movement of three "m-gates" to their hyperpolarizing-favored position) should last approximately three times longer than the sodium tail current generated by the closure of one "m-gate" during channel deactivation. Armstrong and Bezanilla (1974) and Bezanilla and Armstrong (1975) demonstrated that gating and sodium currents observed during activation were qualitatively consistent with the Hodgkin and Huxley model: gating charge moved before the first sodium channels opened. However, upon channel deactivation, the authors documented that the gating currents did not comply with the Hodgkin and Huxley system of three, identical, independent, "m-gates." $I_{Na}$-deactivation (tail current) during repolarizing voltage steps was not three-fold faster than OFF gating currents ($I_g$OFF). In fact the fast component of the sodium channel tail current and $I_g$OFF are characterized by similar kinetics.

Gating current

The delayed increase in sodium conductance after a step depolarization indicates that the channel molecule must undergo a sequence of transitions before it can open. The portion of the gating current preceding the the onset of sodium current arises from some or all of these preliminary transitions. Upon repolarization, this sequence of

transitions presumably is driven backwards. The identical time course of OFF gating current and ionic tail current suggests that the channel-closing transition is the rate-limiting step for the backward reaction. Early studies suggested that within experimental error, gating current transients can be fitted by single exponential functions. Such a conclusion implied that recording methods were inadequate to reveal the complexities expected from the kinetics of sodium conductance changes. As methods have improved, it has become clear that the time course of gating current transients contains important information concerning channel conductance regulation.

It is now apparent that gating current transients have more than one kinetic component. A very rapid kinetic component followed by a slower phase of the decaying wave form has been documented from squid giant axons (Bezanilla and Armstrong, 1975; Armstrong and Bezanilla, 1975, 1977) as well as the node of Ranvier (Neumcke et al., 1976). However, Keynes and Rojas (1974, 1976) and Meves and Vogel (1977a) reported no evidence of two components of gating current ON transients from squid. More recent investigation by Armstrong and Gilly (1979), Greeff et al. (1982), Bekkers et al. (1984), and Keynes (1986) from squid and Starkus et al. (1981) from crayfish has revealed three dissimilar kinetic components from ON gating current transients. The initial, rapid early component largely precedes $g_{Na}$ turn on. A delayed intermediate phase develops as $g_{Na}$ increases, and a slow component continues after $g_{Na}$ is fully activated. The slower components of gating current were examined in detail (Armstrong and Gilly, 1979; Gilly et al., 1981) and found to agree reasonably well with sodium macroscopic currents. The agreement is not particularly surprising, since

the slower components of gating current have a time course similar to the sodium conductance, probably because they reflect transitions closer to the opening of channels. French and Horn (1983) suggested that the early phase of the gating current provided information about the early steps in the activation process. With small depolarizations the initial fast component shows a quick rise and smooth decay, and the slower components are not prominent. The three distinct kinetic components are especially apparent at positive (> +20 mV) membrane voltages. The rates of the fast and intermediate components are voltage sensitive; both increase as the magnitude of the depolarizing test pulse is increased from a single holding potential. Voltage sensitivity of the slower component is not immediately obvious (Starkus et al., 1981). Noting the dissimilar properties of the three gating current components, Starkus et al. (1981) concluded that they may represent either three independent, non-uniform gating particles, or alternatively, a single particle moving through a complex state array.

Fractionation of gating current

When ON gating current is altered in magnitude by change of holding potential (between -120 mV and -80 mV), there is little, if any, change in $I_g$ON kinetics. By contrast, when fast inactivation is induced by short (less than 10 msec) prepulses, marked changes in $I_g$ON kinetics can be observed. The slower (intermediate and slow) kinetic components of the gating current transient are reduced ($Q_i$, immobilized components of total gating charge) by prepulse induced fast inactivation (Keynes and

Rojas, 1976; Keynes, 1983; Greeff et al., 1982; Starkus and Rayner, 1987) or local anaesthetics (Bekkers et al., 1984). The initial fast component ($Q_n$, nonimmobilized component of total gating charge) of $I_g$ON is reduced (immobilized) with prepulse durations exceeding 10 msec. Starkus and Rayner (1987) concluded that there are two separate but interactive charge carriers for each sodium channel: a highly-reactive primary gating current generator ($Q_n$) which is immobilized only by slow inactivation, and a more slowly reactive secondary generator ($Q_i$) which is immobilized only by fast inactivation. Furthermore, the authors stated that both gating current charge generators must be mobilized to permit opening of the sodium channel.

The parallel activation (parallel transfer) model proposed by Keynes (1983) implies that the sodium channel is controlled by two separate gating systems operating in parallel, more or less independently. One system would generate the fast $Q_n$ and the other the slow $Q_i$. Upon depolarization a channel would be open only if both charges had been displaced. Conversely, the return of either of the two charges to the resting state would close the channel. Only the slow $Q_i$ system is proposed to undergo a sequentially coupled process of inactivation taking it out of the activated state. Thus the parallel charge transfer model (Keynes, 1983) could readily explain the selective blockage of slow $Q_i$ both by prepulse induced fast inactivation and by local anaesthetics. Upon repolarization, sodium channels would be closed by the return of the non-inactivating charges (fast $Q_n$) to their resting position, whatever the state of the $Q_i$ system. In the parallel transfer scheme, the charge displacement of fast $Q_n$ is assumed to be independent of whether the slow $Q_i$ charges are fully mobile or are blocked by

prepulse induced fast inactivation or local anaesthetics. Such an independence would require that the charge displacements $Q_n$ and $Q_i$ take place in different parts of the same protein molecule and are effectively shielded from one another. They would thus be prevented from interacting electrically.

## Single channel investigation

The extracellular patch clamp technique has allowed, for the first time, the currents in single channels to be observed (Neher and Sakmann, 1976). In this technique a small heat-polished glass pipette is pressed against the cell membrane, forming an electrical seal with a resistance of the order of 50 MΩ (Neher et al., 1978). The high resistance of this seal ensures that most of the currents originating in a small patch of membrane flow into the pipette, and from there into current-measurement circuitry. The resistance of the seal is important because it determines the level of background noise in the recordings.

Neher (1981) observed that tight pipette-membrane seals, with resistances of 10 - 100 GΩ, can be obtained when precautions are taken to keep the pipette and the membrane surfaces clean, and when suction is applied to the pipette interior. Patch clamp electrophysiologists refer to these high resistance seals as ''giga-seals'' (giga-seal resistance = $10^9\Omega$) to distinguish them from the conventional, megaohm seals.

The high resistance of a "giga-seal" reduces the background noise of the recording by an order of magnitude (signal/noise ratio is increased as the seal resistance is increased), and allows a patch of membrane to be voltage clamped without the use of microelectrodes (Sigworth and Neher, 1980).

Giga-seals are mechanically stable. Following withdrawal from the cell membrane a membrane vesicle forms occluding the pipette tip (Hamill and Sakmann, 1981; Neher, 1981). The vesicle can be partly disrupted without destroying the giga-seal, leaving a cell-free membrane patch that spans the opening of the pipette tip. This allows single channel current recordings from isolated membrane patches in defined media, as well as solution changes during the measurements (Horn and Patlak, 1980; Hamill and Sakmann, 1981). Alternatively, after giga-seal formation, the membrane patch can be disrupted keeping the pipette attached to the whole-cell by means of the giga-seal. This provides a direct low resistance access to the cell interior allowing for current recording and voltage clamping of the small cell.

Sigworth and Neher (1980) calculated approximately 3-5 channels within their 0.5 $\mu m^2$ patch from cultured rat myotube membrane. Depolarizing steps of 10 mV produced mean sodium channel current of -1.6 pA [pico amp (pA) = $10^{-12}$ amps] with an average life time ~0.7 ms, and a single-channel conductance $\gamma$ = 18 pS. The authors assumed that since sodium channels are identical and function independently, the sum of many current records from a few channels should show the same properties as the macroscopic sodium current measured in a conventional voltage-clamp from thousands of channels.

An average time-course derived from 300 depolarizations of the membrane patch shows the typical kinetic behavior with a rapid ($\tau_m$ ~0.8 ms) activation followed by a slower ($\tau_h$ ~2.6 ms) inactivation process. Much of the classical macroscopic voltage-clamp data is being repeated by patch-clamp measurements of microscopic channel currents in the mouse neuroblastoma cell line, N1E-115 (Quant, 1987), and from patches of *Xenopus laevis* oocytes injected with exogenous mRNA coding for rat-brain-II sodium channels (Noda et al., 1986; Stühmer et al., 1987; Conti and Stühmer, 1989). From analysis of microscopic channel kinetics, investigators are uncovering crucial evidence which may help reveal the gating mechanism controlling sodium channel conductance.

## Molecular structure of sodium channels

Recent structural evidence suggests that the principal protein component of voltage-sensitive sodium channels is a glycoprotein of 260 kDa (kilo Daltons) which has a core polypeptide of ~210 kDa (Noda et al., 1984). In mammalian neurons, the $\alpha$ subunit is associated by non-covalent forces with a $\beta_1$ glycoprotein subunit of 36 kDa and by disulfide linkages with a $\beta_2$ glycoprotein subunit of 33 kDa (Messner and Catterall, 1985). In skeletal muscle, one or two small subunits of approximately 37 kDa are also associated with the principal sodium channel polypeptide (Kraner et al., 1985), whereas only a single sodium channel polypeptide of 260 kDa has been observed in eel electroplax (Noda et al., 1984). Purified polypeptide preparations mediate selective

ion transport and voltage-dependent gating when incorporated into pure phospholipid vesicles or planer bilayers (Noda et al., 1984). Complementary DNAs encoding the amino acid sequence of the sodium channel glycoprotein from electroplax (Noda et al., 1984) and the α subunit of the sodium channel from rat brain (Auld et al., 1985), have been cloned and their sequences determined, revealing the primary structure of the principal protein component of the sodium channel. Four internally homologous transmembrane domains of approximately 300 amino acids each are connected by shorter structures of non-homologous amino acids. Noda et al. (1984) have proposed that these four homologous domains surround a central aqueous transmembrane pore which seems to be the ion conducting pathway of the sodium channel. Catterall (1986) suggested that the four pseudosymmetric domains of this tetrameric molecule correspond to the three "m-gates" and single "h-gate" of the Hodgkin and Huxley model. Each of the apparently homologous domains contains ~six (S1-S6) helical transmembrane segments, including a potentially alpha-helical (S4) segment with a high concentration of positively charged groups which would serve as a "voltage-sensor" or "gating particle" for the sodium channel (Noda et al., 1984). Greenblatt et al. (1985), Guy and Seetharamulu (1986) and Catterall (1986) have proposed that these "S4-segments" act as voltage-sensitive channel gates by rotating as "sliding helices" during the gating process. However, Catterall's (1986) assignment of function to S4 segments based on the Hodgkin and Huxley model (three "m-gates" and one "h-gate") is in conflict with the major conclusions reached in recent electrophysiological studies.

Kinetic models of the sodium channel

Conti and Stühmer (1989) analyzed sodium gating current and single channel kinetics from nerve sodium channels in cell-attached macropatches of *Xenopus laevis* oocytes injected with exogenous mRNA coding for rat-brain-II sodium channels. The authors suggest that sodium channel activation might be controlled by three independent, parallel and uniform (2.03*e*) gating particles. This mechanism is consistent with the assumption made by Conti (1986) that sodium channel activation is controlled by three independent voltage-gated transitions which all involve the same gating charge. This also fits the voltage dependence of sodium activation which implies a simple Hodgkin and Huxley type activation scheme in which the opening of a sodium channel is preceded by three independent first order reactions each producing the same transmembrane charge movement. This conclusion, however, is incompatible with the observation that the time course of $I_{Na}$-deactivation is identical to $I_g$OFF (Armstrong and Bezanilla, 1974; Bezanilla and Armstrong, 1975).

However, the conclusion proposed by Conti and Stühmer (1989) is inconsistent with data from studies in crayfish giant axon. Rayner and Starkus (1989) observed from gating current data that gating charge measured at a single test potential from successive changes of holding potential [$Q_{ON}(V_h)$] produced a symmetrical equilibrium distribution of gating charge with a single slope of ~1.8*e*. Using another experimental protocol, where the membrane is held at strongly negative holding potentials (-140 mV and -120 mV), the distribution of gating charge as a function of depolarizing test

potential [$Q_{ON}(V_m)$] shows a single slope of ~1.8*e*. Rayner and Starkus (1989) concluded that the sodium channel gating mechanism does not involve loading of gating charge within intermediate pre-open states at equilibrium (this will be considered further in the Discussion). Therefore, it is possible that channel activation is controlled by either of two mechanisms, a) three parallel and uniform gating particles as was suggested by Conti and Stühmer (1989), or b) only one major gating particle with a valence of 1.8*e* and two other gating particles with lower valences.

Ruben et al. (1990) analyzed channel activation mechanisms from ionic current data by measuring the fraction [$F(V_m)$] of channels open at peak conductance at different test potentials. Their data confirms that a >4*e* high limiting slope appears (at test potentials within 35 mV of the apparent threshold potential) in experiments where less negative holding potentials are used (Keynes and Rojas, 1974, 1976; Almers, 1978; Stimers et al., 1985). However, from holding potentials more negative than -100 mV, the high limiting slope disappears, and channel voltage sensitivity [$F(V_m)$-curve] shows a single valence of ~2.0*e* at all test potentials. Thus, the gating current data of Rayner and Starkus (1989) and ionic current data of Ruben et al. (1990) strongly suggest that the mechanism controlling sodium activation is a multistate system of three independent and parallel gating particles with unequal valences.

Parallel cyclic models vs linear sequential models

Experimental evidence has refuted Hodgkin and Huxley's first order and sequential model of three parallel and identical gating particles. However, recent

investigation has provided considerable insight into other possible models. The main function of kinetic modeling is to suggest experimental designs which will allow investigators to eliminate some types of models, and eventually gain a clearer understanding of the gating mechanism. Models describing sodium channel activation fall within three general classes, (a) parallel and identical particle models, (b) parallel and nonidentical particle models, and (c) sequential linear models.

Channels pass through more than one closed state in going from the resting to the open state. In the process underlying the gating of sodium channels, there are at least two closed states preceding the opening of sodium channels (Bezanilla and Armstrong, 1977; Armstrong and Gilly, 1979; Armstrong, 1981, Bezanilla et al., 1982). This is apparent from the "lag" or sigmoidicity in the activation kinetics in response to a depolarizing voltage step. A similar conclusion can be drawn at the single channel level by measurement of the latency between the onset of the voltage step and the opening of the first channel (Horn et al., 1981a; Patlak and Horn, 1982). The histogram of latencies to first opening has a simple theoretical interpretation. If it has a maximum value at the onset of the voltage step, then the resting closed state leads directly into an open state. However, all published first latency histograms have a maximum value at a time greater than zero. Additional evidence supporting the presence of multiple closed states is the fact that the onset of ionic current after a voltage step is largely preceded by gating current (Keynes, 1975; Meves, 1978). Therefore, opening of channels is a transition subsequent to the movement of gating charge.

(a) Parallel and identical particle models

The Hodgkin and Huxley model, describing sodium channel activation as having "$m^3$" kinetics, can be considered a subunit model. This model suggests that the channel activation gate is controlled by three independent and identical gating particles, in which each is assumed to make a voltage-dependent transition from its hyperpolarized-favored position (closed state) to its depolarized-favored position (open state). Only after all three gating particles have made transitions to their open position is the channel macromolecule able to assume its conducting conformation. Although the Hodgkin and Huxley model describes three parallel gating particles, it can be presented with the linear Scheme 1:

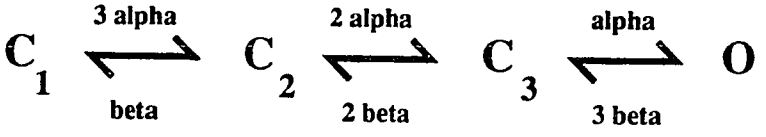


The symbols $\alpha$ (alpha) and $\beta$ (beta) represent the forward and backward rate constants of the activation system. The inactivation "h-gate" is not represented. The voltage-dependent transition rate of each gating particle is a function of particle valence (charge) and the energy barrier it must overcome. At resting potential the value for $\beta$ is greater than for $\alpha$ and the reaction is driven to the left. However, when sufficient energy is imposed upon the system (as with depolarization) $\alpha$ becomes larger than $\beta$,

and the reaction is driven to the right toward the "open" state. The "$m^3$" full activation scheme is shown as:

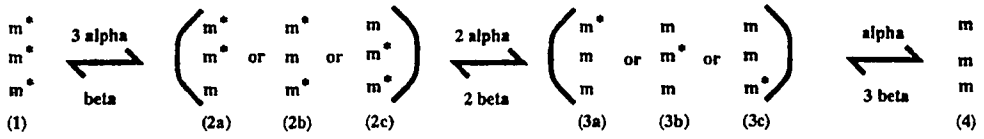


At a hyperpolarized potential, the charged gating particles are in a nonconducting position. This is represented as $m^*$. Upon depolarization the system goes through two intermediate states (between the transitions $3\alpha$ to $2\alpha$ and then from $2\alpha$ to $\alpha$) before all the gating particles enter the conducting position which is represented as "m." However, the model cannot predict which gating particle moves during each transition step. Thus the rate constants represent the probability of any of the gating particles moving from the $m^*$ to the m position times the number in the $m^*$ position. Thus, a gating particle in the first intermediate state ($C_2$) may be either $m^*$ $m^*$ m, $m^*$ m $m^*$, or m $m^*$ $m^*$ (three conditions), and the second intermediate state ($C_3$) may be either $m^*$ m m, m $m^*$ m, or m m $m^*$ (three conditions). Although the model shows eight distinct possibilities for the parallel movement of the gating particles between the closed to open positions, the identical rate constants for all particles permit the full 8-state model to be presented as a 4-state sequence.

(b) Parallel and nonidentical particle models

Like the parallel and independent 4-state Hodgkin and Huxley model (described above), the parallel nonidentical particle model assumes independent voltage-sensitive action from three independent gating particles (''m-gates''). However, this model does not presume identical kinetics. Therefore, the possibilities for the parallel movement of three gating particles (S4 segments) having dissimilar rate constants must be represented by a cyclic 8-state model shown below in Scheme 2.

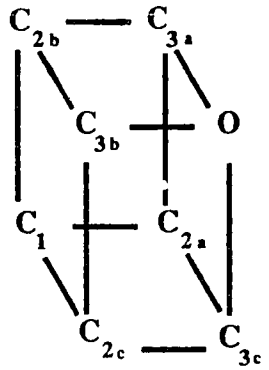


Rayner and Starkus (1989) reported that the sodium channel gating mechanism did not involve significant loading of gating charge within intermediate pre-open states at equilibrium. Therefore, at holding potential, the three gating particles are primarily in the closed ($C_1$) position. Upon depolarization the three gating particles move into the

intermediate closed states, $C_{2a}$, $C_{2b}$ and $C_{2c}$. At this position within the model any one of the gating particles has to undergo two transitions before entering the channel open (0) state. When the gating particles reach the $C_{3a}$, $C_{3b}$ and $C_{3c}$ intermediate closed states, only one transition is necessary before entering the open state. This parallel cyclical model shows three distinct and parallel paths converging to the channel open state ($C_3$ to O step) and three parallel paths diverging from the open state (O to $C_3$).

(c) Linear sequential models

The linear sequential model proposed by French and Horn (1983) describes the mechanisms underlying the conformational changes associated with channel gating. A simple representation of this linear sequential model is shown below in Scheme 3:

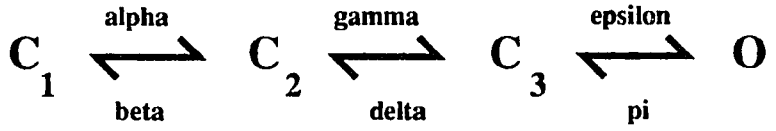


Inactivation is not included. At rest the channels reside in the state $C_1$, and upon depolarization the gating particles are driven to the right. The transitions to the $C_1$ and $C_2$ intermediate states ($\alpha$ and $\gamma$, respectively) are rapid by comparison to the final opening transition ($\varepsilon$) to the channel open state. All rate constants are presumed to be voltage dependent and sequential reaction steps are coupled by electrostatic and/or allosteric

forces. The lag in channel opening after a depolarizing voltage step is explained by the time required for gating charge to proceed from the closed ($C_1$) to open (O) state. French and Horn (1983) suggested that the lag in channel opening depends upon the holding potential, which determines the distribution of gating charge among preopen states. The linear sequential model is consistent with data of Armstrong and Gilly (1979) and Armstrong (1981). Since the final channel opening step ($\varepsilon$) is voltage sensitive, the kinetics of the slower components of gating current will be associated with the kinetics of macroscopic ionic current representing the opening of channels. The relative amplitude of the intermediate component of $I_g$ON described by Armstrong and Gilly (1979) will depend partly on the voltage dependence of the final opening step ($\varepsilon$). French and Horn (1983) point out that in the linear sequential model, channel closure (through deactivation) follows the reverse of the pathway that was taken during primary activation. Data consistent with that hypothesis had been presented by Oxford (1981), although contrary data from the lack of effect of $D_2O$ on tail currents, (see Schauf and Bullock, 1982) was ignored by French and Horn (1983).

## Hypothesis

The fundamental purpose of kinetic modeling is to discriminate between various types of model systems by comparing the behavior of the models to experimental results. Hopefully, this would eventually lead to a greater understanding of the processes underlying the sodium channel gating mechanism. My hypothesis is that linear sequential and parallel cyclical models will behave differently under "appropriate challenge." Certain pharmacologic and pulse protocol challenges should unequivocally determine a model system which best describes the activation mechanism. Therefore, as a result of the electrophysiological investigation presented in this thesis involving the substitution of $D_2O$ for $H_2O$ and the addition of THC, I conclude that a parallel cyclical model best describes the mechanism underlying sodium channel activation.

## Aims and approach

### Chapter 3: Sodium channel activation mechanisms: insights from deuterium oxide substitution.

Schauf and Bullock (1979, 1982), using *Myxicola* giant axons, demonstrated that solvent substitution with deuterium oxide ($D_2O$) significantly affects both sodium channel activation and inactivation kinetics without corresponding changes in gating current

or tail current rates. They concluded, (a) no significant component of gating current derives from the final channel opening step and, (b) channels must deactivate (during tail currents) by a different pathway from that used in channel opening. By contrast, Oxford (1981) found in squid axons that, when a depolarizing pulse is interrupted by a brief (100 μs) return to holding potential, subsequent reactivation (secondary activation) is very rapid and shows almost monoexponential kinetics. Increasing the interpulse interval resulted in secondary activation rate returning towards control, sigmoid (primary activation) kinetics. He concluded that channels open and close (deactivate) via the same pathway.

I have repeated both sets of observations in crayfish axons, confirming the results obtained in both previous studies, despite the apparently contradictory conclusions reached by these authors. I find that secondary activation following a brief interpulse interval (50 μs) is insensitive to $D_2O$, although reactivation following longer interpulse intervals (400 μs) returns towards a $D_2O$-sensitivity similar to that of primary activation. I conclude that $D_2O$-sensitive primary activation and $D_2O$-insensitive tail current deactivation involve separate pathways. However, $D_2O$-insensitive secondary activation involves reversal of the $D_2O$-insensitive deactivation step.

# Chapter 4: Sodium channel activation mechanisms: insights from delta-9-tetrahydrocannabinol substitution.

Early electrophysiological investigation on squid giant axons (Brady and Carbone, 1973) and on small non-myelinated c-fibers of the vagus nerve of the rabbit (Byck and Ritchie, 1973) demonstrated the ability of the natural marijuana constituent, delta-9-tetrahydrocannabinol (THC), to decrease both the action potential amplitude and its conduction velocity. Strichartz et al. (1978) were the first to investigate the effects of THC on sodium channel conductance mechanisms under voltage-clamp conditions. This work was performed on the excitable membrane at the node of Ranvier of myelinated fibers of the frog sciatic nerve. The authors reported that THC modified channel conductance by slowing the activation kinetics of $I_{Na}$ (lengthening the time-to-peak current, $t_p$) and suppressing ionic conductance ($g_{Na}$) in a voltage-dependent manner. They also noted that channel inactivation processes were not affected by THC action. The authors concluded that the lengthening of $t_p$ and the shift in the voltage-dependence of peak $g_{Na}$ are both related to the relative kinetics of sodium activation and inactivation, and since inactivation was unaffected by THC, alterations of activation alone account for these observed changes.

I have repeated the above observations in crayfish axons, but I can confirm only one of the three results obtained in the previous studies. I find that THC affects both activation and inactivation kinetics. However, I find that the normalized $F(V_m)$ curves

are almost identical indicating no significant shift in surface charge following THC treatment. Furthermore, I find that THC selectively alters only the slower components of ionic and gating current kinetics while sparing the very fast processes. These results suggest that fast THC-insensitive processes reflect a THC-insensitive gating mechanism: a "fast m-gate."

The significance of these $D_2O$ and THC actions with respect to channel models will be considered in the Discussion section.

# CHAPTER 2

# GENERAL METHODS

Methodology of the technical and experimental procedures of voltage clamp electrophysiology of sodium channels in nerve membrane is extensive. Therefore, I will discuss only the ideas and theories concerned within the scope of this project. The topics that will be discussed in the Methods section are:

Biological preparation
- (a) crayfish giant axon
- (b) isolation of the giant axon

Voltage clamp techniques
- (a) voltage clamp circuit
- (b) internal perfusion
- (c) electrodes
- (d) liquid junction potentials

Space clamp artifacts
- (a) static
- (b) dynamic
  - (b.1) series resistance
  - (b.2) invasion artifacts

Techniques for measuring gating currents
- (a) subtraction of linear capacity and leakage currents
- (b) subtraction of nonlinear leakage current
- (c) gating current
- (d) crayfish as a premiere preparation

Instrumentation
- (a) data recording
- (b) temperature regulation

Experimental internal and external solutions

Methods for chapter 3: sodium channel activation mechanism: insights

from $D_2O$ substitution

Methods for chapter 4: Sodium channel activation mechanism: insights from THC substitution

Biological preparation

(a) The crayfish giant axon

Axial wire voltage clamp experiments for the measurement of sodium channel ionic ($I_{Na}$) and gating current ($I_g$) discussed in this dissertation were carried out using medial giant axons of the crayfish *Procambarus clarkii*. Voltage clamp techniques for the crayfish were first designed by Shrager (1974) and further developed by Starkus and Shrager (1978). The diameter of the crayfish medial giant axon ranges from 200 and 300 μm. This is smaller than giant axons of the squid *Loligo pealei* which are typically in the order of 500 and 1000 μm in diameter.

The advantages in utilizing the crayfish giant axon are the following: crayfish are readily available from fresh water streams in Hawaii on a year round basis, are cheap to purchase and easy to maintain in circulating fresh water storage tanks at ambient temperature (20° to 22°C). By contrast squid are only available seasonally, maintenance in captivity is exceedingly difficult, and the giant axon has a viscous axoplasm which must be squeezed out from the axon with a small rubber roller. However, the axoplasm of the crayfish giant axon is fluid and can be easily replaced with artificial salt solutions (see internal solutions in Table 2). I elected to work with the crayfish

not only because of its large nerve fiber and consistent accessibility in Hawaii but also because of the fast sodium channel kinetics. The crayfish giant axon has become the premiere preparation for gating charge measurements. Moreover, Drs. Martin Rayner and John Starkus have been improving the experimental techniques of this preparation since 1978.

(b) Isolation of the giant axon

The crayfish was sacrificed, the carapace removed, and the bilateral ventral nerve cord dissected free and immediately placed in the cooled and temperature controlled experimental Plexiglas chamber. For the duration of the dissection procedure the axon was bathed in artificial crayfish extracellular fluid (see Table 2). The connective tissue sheath was removed from the nerve cord using Dumont #5 fine forceps and Vannas microdissection scissors under a Wild M5 stereo dissecting microscope. The abdominal ganglia in the recording region were cut free and removed at this time. Using fine pulled glass needles, the smaller fibers of the nerve bundle were then teased away, exposing the medial giant axon over a length of ~1.5 cm.

The isolated fiber was then ready for cannulation with an internal perfusion pipette and internal electrode assembly.

Voltage clamp techniques

(a) voltage clamp circuit
(b) internal perfusion
(c) electrodes
(d) liquid junction potentials

The voltage clamp technique measures currents passing through ion channels by controlling the potential across the membrane. The experimental procedure was first developed by Marmont (1949) and Cole (1949) and further progress was made by Hodgkin and Katz (1949) and Hodgkin and Huxley (1952,a,b,c,d). Under voltage clamp conditions, the membrane potential is "clamped" constant at a chosen level. Therefore, resulting changes in conductance are observed solely as functions of time. The effects of voltage on conductance could be characterized at different clamped potentials.

In a standard voltage clamp experiment the membrane potential is routinely depolarized for several milliseconds from a holding potential near the normal cell resting potential (~-100 mV). The total membrane current within the voltage clamp circuit is the sum of two terms: ionic current ($I_{ion}$) which is charge carried by ions conducting through the pore and capacity current (symmetric and asymmetric $I_{cap}$) which is the redistribution of charge within and near the membrane. This can both be ionic and molecular charge. Molecular charge is associated with protein and phospholipids.

Detailed discussion of linear (symmetric capacity current) and nonlinear (asymmetric capacity current or gating current) capacity current is considered later in the Methods section. The equation describing this process is:

$$I_{mem} = I_{ion} + I_{cap} = I_{ext}.$$

During the initial stepwise change in voltage (first 5 to 15 μs), which is produced by the command (test) voltage being applied across the terminals of the voltage-clamp amplifier (see Fig. 1), $I_{ext}$ must change rapidly to charge the membrane capacitor to reach the new command voltage, thus:

$$I_{mem} = I_{cap} = I_{ext}.$$

A brief capacity current ($I_{cap}$) will flow while the membrane is charging. Afterward $I_{cap}$ will fall to zero as dV/dt approaches zero, and the current flow in the external circuit will be determined solely by the ionic currents across the membrane, thus:

$$I_{mem} = I_{ion} = I_{ext}.$$

If the direction of $I_{ion}$ is inward and $I_{ext}$ is in the outward direction (see Fig. 1), and if the magnitude of $I_{ext}$ can be rapidly adjusted so that the potential remains constant (dV/dt = 0), then there can be no further capacity current across the membrane. To maintain the constant potential, it is necessary that the voltage-clamp circuit have a feedback amplifier with a good high-frequency adjustment capability of passing current in either direction in the external circuit.

Under these circumstances, $I_{cap}$ will always be zero, while the magnitude of $I_{ion}$ will be equal and opposite polarity to $I_{ext}$:

$$I_{ion} = I_{ext}, \text{ and } I_{ion} - I_{ext} = 0.$$

If $I_{ext}$ is monitored, then $I_{ion}$ will always be known. Thus the voltage-clamp circuit provides a moment-by-moment measure of the ionic currents flowing across the axon membrane.

(a) Voltage clamp circuit

The voltage clamp circuit used in this study was designed by Lee Chabala (unpublished), which is a modified version of the standard voltage clamp circuit described by Moore and Cole (1963).

The internal and external membrane potentials were measured by high input impedance amplifiers (#1 and #2, Fig. 1) and were fed into the differential amplifier (#3) to record the transmembrane potential ($V_m$). The transmembrane potential was compared with the command signal at the summing junction of the control amplifier (#4). When these two signals were unequal, the control amplifier delivered current into the axon until the membrane potential matched the command signal. To hold the membrane potential at a constant level this injected current is equal and opposite to the membrane ionic current. The command signal consisted of an adjustable holding potential ($V_h$) and an adjustable step voltage pulse under computer control. Ionic current, produced by the step wise changes in membrane potential ($V_m$), was measured

by the currentometric amplifier (#5) via an external electrode. The current measuring electrode was flanked on both sides by two driven "virtual ground" guard electrodes (see Electrodes below).

(b) Internal perfusion

The internal perfusion system was designed for the crayfish preparation by Shrager (1974). After dissection and isolation of the cleared giant axon, holes were cut at each end of the fiber for insertion of the voltage clamp electrode assembly into one end of the fiber and the perfusion pipette into the other. The perfusion pipette (~100 μm in diameter) was cannulated into the axon next to the esophageal ganglion. The voltage clamp electrode assembly was cannulated into the axon next to the abdominal ganglion. Since the axoplasm in the crayfish giant axon is very fluid, it can be readily replaced with artificial salt solutions (see Solutions in Table 2). This internal perfusate was held in a 10 cc syringe and delivered inside the axon via a glass pipette and polyethylene tubing #190. Flow of internal solution to the axon was maintained by a 3-4 cm hydrostatic pressure head between the axon and the top of the solution reservoir. This internal perfusion system provides a simple, fast and effective means of changing internal solutions in crayfish giant axons.

(c) Electrodes

Three types of electrodes were used for voltage clamp experiments, (1) internal electrode assembly, (2) external reference electrode, and (3) external current measuring electrode and guard electrode assembly (Fig. 1).

The internal clamp electrode was of the "piggyback" type described by Chandler and Meves (1965). It consisted of a 50 μm (internal diameter) glass capillary used for measuring internal potential and a 25 μm 95% platinum - 5% iridium wire for injecting current. The final diameter of the wire after plating was ~30 μm. The internal glass capillary contained a floating 18 μm platinum-iridium wire to reduce high frequency impedance (Fishman, 1973) and was filled with 200 mM KCl solution (KCl 172 mM, $K_3$ citrate 37 mM to pH 7.5). The proximal end of the glass capillary was inserted with a Ag-AgCl pellet and connected to a high impedance amplifier (#1, Fig. 1). The internal current-injecting wire was attached to the capillary and insulated with Insul-X lacquer except for the distal 9 mm portion which was left bare. The bare portion of the electrode was carefully cleaned and platinized according to the method described by Moore and Cole (1963). This wire was briefly electroplated in a platinum solution (Kolhrausch Solution) to reduce wire resistance.

The external membrane potential was measured by a glass capillary with a tip diameter of 200 to 400 μm. The capillary was filled with a 2% agar gel of normal Van Harreveld solution (Van Harreveld, 1936, see Table 2) and was connected to a potentiometric amplifier (#2, Fig. 1) via a Ag-AgCl pellet.

The membrane current was measured using three external current electrodes (Fig. 1). The central electrode (3 mm) was connected to the currentometric amplifier (#5, Fig. 1) and the remaining two electrodes (3 mm) were directly grounded to serve as driven "virtual ground" guard electrodes. With this arrangement of external electrodes the current flowing through the central electrode becomes perpendicular to the membrane, eliminating the longitudinal spread of current (see Space clamp artifacts below).

(d) Liquid junction potentials

In the voltage clamp circuit, the ion solutions of the internal and external electrodes produce a potential difference. The magnitude of this potential arises from the different mobilities of these electrolytes. The internal potential electrode is filled with an electrolyte solution which $K^+$ is the dominant cation. This electrode is positioned inside the axon which is normally perfused with K 250, Cs 230 or TMA 230 solutions (see Table 2). The external potential electrode is filled with an electrolyte solution which $Na^+$ is the main cation. This electrode is placed near the external surface of the axon which is normally bathed in external sodium solution (see Table 2). When the internal and external potential electrodes are brought together during the beginning of the experiment, a liquid junction potential of ~-6 to -8 mV results. Therefore, correction of the junction potential is accomplished by adjustment of the DC offset potentiometer. At the conclusion of each experiment another measurement is made for the

liquid junction potential. After 3 to 6 hours of continuous data recording, the junction potential routinely drifts approximately 1 to 3 mV and rarely more than 5 mV. There are two reasons which explain for the observed drift of the liquid junction potentials , (1) gradual exchange of electrolytes from the electrode filling solutions, and (2) drifting of the operational amplifier hardware.

Space clamp artifacts

(a) static
(b) dynamic
    (b.1) series resistance
    (b.2) invasion artifacts

An axial wire voltage clamp system requires the basic assumption that a "space clamp" (Cole, 1968), or proper membrane potential control is imposed over the entire region of membrane from which current is collected. Ideally there would be no variations of membrane potential with distance along the length of the axon within the measuring region. In practice this condition may be closely approximated (Rojas et al., 1969). Moreover, the "space clamp" insures that the entire region of membrane under the current collecting electrode experiences the same potential changes at exactly the same time, and that this clamped region of membrane is isolated from the remainder of the cell. Current densities ($mA/cm^2$) are uniform across the entire membrane area under the recording electrode. The important function of the two guard electrodes is to maintain a uniform potential across the region of membrane from which current is being recorded by minimizing "edge effects" at the ends of the current collecting electrode. There are two types of space clamp errors that may exist and, therefore distort the voltage uniformity across the membrane, (a) "static, and (b) "dynamic."

(a) Static space clamp artifacts

"Static" errors occur when the membrane voltage ($V_m$) is not uniform along the clamped region of axon in steady state conditions. Thus there could be regions of the membrane which are not at the exact command or test potential generated by the clamp. A test for voltage uniformity along the space clamped region of the axon is to depolarize the membrane to the equilibrium potential for sodium ion ($E_{Na}$) and observe the ionic current. $E_{Na}$ can be calculated from the Nernst equation (Briggs, 1930; Goldman, 1943; Hodgkin and Katz, 1949; Patlak, 1960; Mullins and Noda, 1963) which is determined from the ratio of the external and internal sodium ion concentrations (Hodgkin and Huxley, 1952a; Dodge and Frankenhaeuser, 1959; Moore and Adelman, 1961; Julian et al, 1962).

$$E_{Na} = RT/FZ \ln [Na]_o / [Na]_i$$

Where:

$E_{Na}$ = sodium equilibrium potential

R = universal gas constant (8.31 joules/mol/° absolute)

F = Faraday constant (96,500 coulombs/mol)

T = temperature in ° absolute

Z = valence of the ion

$[Na]_o$ = concentration of sodium outside the cell

$[Na]_i$ = concentration of sodium inside the cell

Where $E_{Na}$ is required in millivolts, assuming the temperature is 9.5°C and converting to logarithms to the base 10 [ln (2.303) = $\log_{10}$], the Nernst equation can be simplified by combining all the constants into a single value:

$$E_{Na} = 56/Z \log [Na]_o / [Na]_i$$

When the membrane is depolarized to $E_{Na}$, there should be no noticeable sodium current if the voltage is uniform across the membrane. The recorded current following the test voltage step should consist of a small outward gating current followed by a flat baseline for the duration of the depolarizing pulse. If the voltage is not uniform along the clamped region of membrane, then an inward sodium current would be observed where the command (test) potential is more negative than $E_{Na}$, and/or an outward sodium current where the command potential is more positive than $E_{Na}$.

(b) Dynamic space clamp artifacts

(b.1) Series resistance compensation

(b.2) Invasion artifacts

(b.1) Series resistance compensation

When using voltage clamp procedures on any membrane preparation, it is crucial to accurately compensate for resistance in series ($R_s$) with the membrane. Uncompensated resistance in series with the voltage clamped membrane will produce a voltage drop proportional to the current output of the clamp, and therefore the command potential measured between the voltage following electrodes will not represent the actual transmembrane potential. Fig. 2 shows the location of anatomical resistors aligned in series between the extracellular fluid and the axoplasm (intracellular fluid). The clamp potential is measured between the internal and external potential electrodes. However, there is an array of fluid, connective tissue and glial structures that partition the membrane from the clamp potential measuring external electrodes. The contribution to total series resistance by external and internal fluid is negligible. Therefore, the two major sites of series resistance lie at the Schwann cell clefts and the periaxonal space (fluid layer between the axon and Schwann cell). Fig. 3 illustrates a simplified model of a physical system from squid (Stimers et al., 1987). The figure shows a cleft between two Schwann cells that would contribute to the normal series resistance ($R_s$). The cleft is continuous with the periaxonal space (also known as the F-H space, as

first noted by Frankenhaeuser and Hodgkin, 1956), which is between the Schwann cells above and the axon membrane below. The resistance of the F-H space ($R_{FH}$) is variable depending upon its volume. $R_s$ can be compensated for electronically, and the patch of membrane directly under the cleft (which has access to the extracellular fluid via a tortuous route) will be clamped with a square potential that rises with the speed to the clamp, or the duration of the fast component of the capacity current (this is discussed in further detail below). However, $R_{FH}$ cannot be compensated since this would result in overcompensation of $R_s$. The additional contribution to total series resistance, produced by this high $R_{FH}$, should slow clamp rise time in membrane areas not directly beneath Schwann cell clefts. Hence, slowing of clamp speed would result from these relatively undercompensated membrane regions.

Stimers et al. (1987) showed in squid that hyperosmolar external perfusates (or hypoosmolar internal perfusates) created outward water movements which altered the fast kinetic of gating current. They suggested that outward water shifts across the axolemma increased the volume to the periaxonal space, thus decreasing the total series resistance and increasing the clamp speed. Adelman et al. (1977) reported that changes in the periaxonal space volume appear linearly related to inward or outward water movements, for small osmolar differences. Alicata et al. (1989) suggested that inward water shifts across the axolemma, generated by a hyperosmolar internal perfusate should therefore reduce the volume of the periaxonal space and increase $R_s$. Alicata et al. (1989) tested their hypothesis and showed that inward water movements, (a) slowed the clamp rise time, (b) reduced the peak of the linear capacity currents,

and (c) reduced the peak of the fast component of the gating current. However, the data showed that fast $I_g$ returned to normal in the presence of the hyperosmolar internal perfusate when clamp speed was also returned to its control rate by increasing series resistance compensation during hyperosmolar perfusion.

Fig. 4 shows that changes in series resistance compensation can have substantial impact on the early time course of gating current. Trace *a* (Fig. 4 A) shows the control record obtained with 10 $\Omega.cm^2$ $R_s$ series resistance compensation (~90 - 95% of the estimated $R_s$ in this axon). Traces *b-f* show the gating currents obtained when compensation for series resistance was readjusted to 9, 8, 7, 5 and 0 $\Omega.cm^2$, respectively. These records demonstrate progressive reduction of the initial fast component of gating current, as series resistance compensation is reduced. Neither total gating charge nor the time constants of the slower $I_g$ components were affected by change in series resistance compensation.

While recording the gating currents shown in Fig. 4 A, P/n control capacity currents associated with each level of series resistance compensation were separately recorded. These capacity currents are shown in Fig. 4 B, traces *a-f*. Peak capacity current falls as the uncompensated component of series resistance increases, indicating a reduction in the maximum rate of rise of clamp voltage, while the falling phase slows significantly. The fast linear capacity currents were integrated (see Fig. 4 C) to provide a more readily comprehensible measure of clamp rise time. This relationship remains similar to that noted by Stimers et al. (1987): the greater the uncompensated fraction of series resistance, the slower the rise time of the clamp (Fig. 4 C).

Since changes in $R_s$ compensation affect clamp rise in the axon, a cause and effect relationship can be presumed between the clamp rise time changes (indicated in Fig. 4 C) and the changes in gating current wave form shown in Fig. 4 A. For the traces obtained with 10 $\Omega.cm^2$ series resistance compensation (trace *a* in each figure), the peak of the gating current occurs well before final voltage is reached and a clear "fast $I_g$" component is visible. In contrast, when series resistance compensation is turned off (trace *f*) in each figure, the gating current peaks considerably later, closer to the time at which final potential is reached, and fast $I_g$ cannot be separately identified. These kinetic shifts did not involve any change in total gating charge, which remained at 43 $nC/cm^2$ in Fig. 4 A for trace *a* and 44 $nC/cm^2$ for trace *f*. Alicata et al. (1989) concluded that slowing the clamp does not "remove" fast $I_g$. Fast $I_g$ only becomes readily apparent in gating current records when the rate of rise of the clamp approaches the rate of the kinetic event characteristic of this very rapid component.

The nature of the periaxonal space in crayfish axons has been investigated by Shrager et al. (1983) using a combination of voltage clamp, thin section, and freeze fracture techniques. At the ultrastructural level, a complex lattice of tubules was found to cross the inner most glial layers in crayfish axons. No such structure has been reported for squid, where a narrow periaxonal space opens into clefts between the Schwann cells at intervals of 5 - 13 μm. By contrast, in crayfish, the spacing between openings of the tubular lattice was only ~0.2 μm. Shrager et al. (1983) concluded that crayfish sodium channels are located in regions with relatively unrestricted access to bulk extracellular fluid. Thus, effective $R_{FH}$ may well remain small, by comparison

with total $R_s$, in crayfish axons under most experimental conditions. I was able to measure the fast kinetic component of gating current with normal series resistance compensation (10 $\Omega/cm^2$). However, as noted by Stimers et al. (1987), the volume of the squid giant axon periaxonal space (F-H space) had to be increased by bathing the axon in a solution that was 10-20% hyperosmotic with respect to the internal solution in order to uncover the fast kinetic of $I_g$.

Series resistance compensation was achieved with an electronic feed back circuit (Levis, 1979) which summed an appropriate proportion of the injected clamp current back into the clamp circuit output. In internally perfused crayfish axons routine compensation of 10 $\Omega.cm^2$ removes detectable dependence of $I_{Na}$ kinetics on sodium current magnitude (Fig. 5). Control axon kinetics remain stable whether sodium current is reduced by changing pore number without altering pore current, as by changing the holding current or applying low concentrations of TTX (Fig. 5 A), or by changing pore current without altering pore number, as by changing the extracellular sodium concentration (Fig. 5 B). By contrast, if membrane potential is intentionally shifted by as little as 5 mV (Fig. 5 C), and the currents are scaled, a clear kinetic discrepancy is apparent. Therefore, series resistance errors under these experimental conditions must be less than 5 mV.

(b.2) Invasion artifacts

Dynamic errors (space clamp artifacts) in membrane voltage can be also be produced by invasion artifacts. Invasion artifacts in sodium current usually arise from action potentials originating in membrane regions outside the guard electrodes. The invading external currents enter the inadequately space clamped region and distort the voltage uniformity of the membrane. These dynamic errors appear as "notches" (sharp discontinuities) in the sodium current waveform (see Fig. 6). This is usually observed near threshold test potentials between -60 and -30 mV. Artifacts are most readily avoided by maintaining inward sodium current density at approximately ~1.0 - 1.5 $mA/cm^2$, or by perfusing the axon with media which do not support action potentials (such as recording outward rather than inward sodium currents). However, it may be reasonable that the artifact shown in Fig. 6 was produced by improper insulation of the internal voltage clamp electrode. After the electrode was rebuilt and reinsulated prevention of external current from entering the space clamped region of the membrane appeared adequate, and the invasion artifacts observed in $I_{Na}$ records were eliminated. Space clamp artifacts which are routinely encountered during voltage clamp experiments are shown in Table 1. The table also includes the magnitude of the voltage and current errors in control conditions following appropriate corrections.

# TABLE 1

**Voltage Errors Associated**

**with the Voltage Clamp**

| Voltage Errors | Magnitude of Error |
|---|---|
| Liquid junction potential | ± 1 mV |
| Series resistance | < 1 mV |
| Invasion artifacts | < 1 mV |
| Space clamp errors | < 1 mV |

Techniques for measuring gating currents

(a) Operational definition of gating current
(b) Subtraction of linear capacity and leakage currents
(c) Subtraction of nonlinear leakage current
(d) Crayfish is a premiere preparation for gating current measurements

(a) Operational definition of gating current

The molecular events that regulate opening and closing of sodium channels in axon membrane are driven by the rearrangement of charged gating structures in response to a potential change in the electric field. Movement of these charged components generates a detectable "gating current" (Armstrong and Bezanilla, 1973, 1974; Keynes and Rojas, 1973, 1974; Meves, 1974). Gating current is the nonlinear (asymmetric) component of the membrane capacitance. Therefore, isolation and measurement of gating current involves subtraction of the linear and nonlinear components of the membrane capacity current. This experimental procedure is described below.

(b) Subtraction of linear capacity and leakage currents

The total membrane current ($I_{total}$) is equal to the linear capacity current ($I_{cap}$ linear) plus the nonlinear capacity current or gating current ($I_{cap}$ nonlinear) plus ionic current ($I_{ionic}$) plus leakage current ($I_{leak}$). The expression is given as:

$$I_{total} = I_{cap}\ (\text{linear}) + I_{cap}\ (\text{nonlinear}, I_g) + I_{ionic} + I_{leak}.$$

Ionic current was eliminated by application of specific channel blockers such as TTX and STX, or by replacing the permeant monovalent cations with impermeant tetramethylammonium.

Linear capacity currents were subtracted directly on the Nicolet 1170 signal averager by utilizing modified versions of the P/n protocols reported by Armstrong and Bezanilla (1974) and Bezanilla and Armstrong (1977). A schematic representation of test pulse (P) and control pulse (P/n) protocols is shown below:

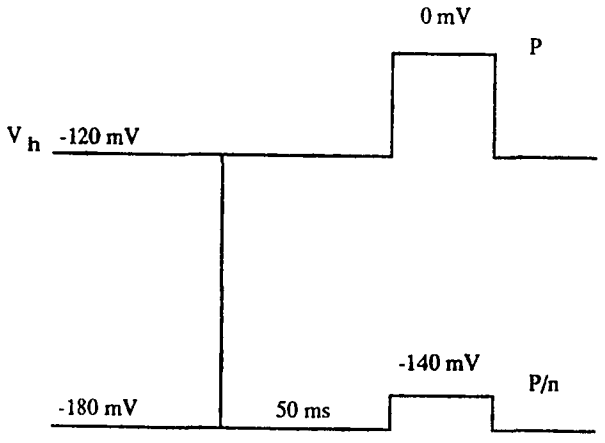

To isolate and measure the gating currents ($I_{cap}$ nonlinear), the linear capacity current must be subtracted by using the P/n subtraction procedure. During a depolarizing step change in voltage from the holding potential, referred to as the P pulse, two different components of capacity currents are generated. One component of capacity current is a linear function of the size of the voltage step and is therefore referred to as linear capacity current. The second component is the nonlinear capacity current or gating current which is generated only when the sodium channels open. To subtract the linear capacity current and isolate the gating current, P/n pulses are generated in a voltage range which does not activate channel opening and therefore does not generate gating current. These P/n pulses are limited to a voltage range -180mv to -140mv and have been shown to be free of any gating charge (Fig. 7, see also Starkus et al., 1981). Subtracting the P/n from the P pulses, subtracts the linear capacity current and therefore isolates the gating current. The total current is now gating current and leakage current.

When sodium ionic current is blocked with external TTX, and potassium current is blocked with internal cesium or tetramethylammonium, some small "leakage" current remains which is apparently not time dependent (Meves and Vogel, 1977a). It is as if some channels were open at all voltages. This small voltage-dependent "leakage" current could be expected to obey an equation such as $I_{leak} = g_{leak} (V_m - E_{leak})$ under most circumstances. Unfortunately, no currents through channels are exactly "linear" in the sense that the above equation is exactly obeyed. As was discussed above, the P/n control pulse subtracts the linear capacity and linear leakage current from the P test pulse. However, some leakage current remains after this subtraction

procedure. I will refer to this leak as the nonlinear leakage current and is corrected by a method discussed below.

(c) Subtraction of nonlinear leakage current

The linear subtraction (P/n) method, used for subtraction of linear capacity and leakage currents, does not remove the nonlinear component of steady state leak. The magnitude of nonlinear leak becomes greater at depolarized test potentials. Since leakage current is time invariant, any nonlinearity produces an offset in the baseline to which gating current decays to. Correction for nonlinear leakage current was made by defining the steady-state leakage line as zero current in the subtracted data. Therefore, each gating current was zeroed to a baseline by fitting a straight line through at least the last 3 - 8 ms of the data trace. Gating current occurs within the first 2 ms of the data record, and the portion of the record after 2 ms is time-invariant, nonlinear leak.

Gating current from crayfish giant axons

Fig. 8 A compares the capacity current associated with a test depolarization (P) to 0 mV with its control-pulse capacity current (P/n) of equal magnitude but generated in a voltage range more negative than the cell resting potential (-180 mV to -280 mV, Starkus et al., 1981). Fig. 8 A shows that the two current traces nearly overlie in the rising phase, but the test current (P) diverges from the control current (P/n) during the falling phase. Fig. 8 B shows the same P and P/n records at a greater amplifier gain, but here emphasizing the diverging sections of the falling phase for the two capacity

current traces. The trace associated with the P test pulse decays more slowly in comparison to the fast component of the linear capacity current associated with the P/n control pulse. The fast component of the P/n control capacity current indicates a clamp settling time of ~25 μs leaving a barely discernible residual slow component. Fig. 8 C shows the nonlinear component of the test (P) capacity current (gating current) at a higher gain after subtracting the control (P/n) and test (P) currents. In this study gating currents were measured by signal averaging 16 consecutive depolarizing test P pulses at a frequency of 1 Hz followed by 64 (if P/4) consecutive control P/n pulses, previously calculated to match the divided pulse protocol (P/n, Armstrong and Bezanilla , 1974).

(d) Crayfish is a premiere preparation for gating current measurements

Although the classical preparation for gating current investigation has been squid giant axon (Almers, 1978; Armstrong, 1981; Bezanilla, 1982; Keynes, 1986), the crayfish preparation offers superior resolution of the multiple components associated with the gating current waveform. Almers (1978) noted that the magnitude of gating current depends on three factors: (a) the number and valence of gating charges at each pore, (b) the kinetics of gating charge movement, and (c) the pore density. Starkus et al., (1981) reported that the maximum amount of charge movement in crayfish axon is ~2,200 electron charges/$\mu m^2$. This is slightly greater than the 1,500 to 1,900 reported for squid axons (Armstrong and Bezanilla, 1974; Keynes and Rojas, 1974; Hille, 1984). Because the $Q_{ON}/V_m$ distribution is not significantly steeper for crayfish than

for squid, indicating a similar charge number per channel, larger total charge movement in crayfish may well be accounted for by a higher sodium pore density. Starkus et al. (1981) concluded that the larger gating currents arise primarily from approximately four-fold faster kinetics in crayfish axon than in squid. The gating current signal in crayfish occurs within a time duration of approximately 2 ms, while in squid the time window is approximately 8 ms. Therefore, the slightly greater number of gating charges (~2,200 electron charges/$\mu m^2$) moving in a shorter time duration produces a larger gating current data trace. Moreover, the crayfish axon can be readily held at more negative potentials (i.e., -120 mV), and P/n control pulses in the voltage range of -150 to -200 mV may be imposed without [the dangers of] introducing membrane breakdown.

Instrumentation

(a) Data recording
(b) Temperature regulation

(a) Data recording

Experiments were carried out under computer control using a programmable pulse generator with 12 bit resolution, accurate to within ±0.1 mV (Adtech Inc., Honolulu, HI). Data traces were also digitized with 12 bit resolution using a Nicolet digital oscilloscope (model 1090A; Nicolet Instrument Corp., Madison, WI) and signal averaged on a Nicolet 1170. Sample intervals of 1 or 2 μs/pt were used for these studies. The signal averaged records (4090 data points per record) were then transferred and

archived onto a hard disk unit using a Sun 3/60 (Sun Microsystems, El Segundo, CA) running the UNIX operating system in a multiuser and multitasking mode. To compensate for the lack of real time processing ability on the UNIX system, the Digital/Analog (D/A) and Analog/Digital (A/D) circuits were separate devices external to the Unix computer system. The Unix computer controlled the initiation of the D/A and A/D devices during data acquisition by a master program. The master program also controlled data storage and retrieval, and provided data analysis procedures (including scaling, linear offsets, numerical integration, and operator-controlled digital filtering).

(b) Temperature regulation

All experiments were run at 9.5°C. A Teflon-coated aluminum block formed part of the bottom of the Plexiglas chamber, and was clamped to two thermoelectric cooling (Peltier) devices (Cambion Corp., #806-1067-01, Cambridge Thermionic Corp., Cambridge, Mass.). A thermilinear thermistor (YSI 44202, Yellow Springs Instrument, Co., Yellow Springs, OH) was placed close to the axon, and an electronic feedback system held the temperature to within ± 0.1°C of the set point.

Experimental solutions and reagents

Dissection of crayfish giant axon were begun in modified Van Harreveld external solution (MVH, Table 2). The external solutions were adjusted to pH 7.55 and 430 to

440 mosM. The osmometer (uosmette, Precision Systems, Inc., Natick, MA) determined solution osmolarity from its freezing point depression. The composition of both external and internal solutions are given in Table 2. Depending on the experimental protocol, the extracellular sodium concentration was adjusted by the appropriate mixing of tetramethylammonium (0 Na MVH) for sodium (210 Na MVH).

Internal perfusion solutions were prepared to be isosmotic with the external solution at 430 to 440 mosM, and the pH adjusted to 7.35. Separate internal perfusates were prepared with either potassium (250 K), cesium (230 Cs) or TMA (230 TMA) as the major cation. The use of either TMA or cesium (Cs) in the internal perfusate reduces leakage current, and prevents potassium currents from contaminating analysis of sodium channel current kinetics. Therefore, either 230 Cs or 230 TMA was utilized as the internal perfusate during data recording. The sodium ion concentrations are noted in the figure legend as ($[Na]_{in}$ // $[Na]_{out}$).

Tetrodotoxin (TTX), obtained from Calbiochem-Behring Corp. (La Jolla, CA), was included to the external media at 200 nM for all gating current recordings. In experiments involving the removal of fast inactivation, chloramine-T (Sigma Chemical Co., St. Louis, MO) was added to the internal solution and was prepared following the procedures originally described by Huang et al. (1987). Optimal results in removing all fast inactivation were achieved using freshly prepared 10 mM chloramine-T and lowering the pH of the internal media to 6.50.

Since chloramine-T also blocks the sodium channel (Wang et al., 1985; Huang et al., 1987), the internal chloramine-T perfusate was washed out as soon as reduction in peak current magnitude of $I_{Na}$ was noticed.

In heavy water experiments, internal and/or external solutions were prepared with 99.8% deuterium oxide (Sigma Chemical Co., ST. Louis, MO). Delta-9-tetrahydrocannabinol (THC) was obtained through licensing to Dr. John Starkus, and the THC solubilizing agent Pluronic F68 (see Methods for Chapter 4 below) was purchased from BASF Wyandotte Corp. (Wyandotte, Mich.).

# TABLE 2

## External Solutions

| Name | $Na^+$ | $K^+$ | $Mg^{++}$ | $Ca^{++}$ | $TMA^+$ | $Cl^-$ | Hepes | pH |
|---|---|---|---|---|---|---|---|---|
| | | | | mM | | | | |
| NVH* | 210 | 5.4 | 2.6 | 13.5 | 0 | 247.6 | 2 | 7.55 |
| 0 Na MVH† | 0 | 0 | 2.6 | 13.5 | 210 | 242.2 | 2 | 7.55 |
| 210 Na MVH‡ | 210 | 0 | 2.6 | 13.5 | 0 | 242.2 | 2 | 7.55 |

* (NVH) normal Van Harreveld solution (Van Harreveld, 1936).
† (MVH) modified Van Harreveld solution.
‡ Low external sodium solution achieved by appropriate mixing of 210 Na MVH with 0 Na MVH.

## Internal Solutions

| Name | $K^+$ | $Cs^+$ | $Na^+$ | $TMA^+$ | $F^-$ | glutamate$^-$ | Hepes | pH |
|---|---|---|---|---|---|---|---|---|
| | | | | mM | | | | |
| 250 K | 250 | 0 | 0 | 0 | 60 | 190 | 1 | 7.35 |
| 230 Cs | 0 | 230 | 0 | 0 | 60 | 170 | 1 | 7.35 |
| 230 Na* | 0 | 0 | 230 | 0 | 60 | 170 | 1 | 7.35 |
| 230 TMA | 0 | 0 | 0 | 230 | 60 | 170 | 1 | 7.35 |

All internal and extenral solutions checked for osmolarity in the range 430-440 mosM.
* Low internal sodium acheived by appropriate mixing of 230 Na and 230 TMA.

Methods for chapter 3: sodium channel activation mechanisms:

insights from deuterium oxide substitution.

Schauf and Bullock (1979) reported from *Myxicola* that $D_2O$ (at 5 °C) alters sodium channel kinetics by dramatically slowing the activation and inactivation components of $I_{Na}$. However, at higher temperatures of 16 –18°C sodium channels behaved similarly in $H_2O$ and $D_2O$ thus eliminating kinetic sensitivity of the channel to $D_2O$ action. The objective of this study was to confirm in crayfish axons the slowing action of $D_2O$ on channel kinetics observed in *Myxicola*. Since the freezing point for $D_2O$ is ~4.0 °C, ice crystal formation in the external bathing solution prevented data recording at lower temperatures. My initial experiments with external $D_2O$ were done at 5.0 °C which produced severe icing along the edges of the experimental chamber. Therefore, temperature was maintained at 9.5 ± 0.1°C for all experiments described in this study.

Schauf and Bullock (1979, 1980, 1982) and Schauf (1983) exposed both internal and external membrane surfaces to $D_2O$. In this study $D_2O$ (M. W. 20) was perfused either internally or externally. I find that $D_2O$ action on sodium channel kinetics is independent of route of application (see chapter three Results). When $D_2O$ is perfused internally, the membrane remains stable through two to three hours of recording. However, when $D_2O$ is placed only on the outside of the axon, crayfish axons remain stable for no more than 15 to 20 minutes before a marked increase in the linear leak current is observed.

Moreover, with external $D_2O$ application the membrane becomes increasingly intolerant of capacity current subtraction protocols (P/n) at hyperpolarized potentials. In my experiments with external deuterium oxide, $D_2O$ was substituted for external $H_2O$ and chilled to approximately 8 to 9 °C. The volume of the experimental chamber was then exchanged three times and continuously perfused. Bath temperature equilibrated to 9.5 °C within one minute.

During the use of either internal or external $D_2O$, the following criteria were therefore established for monitoring membrane integrity: (a) the holding current should not exceed that required to maintain membrane voltage within ±0.2 mV of the desired holding potential; (b) the peak magnitude of the fast component of linear capacity current could not fluctuate more than ±10% of control conditions; (c) the zero time intercepts of the two slower kinetic components of the capacity current should not increase from control levels; and (d) leakage current (observed during hyperpolarizing steps) must remain parallel to the baseline and not exceed by >10 - 20 $\mu A/cm^2$ the measured leakage current in control conditions. P/n control capacity currents were separately recorded throughout the experiment to check for changes in clamp speed and linear leak. Experiments were terminated when any of the above monitors exceeded criterion levels.

Methods for chapter 4: sodium channel activation mechanisms:

insights from delta-9-tetrahydrocannabinol substitution.

Delta-9-tetrahydrocannabinol (THC) is a hydrophobic compound (see Fig. 9 for structure and M.W.), essentially insoluble in aqueous solution. Therefore, THC was dissolved in the crayfish aqueous solution through the use of the polyhydroxy solubilizing agent Pluronic F68 according to the procedures originally described by Byck and Ritchie (1973) and Strichartz et al. (1978). A small volume (100 μl) of stock THC solution (318 mM THC) in 95% ethanol was added to 25 mg of dry Pluronic F68 and 1 ml of internal solution. The solution was gently heated at 50-60 °C until the Pluronic F68 dissolved. The ethanol was evaporated by gentle exposure to nitrogen gas for approximately 30 min. The THC and Pluronic F68 solution was then diluted with 24 ml of crayfish internal solution at room temperature to yield a final concentration of 1.27 mM. Serial dilutions were then made from this final concentration.

Long exposure times with low concentrations of THC (100 μm) were required to reach equilibrium block and slowing of $I_{Na}$ kinetics. Therefore, I encorporated the ''pulse'' method described by Strichartz et al. (1978). The procedure involved a brief exposure to higher concentrations of THC (635 μm and 1.27 mM) for ~1 to 2 minutes.

Sodium currents were reduced approximately 50%, slowed ~two-fold and remained at this level for up to 1 - 2 hours after replacement with the Pluronic F68 control solution.

The criteria for monitoring membrane integrity, as discussed above in the $D_2O$ study, were also used here. All experiments were run at 9.5 ±0.1 °C.

# CHAPTER 3

Sodium Channel Activation Mechanisms:

Insights from Deuterium Oxide Substitution

## Introduction

The exact relationship between "voltage-sensitive" gating current ($I_g$), and the molecular events constituting the "opening" or "gating" of the sodium channel remains unclear. Schauf and Bullock, (1979; 1980; 1982) and Schauf and Chuman (1986), have reported that solvent substitution of 98% deuterium oxide ($D_2O$) in *Myxicola* selectively slows macroscopic sodium current kinetics without corresponding action on gating current. No significant component of ON gating current had a time course which followed the altered kinetics of the final channel opening step. Schauf and Bullock (1979) conclude that physiologically detectable gating current must be generated exclusively within non-conducting, pre-open transitions of the channel rather than by the movement of the channel "gates" themselves. Furthermore the channel activation gates must be exposed to a hydrophilic phase and hence affected by $D_2O$, whereas the principle gating current generator appears protected from the effects of solvent substitution. On the other hand, Schauf and Bullock (1982) also observe that closure (deactivation) of conducting sodium channels is insensitive to the effects of

$D_2O$. The rate constants of the fast and slow components of sodium tail current remain unaltered during solvent substitution. The authors suggest that conducting sodium channels may deactivate by a route dissimilar from that taken during initial activation of sodium channels. Schauf (1983) also showed that prepulse-induced ("Cole-Moore-type") shifts in sodium channel activation are not affected by solvent substitution with $D_2O$.

Structural models describing sodium channel gating have been proposed by Noda et al. (1984); Guy and Seetharamulu (1986) and Catterall (1986). These models suggest that voltage-dependent channel gating results directly from rotation of the highly charged and highly conserved S4 $\alpha$ helix in response to membrane depolarization, such that a significant component of gating charge would move in the final channel opening step. The assumptions of these structural models appear in conflict with the experimental data presented by Schauf and Bullock (1979).

Oxford (1981) demonstrated that when a maintained depolarizing pulse was interrupted by a brief return to holding potential, subsequent reactivation (secondary activation) of the sodium channel proceeded rapidly with almost monoexponential kinetics. During the brief interpulse interval, channels were apparently captured in a nonconducting transition state adjacent to the open state. He concluded that channel deactivation occurs by reversal of the multi-state primary activation path. This evaluation of channel behavior also seems in conflict with a major conclusion reached by Schauf and Bullock (1979, 1982) from their $D_2O$ studies, namely that activation and deactivation occur by separate paths.

I report here the effects of $D_2O$ substitution on sodium channel gating current, ionic current and tail current in the crayfish. My results provide detailed confirmation for both Schauf and Bullock's findings in *Myxicola* and Oxford's observations on secondary activation. However, secondary activation, following brief interpulse intervals, is $D_2O$-insensitive.

The significance of $D_2O$ action with respect to channel models will be considered in the Discussion.

## Results

The initial purpose of this project was to confirm in crayfish axons the observations reviewed by Schauf and Chuman (1986) concerning the effects of $D_2O$ on sodium channel kinetics in *Myxicola.* I find that solvent substitution with $D_2O$ significantly slows sodium channel activation and inactivation kinetics (Fig. 10 A, and Fig. 12 A, B and C) in crayfish without corresponding changes in tail current kinetics (Fig. 10 A) or the ON and OFF gating current (Fig. 10 B). Ionic current (Fig. 10 A) was recorded before (trace *a*), during (trace *b*) and after (trace *c*) washout of internally perfused $D_2O$. It is clearly visible that activation and inactivation kinetics of $I_{Na}$ are slowed by $D_2O$ (trace *b*) in comparison to the records in $H_2O$ (traces *a* and *c*). The tail currents (Fig. 10 A) however are indistinguishable and appear insensitive to $D_2O$ action. In Fig. 10 B I show records of $I_g$ON and $I_g$OFF taken in $H_2O$ (trace *a*) and in $D_2O$ (trace *b*). No kinetic effects of $D_2O$ on $I_g$ are apparent at this level of resolution. Thus this figure provides a preliminary confirmation of the major findings reported from *Myxicola* axons. $D_2O$ significantly slows $I_{Na}$ activation and inactivation kinetics without corresponding affect on gating current and ionic tail current (Schauf and Bullock, 1979, 1982; Schauf 1983; Schauf and Chuman, 1986).

More careful examination of the effects of $D_2O$ on $I_g$ON kinetics (Fig. 11) shows small changes in the initial peak $I_g$ON during exposure to $D_2O$ as noted by Schauf and Bullock (1979). Small changes in peak $I_g$ were also detected in our data, although this is not clearly visible in Fig. 11, A or B, due to the compressed time base. However,

Alicata et al. (1989) have demonstrated that changes in series resistance ($R_s$) alter clamp rise time, thus affecting both capacity current waveform and the fast component of gating current. I therefore looked for changes in $R_s$ during the course of the experiment by using the waveform of the separately recorded P/n control capacity currents as an indicator of changes in clamp rise time. $D_2O$ induced a small reduction in peak capacity current (<10%) which corresponds to an increase in $R_s$ and a reduction in clamp speed. In every instance in which reduction of peak $I_g$ was noted, I also noted a corresponding reduction in peak capacity current. I conclude that changes in peak $I_g$ result from indirect effects of $D_2O$ on $R_s$ rather than from direct solvent action on the gating currents.

Fig. 11 shows that no $D_2O$-induced changes are readily apparent in the slower components of gating current. However, integrations of these gating current records suggest small (but consistent) rate changes in charge movement between the records in $H_2O$ (traces *a*) and in $D_2O$ (traces *b*). Gating current was integrated over a 2 ms time course, and there was essentially no significant change in total charge movement between $H_2O$ and $D_2O$ conditions (see Figure legend). The gating currents in Fig. 11, A and B, were recorded at 0 mV where total charge movement is close to $Q_{max}$ (see Fig. 6 of Rayner and Starkus, 1989) and $I_g$ kinetics are still relatively slow.

These conditions maximize the opportunity for recording small kinetic changes in gating currents. My results confirm the lack of major effect on $I_g$ kinetics noted in *Myxicola* (Schauf and Bullock, 1979, 1980 and 1982) and squid axons (Meves, 1974). Nevertheless my data suggests that future work may be able to resolve and quantify small effects of $D_2O$ on the kinetics of the slower components of gating current. I find no differences between the effects of internal (Fig. 11 A) and external (Fig. 11 B) $D_2O$ application on gating current.

In Fig. 12 records of ionic current are shown at voltages of -20 mV (A), 0 mV (B) and +20 mV (C). Because $D_2O$ decreases maximal sodium channel conductance (~20%), currents recorded in the solvent (traces *b* in each panel) have been scaled to the peak inward current magnitude of the record taken in $H_2O$ (traces *a* in each panel) to aid visual comparison of the $D_2O$ effects. I have quantified these effects for the voltage range -40 to +60 mV (see Table 3) . The ratio of $D_2O$ / $H_2O$ was determined both for time to peak inward current magnitude ($t_p$) and the time to one-half peak current magnitude ($t_{½}$) in a series of six axons. My results show this ratio as 1.31 ± 0.07 and 1.33 ± 0.18 for $t_p$ and $t_{½}$, respectively. Ionic current was analyzed over an 8 ms time course, and I find that the asymptotic value for steady-state $I_{Na}$ is not changed during exposure to $D_2O$. This is not readily apparent in Fig. 12 A where I show $I_{Na}$ traces recorded at -20 mV and plotted on a short time base. However, at the more positive voltages such as +20 mV (Fig. 12 C) where the kinetics are faster, it becomes more visible that the asymptotes are analogous in $H_2O$ and $D_2O$. Thus my data confirms the major findings reported from *Myxicola* by Schauf and Bullock

(1979). $D_2O$ significantly slows activation and inactivation kinetics of $I_{Na}$, and this slowing action is voltage-insensitive (see Table 3).

## TABLE 3

**Effects of $D_2O$ Across Voltage ($V_m$)**

| $V_m$ | Time to peak $I_{Na}$ $t_p$ (μs) | | Time to 1/2 peak $I_{Na}$ $t_{½}$ (μs) | | Ratio $D_2O$ / $H_2O$ | |
|---|---|---|---|---|---|---|
| mV | $H_2O$ | $D_2O$ | $H_2O$ | $D_2O$ | $t_p$ | $t_{½}$ |
| -40 | 902*(1) | 1,232 (1) | 328 (1) | 528 (1) | 1.37 | 1.60 |
| -20 | 531 ±36.9 (6) | 640 ±17.6 (6) | 219 ±20.8 (6) | 265 ±13.5 (6) | 1.21 | 1.21 |
| 0 | 391 ±41.1 (4) | 550 ±76.8 (4) | 156 ±23.7 (4) | 247 ±49.3 (4) | 1.41 | 1.58 |
| 20 | 256 ±4.1 (3) | 318 ±10.3 (3) | 128 ±0 (3) | 149 ±4.62 (3) | 1.24 | 1.16 |
| 40 | 208 (1) | 278 (1) | 106 (1) | 128 (1) | 1.34 | 1.21 |
| 50 | 174 ±4.9 | 228 ±6.1 | 84 ±1.1 (3) | 105 ±14.1 (3) | 1.31 | 1.25 |
| 60 | 174 (1) | 226 (1) | 90 (1) | 114 (1) | 1.30 | 1.27 |

* Values presented as mean, ± S.D. and (n).

Schauf and Bullock (1982) also reported that the sodium channel tail current was apparently insensitive to the solvent effects. They noticed that when the tail current records in $H_2O$ and $D_2O$ were scaled and superimposed, the fast components were identical while the slower components showed slight sensitivity or variability in $D_2O$. In Fig. 13, I show tail currents recorded at -80 mv following a test potential to +20 mV for 1 ms (see pulse pattern in Fig. 13 A; I plot only the portion of the current trace corresponding to the continuous line of this pulse diagram). Both the fast and slow kinetic components of the decaying tail current are clearly visible in these records. In Fig. 13 A, I have scaled the $D_2O$ record such that the slow components

overlie; these records superimpose exactly with no detectable kinetic dissimilarity in their rates. Trace *a* was recorded in $H_2O$ and trace *b* in $D_2O$. I then rescaled the $D_2O$ record to match the control peak tail current (see Fig. 13 B). The fast components of these traces now overlie with no apparent dissimilarities in their rates. However, I also noticed (as did Schauf and Bullock [1982] from *Myxicola*) that when the fast components are scaled as in Fig. 13 B, reduction in the relative intercept of the slow component (trace *b*) in $D_2O$ is more evident. I found a similar change at all prepulse durations investigated (0.4-6 ms).

Could series resistance errors be obscuring kinetic effects of $D_2O$ on tail current kinetics? If the axon were markedly undercompensated in control conditions, reduction in peak tail current during exposure to $D_2O$ could reduce the voltage error and so lead to an artifactual increase in deactivation kinetics. The artifactual voltage shift could mask a slowing by $D_2O$; this problem would be accentuated if $D_2O$ reduced series resistance. I recognize that $D_2O$ reduces the equivalent conductivity of electrolyte solutions (Swain and Evans, 1966) and thus would be expected to increase $R_s$, however, series resistance may be markedly affected by other factors (such as osmotic changes in Schwann cells as well as inward versus outward solvent fluxes [see Stimers et al., 1987; Alicata et al., 1989]). Thus other, less readily predictable, changes might override the conductivity effect.

Schauf and Bullock (1982) were careful to recompensate their axons after exposure to $D_2O$. In my experiments I changed external sodium concentration to maintain approximate equivalence of peak currents before and after $D_2O$ exposure.

Additionally, I monitored $R_s$ changes throughout the course of these experiments, using peak capacity current as the measured parameter (see Alicata et al., 1989). $D_2O$ initially produces a small increase in $R_s$, but this increase disappears over time, and $R_s$ is typically slightly reduced later in the experiment. Neither the peak magnitudes nor the kinetics of the tail currents were significantly affected by these small $R_s$ changes. I therefore conclude that tail current kinetics are insensitive to $D_2O$.

Armstrong and Bezanilla (1974) and Keynes and Rojas (1976) (squid giant axon) and Hahin and Goldman (1978) and Bullock and Schauf (1978) (*Myxicola*) have observed that a conditioning prepulse alters the time-dependent onset (''Cole-Moore-type'' shift) in sodium channel activation after a subsequent membrane depolarization (see pulse pattern *b* in Fig. 14, B and C). Schauf (1983) reported that although $D_2O$ causes significant slowing of channel activation and inactivation, it was without effect on prepulse-dependent delays in channel activation visible after conditioning hyperpolarizing prepulses. Schauf had predicted this result on the premise that since $D_2O$ was unable to alter

gating current, which he presumed to arise from transitions between non-conducting precursor states, it would also have no affect on ''Cole-Moore-type'' shifts (which have also been supposed to arise from changes in relative occupancy of early preopen states [see Taylor and Bezanilla, 1983]).

Fig. 14 A shows the single pulse control records at 0 mV in $H_2O$ and $D_2O$. The $D_2O$ record is not scaled demonstrating that $D_2O$ decreases maximum sodium conductance by ~20%. In Fig. 14 B I demonstrate the time shift of channel activation

kinetics, in $H_2O$, after a conditioning depolarizing prepulse to -65 mV (trace *b*) by comparison with the single pulse record (trace *a*). Trace *b* was scaled to match the peak current of the single pulse record to aid visual comparison of the shift in activation. I evaluated the "Cole-Moore-type" shift by determining the difference in $t_{½}$ between single pulse and double pulse records. In $H_2O$ (Fig. 14 B) the shift in activation ($\Delta\ t_{½}$) is 20 μs. I repeated the above protocol in $D_2O$ (Fig. 14 C) and found the magnitude of the "Cole-Moore-type" shift ($\Delta\ t_{½}$) to be 32 μs. At a different test potential of +50 mV the magnitude of the shift ($\Delta\ t_{½}$) in $I_{Na}$ was 13.5 μs in $H_2O$ and 17.0 μs in $D_2O$. My results for the "Cole-Moore-type" shift experiments are summarized in Table 4. I noticed, at the two voltages tested, the magnitude of the prepulse-dependent shift in activation was ~1.4 fold greater in $D_2O$ than in $H_2O$. However, when the magnitude of the shift is expressed as the ratio of $\Delta\ t_{½}$ / $t_{½}$ (single-pulse), this ratio is not changed by $D_2O$. Thus my data confirms the results reported from *Myxicola* by Schauf (1983).

**TABLE 4**

**Comparison of "Cole-Moore-type" Shifts in $H_2O$ and $D_2O$ at 0 and 50 mV**

| Time (μs) | 0 mV | | +50 mV | |
|---|---|---|---|---|
| | $H_2O$ | $D_2O$ | $H_2O$ | $D_2O$ |
| $t_{1/2}$ single pulse | 174.0 | 244.0 | 94.0 | 123.5 |
| $t_{1/2}$ double pulse | 154.0 | 212.0 | 80.5 | 106.5 |
| * $\Delta$ $t_{1/2}$ "C-M shift" | 20.0 | 32.0 | 13.5 | 17.0 |
| $\Delta$ $t_{1/2}$ / ($t_{1/2}$ single pulse) | 0.12 | 0.13 | 0.14 | 0.14 |

*$\Delta$ $t_{1/2}$ = $t_{1/2}$ single pulse − $t_{1/2}$ double pulse
data from axon 880928b

If sodium channel activation and inactivation are sequentially coupled processes, (Bezanilla and Armstrong, 1977; see also review by French and Horn, 1983), then a specific effect of $D_2O$ on inactivation might affect activation only indirectly. Does $D_2O$ slow $I_{Na}$ activation kinetics after removal of fast inactivation with 10 mM chloramine-T (ch-T)? In Fig. 15 I show that the slowing effect of $D_2O$ on activation kinetics remains after >90% of fast inactivation was removed with a single treatment of 10 mM ch-T (trace *d*). The control record ($H_2O$) following ch-T treatment is shown in trace *c*. For comparison I also provide records from the same axon before removal of fast inactivation, before (trace *a*) and during exposure to $D_2O$ (trace *b*).

In this axon the $D_2O$ / $H_2O$ ratios (cf Table 3) determined for $t_p$ and $t_{½}$ at 0 mV are 1.41 and 1.36 where fast inactivation is intact and 1.41 and 1.36 after ch-T treatment. This evidence demonstrates that activation is the primary target site for the observed $D_2O$ action on $I_{Na}$ kinetics.

Oxford (1981) showed that when a maintained depolarization was interrupted by a brief return (~100 μs) to holding potential (see Fig. 16 A, pulse pattern insert), reactivation turns on rapidly with almost monoexponential kinetics. He referred to this faster activation process as secondary activation. When the interpulse interval was progressively increased, secondary activation increasingly assumed the sigmoidal appearance of primary activation. I was interested to see whether primary and secondary activation were equally sensitive to the slowing effects of $D_2O$. In Figures 16 and 17 I show results obtained using this double-pulse protocol. All experiments were performed after treatment with 10 mM ch-T. Fig. 16 A shows secondary activation obtained after an interpulse interval of 50 μs (trace *b*). In crayfish axons, as in Oxford's squid axons, secondary activation turns on very fast without the usual sigmoid kinetics shown in the single pulse record (trace *a*). However, when interpulse interval is increased to 400 μs (Fig. 16 B, trace *b*), the reactivation process nearly overlies the sigmoid primary activation kinetics shown in the single pulse control record (Fig. 16 B, trace *a*).

Fig. 17 A shows $I_{Na}$ records obtained from the double pulse protocol (in both $H_2O$ and $D_2O$) with a 50 μs interpulse interval. Secondary activation in $H_2O$ and $D_2O$ are indistinguishable, and $D_2O$ appears to have no affect on this component of activation. On the other hand, primary activation is markedly slowed by $D_2O$. After an interpulse interval of 400 μs (Fig. 17 B) the kinetics and $D_2O$-sensitivity of secondary activation return towards those of primary activation. The $D_2O$-insensitivity of secondary activation after brief (50 μs) interpulse intervals will be further considered in the Discussion section.

In this series of experiments I have been careful to repeat all major observations with both internal and external $D_2O$ perfusion. I have noted no qualitative or quantitative differences resulting from method of solvent application other than a marked negative effect on axon survival when $D_2O$ is applied externally. The similar effects of internal and external $D_2O$ application may be seen for gating current (compare Figs. 11 A and B), for ionic current activation (compare Figs. 12 and 15) and for tail currents (compare Figs. 10 A and 13).

Summary

Schauf and Bullock (1979, 1982), using *Myxicola* giant axons, demonstrated that solvent substitution with deuterium oxide ($D_2O$) significantly affects both sodium channel activation and inactivation kinetics without corresponding changes in gating current or tail current rates. They concluded, (a) no significant component of gating current derives from the final channel opening step and, (b) channels must deactivate (during tail currents) by a different pathway from that used in channel opening. By contrast, Oxford (1981) found in squid axons that, when a depolarizing pulse is interrupted by a brief (~100 μs) return to holding potential, subsequent reactivation (secondary activation) is very rapid and shows almost monoexponential kinetics. Increasing the interpulse interval resulted in secondary activation rate returning towards control, sigmoid (primary activation) kinetics. He concluded that channels open and close (deactivate) via the same pathway.

I have repeated both sets of observations in crayfish axons, confirming the results obtained in both previous studies, despite the apparently contradictory conclusions reached by these authors. On the other hand, I find that secondary activation following a brief interpulse interval (50 μs) is insensitive to $D_2O$, although reactivation following longer interpulse intervals (~400 μs) returns towards a $D_2O$-sensitivity similar to that of primary activation.

I conclude that $D_2O$-sensitive primary activation and $D_2O$-insensitive tail current deactivation involve separate pathways. However, $D_2O$-insensitive secondary activation involves reversal of the $D_2O$-insensitive deactivation step.

# CHAPTER 4

## Sodium Channel Activation Mechanisms:

## Insights from Delta-9-tetrahydrocannabinol Substitution

### Introduction

### Kinetic studies

The Hodgkin and Huxley model had assumed (mostly for computational convenience) that inactivation and activation were independent (uncoupled) and parallel gating systems. This concept suggests that if inactivation were an independent process bearing innate voltage-sensitivity, it should develop immediately after the onset of a depolarizing voltage step.

Hodgkin and Huxley (1952b) showed that upon depolarization, the time course of inactivation develops exponentially without an apparent initial delay. However, Goldman and Schauf (1972) (*Myxicola*) and Bezanilla and Armstrong (1977) reported that the time course of inactivation was sigmoid having a pronounced initial delay. Therefore, the question whether inactivation is best described with an exponential or a

sigmoid time course is related to the question of whether activation and inactivation are independent/uncoupled (as proposed by Hodgkin and Huxley) or dependent/coupled systems.

If inactivation is an independent and parallel voltage-sensitive process distinct from activation, then inactivation should develop immediately following a depolarizing voltage step. Using a single pulse experiment Bezanilla and Armstrong (1977) compared control $I_{Na}$ (where both activation and inactivation components were intact) with records after inactivation was destroyed by treatment with the proteolytic enzyme pronase. Treatment with pronase also destroys some channels in the process of removing inactivation, therefore these records would have to be scaled appropriately to the control records. Scaling the pronase-treated record was determined by a scaling factor required to match the amplitude of the gating current after enzyme exposure to the gating current in control. After proper scaling the two data traces were subtracted producing the time course of inactivation. Using this procedure the investigators found that the time course of inactivation was sigmoid and the onset of inactivation was delayed by several hundred microseconds.

In an additional experiment, Bezanilla and Armstrong (1977) showed that with a conditioning double pulse procedure, the onset of inactivation developed after a noticeable delay. Moreover, the rate of inactivation was sigmoid and proportional to the time course of $I_{Na}$. These experiments involved a conditioning depolarization prepulse at three potentials for varying durations followed immediately with a test pulse. At very short conditioning pulse durations (<0.2 ms) the test pulse current magnitude

remained unchanged showing that inactivation was not evident. However, when the conditioning pulse duration was increased, the population of activatable sodium channels in the test pulse decreased resulting in a decrease of the peak current amplitude. Therefore, the peak amplitude of the test current is related to the fraction of channels that were activatable at the end of the conditioning prepulse. An imaginary curve (envelope) through the current peaks gave an accurate estimation of the rate of inactivation during the conditioning pulse. Moreover, this inactivation envelope showed that the initiation of inactivation developed with a noticeable delay, and its sigmoid rate was similar to the time course of inactivation derived from the single pulse (pronase) experiment described above. The authors concluded from their results that it was necessary for the activation gate of the channel to open before the inactivation gate could close. Therefore, the rate of inactivation is closely proportional to the number of open (conducting) channels, suggesting that the two gating systems are dependent/coupled.

Further evidence disputing the premise that inactivation is an independent/uncoupled voltage-sensitive process was reported from *Myxicola* giant axon (Schauf and Davis, 1975; Goldman, 1976; Goldman and Kenyon, 1982). These investigators demonstrated that the delay (''lag'') in the onset in inactivation observed during two-pulse experiments was dependent on the activation rate of the conditioning pulse. Goldman and Kenyon (1982) concluded that either inactivation was

dependent/coupled to activation or else it was independent/uncoupled and had the same rates as activation.

Gillespie and Meves (1980) also reported that the time course of inactivation was sigmoid with a prominent delay when the data was produced using the double pulse procedure where the conditioning pulse was followed immediately by the test pulse. Contrary to other investigators, they reported that the time course of inactivation was exponential for conditioning durations greater than 50-100 μs when the conditioning pulse and test pulse were separated by at least 1 ms. The authors concluded that since the time course of inactivation was exponential with a delay <50-100 μs, the inactivation event begins well before all the gating particles have moved to their opening position activating the channel, suggesting an independent/uncoupled voltage sensor for the inactivation process. This conclusion was contradictory to the dependent/coupled activation-inactivation hypothesis.

If inactivation gating is completely independent from activation, then the inactivation gate would require a gating charge which should be detectable as a slower component of $I_g$. However, the gating current data reported by Armstrong and Bezanilla (1977) lacked any such slow component, thus providing no evidence for gating charge movement associated with the inactivation process.

Armstrong and Bezanilla (1977) described both the prominent delay (several hundred μs) in the onset of inactivation (Bezanilla and Armstrong, 1977) and the apparent voltage-sensitivity of inactivation (Hodgkin and Huxley, 1952b; Bezanilla and Armstrong, 1977) with a coupled state linear model. The model shows that at

hyperpolarized potentials the activation gates are closed, and the inactivation gate is open. The inactivation gate is unable to close at this point because the closed activation gates are blocking its path. However, following deplorization the activation gates move to their conducting positions and the channel can open. The inactivation gate is then free to move into its closed position after an appropriate delay. In accordance with the coupled state model the apparent voltage-sensitive rate of inactivation depends on the state of activation, with inactivation having no innate voltage sensitivity of its own. In summary, while much evidence has been assembled suggesting sequential activation-inactivation coupling, the kinetic evidence is not yet fully conclusive.

## Pharmacological studies

Pharmacological studies have also contributed to the debate as to whether activation and inactivation are distinct and parallel voltage-sensitive processes, or if their mechanisms are coupled. Armstrong et al. (1973) demonstrated that the inactivation component of $I_{Na}$ was destroyed after internal perfusion of the proteolytic enzyme pronase. Activation kinetics were apparently insensitive to this treatment. This evidence was presumed to provide experimental conformation supporting the Hodgkin and Huxley concept of two independent and uncoupled gating systems. However, pronase could equally well remove the "inactivation-gate" within a sequentially coupled process. Moreover, the pronase experiment showed that the "h-gate" responsible for closing the conducting sodium channel was located on the internal surface of the

macromolecule in contact with the axoplasmic side of the membrane.

Many chemical agents have been used to help elucidate the structure and function of the sodium channel. Some of these agents which selectively affect only inactivation by marked slowing or complete removal are: N-bromoacetamide (NBA), chloramine-T (ch-T), tannic acid, iodate, dilute formaldehyde and glutaraldehyde (Hille, 1984). It was also demonstrated that high internal pH > 9.5 reversibly affects inactivation in the squid giant axon (Hille, 1984). These agents do not affect the voltage-sensitive kinetics of activation or the exponential time course of $I_{Na}$ tail currents. This evidence suggests that activation and inactivation are distinct processes, however, it does not determine whether they are dependent/coupled or independent/uncoupled systems.

In contrast to the effects of pH and proleolytic enzymes, which remove inactivation only when added to the inside of the membrane, there are many peptide toxins from scorpions and sea anemones which selectively affect inactivation when applied externally. *Leiurus quinquestriatus* and *Anemonia sulcata* toxins bind reversibly and competitively to external channel receptors distinct from TTX and STX binding sites. Modification of sodium channel function by toxin prolongs the time course of the action potential. Voltage clamp experiments show the toxin effect as a several-hundred fold slowing of inactivation. The voltage-sensitive kinetics of activation are apparently not altered by toxin action (Hille, 1984).

Two scorpion peptide toxins, *Centruroides sculpturatus* and *Tityus serrulatus*, were found to alter the voltage-sensitive process of activation when these hydrophilic toxins were applied externally. The toxins bind to external receptor sites distinct from

those of the inactivation modifiers. Cahalan (1975) showed that *Centruroides sculpturatus* toxin shifted the voltage dependence of activation to the left by ~40 to 50 mV without significant effect on inactivation. Caution is required for the interpretation of Cahalan's (1975) data. *Centruroides sculpturatus* toxin apparently has no effect on $I_{Na}$ activation or inactivation during a depolarizing test pulse. However, scorpion venom treatment causes the appearance of a new component of sodium current, which Cahalan refers to as "venom-induced current." During a depolarizing pulse, $I_{Na}$ currents activate and inactivate normally. However, after the conclusion of the pulse, when the membrane is repolarized, about one third of the available channels reopen and remain open for hundreds of milliseconds. Cahalan (1975) observed that the onset of the "venom-induced current" followed closely to the recovery of the sodium channel from inactivation after a depolarizing pulse. The author concluded from the analysis of the "venom-induced sodium currents" that toxin exposure shifted the voltage-dependence of channel activation to more hyperpolarized potentials by ~40 to 50 mV while the inactivation process remained intact and almost unaltered from normal. Cahalan (1975) concluded that activation "m-gates" and inactivation "h-gate" operate independently and can be uncoupled by pharmacologic treatment.

Lipid soluble alkaloid plant toxins (aconitine and veratridine) and the Colombian poison-arrow frog toxin, batrachotoxin (BTX) open sodium channels at rest. These toxins bind to sites distinct from those for the channel blocking toxins, TTX and STX. Hille (1984) proposed that the uncharged lipophilic compounds may bind to a receptor site deep within the interface between the hydrophobic region of the channel

macromolecule and the membrane lipids. Aconitine and BTX have long-lasting action and show similar electrophysiological effects on sodium channels. Mozhayeva et al. (1977) showed that aconitine reduced the threshold potential for activation and altered both the voltage-sensitivity and equilibrium potential of channel conductance. The authors showed that the normal threshold potential for frog node sodium channels is ~-50 mV. However, after treatment with 150 μM aconitine, channels opened at ~-90 mV. Current-voltage curves showed a shift of channel conductance to more negative potentials of ~50 mV, and the equilibrium potential for sodium ion ($E_{Na}$) was shifted to more hyperpolarized potentials after toxin exposure. The authors concluded that the toxin increased the permeability properties of the sodium channel to other ions such as ammonium, potassium, cesium and possibly tetramethylammonium. In addition to the effects on activation, these alkaloid toxins markedly slowed or completely removed inactivation.

Electrophysiological investigation on squid giant axons (Brady and Carbone, 1973) and on small non-myelinated c-fibers of the vagus nerve of the rabbit (Byck and Ritchie, 1973) demonstrated the ability of the natural marijuana constituent, delta-9-tetrahydrocannabinol (THC), to decrease both the action potential amplitude and its conduction velocity. Strichartz et al. (1978) were the first to investigate the effects of this highly lipophilic and uncharged compound on sodium channel conductance mechanisms under voltage-clamp conditions. This work was performed on the excitable membrane at the node of Ranvier of myelinated fibers of the frog sciatic nerve. Strichartz et al. (1978) demonstrated that THC exposure lengthened the

time-to-peak inward current magnitude ($t_p$) and suppressed ionic conductance ($g_{Na}$) in a voltage-dependent manner. Moreover, the investigators noted that THC did not affect channel inactivation processes. The authors concluded that the lengthening of $t_p$ and the shift in the voltage-dependence of peak $g_{Na}$ are both related to the relative kinetics of sodium activation and inactivation, and since inactivation was unaffected by THC, alterations of activation alone could account for these observed changes. This THC data proves that activation and inactivation are independent/uncoupled systems.

This evidence from the THC studies, along with the data reported by Cahalan (1975) discussed above, suggested that the tightly coupled activation and inactivation systems could be uncoupled by pharmacologic treatment. Moreover, the results seemed in strong agreement with the Hodgkin and Huxley concepts suggesting that the mechanisms of activation and inactivation operated as parallel and independently voltage-sensitive processes. More recently Catterall (1986) has proposed that the four highly charged S4 segments of the sodium channel tetramer corresponded to three independent and parallel activation (''m-gates'') and one inactivation (''h-gate'') voltage sensors.

As described above a wide range of pharmacologic agents affect both activation and inactivation or alter inactivation only, thus supporting the kinetic evidence suggesting that activation and inactivation are dependent/coupled mechanisms. Only THC and the scorpion venom *Centruroides sculpturatus* were reported to affect activation without changing inactivation kinetics. These results would support independent/uncoupled systems. However, Cahalan (1975) reported that the toxin was

without affect on normal $I_{Na}$ activation and inactivation kinetics during depolarization. His conclusions were derived from the analysis of "venom-induced current" generated after membrane repolarization. On the other hand, THC was reported to only affect activation kinetics while leaving inactivation unaltered in normal $I_{Na}$ currents (Strichartz et al., 1978). Since this single agent provides the strongest apparent evidence favoring the re-introduction of the Hodgkin and Huxley concepts of independent and parallel gating systems, I was interested to discover whether the data reported by Strichartz et al. (1978) was reproducible in crayfish axons on this crucial point. My results show that THC significantly slows both activation *and* inactivation kinetics, without a corresponding shift in the $F(V_m)$ curves. The conclusions which I derive from my THC study favor the hypothesis that activation and inactivation maybe dependent/coupled systems.

Results

Control ionic current data was recorded during internal perfusion of Pluronic F68 (see Methods). THC (~1 mM) and Pluronic F68 was perfused for ~2 to 5-min and then washed from the axon with Pluronic F68. In THC peak sodium current amplitude was reduced to ~50% of control and remained at this level for up to 1 to 2 hr after replacement with control Pluronic F68. In Fig. 18 records of ionic current are shown at test voltages of -20 mV (A), 0 mV (B), and +20 mV (C) from a holding potential of -120 mV. As was observed in frog node (Strichartz et al., 1978), THC also decreases maximal sodium channel conductance (~50%) in crayfish, therefore the ionic currents recorded after THC exposure (traces *b* in each panel) were scaled up to the peak inward current magnitude of the control record (traces *a* in each panel) to aid visual comparison of the THC effects on axon kinetics. At the test voltage of -20 mV (Fig. 18 A) it is easier to observe the ~two-fold slowing of both the rising (activation) and falling (inactivation) components of ionic current by THC (trace *b*). The action of THC on ionic current activation and inactivation kinetics have been quantified for the voltage range -60 mV to +40 mV (see Table 5). The ratio of THC/control was determined for time to peak inward current magnitude ($t_p$), the time to one-half peak current magnitude ($t_{1/2}$), and the time constant for inactivation ($\tau_h$) in a series of three axons. The values presented for 0 mV (Table 5) were determined from a series of eight axons. The results show this ratio as 1.95 ± 0.34, 1.85 ± 0.17 and 2.32 ± 0.60 for $t_p$, $t_{1/2}$ and $\tau_h$, respectively. These ratios are not significantly different. The

observed variability in the magnitude of THC slowing of $I_{Na}$ kinetics was dependent upon the duration of THC exposure. Ionic current was analyzed over an 6 ms time course, and the asymptotes for steady-state $I_{Na}$ changed in proportion to the delay in peak $I_{Na}$ ($t_p$) during exposure to THC. This is not apparent in Fig. 18 A where $I_{Na}$ traces are recorded at -20 mV and plotted on a short time base. However, at more positive voltages such as +20 mV (Fig. 18 C), where the kinetics are markedly faster, it becomes more visible that the asymptotes are analogous in control and THC.

Additional quantitative analysis was conducted on the THC/control ratios for $t_p$, $t_{½}$, and $\tau_h$. The ratios were converted to $\log_e$ (ln) and plotted (figure not shown) as a function of test potential for a voltage range of 70 mV (-30 mV to 40 mV). A peculiar behavior of the activation-inactivation system was noted, providing interesting speculation into the nature of the sodium channel conduction system. The THC/control ratios for $t_{½}$ were observed to be converging in the 70 mV voltage range while the ratios for $\tau_h$ were found to be diverging. Moreover, the ratios for $t_p$ were observed to be constant or only slightly converging across voltage. These observations may suggest a possible equilibration from the juxtaposition of the activation (measured as $t_{½}$) and inactivation (measured as $\tau_h$) coupled processes reacting in contrasting actions to the change in membrane potential.

Strichartz et al. (1978) reported that the action of THC on $I_{Na}$ activation kinetics was voltage-dependent. Their results suggested that exposure to THC shifted the $I(V_m)$ and $g_{Na}(V_m)$ curves to more depolarized potentials. Thus they concluded that the membrane after exposure to THC had to be depolarized by 10.5 mV more than in control conditions to activate half of the sodium conductance. This would mean a depolarizing shift in the midpoint ($V_o$) of the THC conductance [$g_{Na}(V_m)$] curve by ~10.5 mV. I have analyzed my $I_{Na}$ data in a similar manner and present the $I(V_m)$ and $g_{Na}(V_m)$ results below. Fig. 19 A shows $I(V_m)$ curves in control (open circles) and THC (closed circles) conditions. The THC data was recorded after ~1 to 2-min. exposure to ~1 mM THC. The peak magnitude of the inward sodium current was measured and plotted as a function of the test potential from a single holding potential of -120 mV (see legend). In both control and THC conditions the currents reach their maximum amplitude at ~0 mV. Thus there are no significant voltage shifts in the $I(V_m)$ data and the reversal potential ($E_{Na}$) for $I_{Na}$ changed less than ± 5 mV, indicating that the relative permeability properties of the channel to sodium ion were not altered by THC exposure. The discrepancy between my data and that of Strichartz et al. (1978) is further considered below.

In Fig. 19 B peak sodium conductance ($g_{Na}$) has been calculated from the $I(V_m)$ data and plotted as the fraction of conducting channels as a function of the depolarizing test voltage [$F(V_m)$]. The midpoints ($V_o$) of the $F(V_m)$ curves, where 50% of the channel population are conducting, correspond to the test potential of ~-20 mV in both control (open circles) and THC (solid circles) conditions. It is apparent that there

is no significant shift in surface charge that would account for the ~two-fold slowing in both activation and inactivation kinetics noted in ionic current.

Additional evidence is provided to support the hypothesis that THC does not affect the voltage-sensitivity of channel activation in crayfish giant axons. Fig. 19 C shows the $\log_e$ (ln) of the time to one-half peak current amplitude ($t_{½}$) of $I_{Na}$ presented as a function of the depolarizing test voltage [ln $t_{½}(V_m)$]. The slope for the control curve (open circles) corresponds to a voltage change of 76 mV per one *e*-fold change in ln $t_{½}$ (between 6.5 and 5.5). The slope for the THC curve was slightly steeper (solid circles) corresponding to a voltage change of 58 mV per one *e*-fold change in ln $t_{½}$. Although THC markedly slows channel activation, the slopes for these data curves are not significantly different. In crayfish axon THC exposure slows activation (measured as $t_{½}$ and $t_p$) and inactivation (measured as $\tau_h$) kinetics ~two-fold (see Table 5). However, there are no apparent shifts in surface charge [see $F(V_m)$ curves in Fig. 19 B] that would account for the dramatic slowing observed in channel $I_{Na}$ kinetics. Moreover, the voltage-sensitivity of sodium channel activation kinetics, measured as the valence of the ln $t_{½}(V_m)$ curves, is essentially unaltered by THC exposure (see Fig. 19 C).

Since THC is an extremely strong lipophilic agent (Strichartz et al., 1978), it is highly plausible for the THC molecule to gain access into the hydrophobic regions of the channel protein and influence the gating mechanism. Therefore, THC-induced slowing of $I_{Na}$ activation and inactivation kinetics may be associated with corresponding action on gating current. Careful examination of the effects of THC on $I_g$ON

kinetics are shown in Fig. 20 A. Alicata et al. (1989) have demonstrated that changes in series resistance ($R_s$) alter clamp rise time, thus affecting both capacity current waveform and the fast component of gating current. Changes in $R_s$ were monitored during the course of these experiments by using the waveform of the separately recorded P/n control capacity currents as an indicator of changes in clamp rise time. THC induced a small increase in peak capacity current (<10%) which corresponds to a decrease in $R_s$ and an increase in clamp speed.

In Fig. 20 A Gating current (trace *b*) was recorded after exposure to 0.5 mM THC and scaled to the control gating current (trace *a*) by matching the plateau (flat) region of the integration in THC (trace *b*) to the integration in control (trace *a*). THC-induced changes are readily apparent in the intermediate and slow components of ON gating current (Fig. 20 A). However, the initial fast component of $I_g$ON (trace *b*) remains insensitive to THC action (trace *b*) and closely overlies the fast component of control $I_g$ON (trace *a*). Integration of gating current over a 4 ms time course shows that total gating charge movement was suppressed from 27 nC/cm$^2$ in control (trace *a*) to 20 nC/cm$^2$ in THC (trace *b*). When the gating current integration in THC (trace *b*) was scaled to match the integration in control (trace *a*), marked slowing is clearly visible on both the intermediate and slow regions. The gating currents in Fig. 20, A and B, were recorded at 0 mV (from a holding potential of -120 mV) where total charge movement is close to $Q_{max}$ (see Fig. 6 of Rayner and Starkus, 1989) and gating current kinetics are relatively slow. These conditions maximize the opportunity for recording small kinetic changes in gating currents. These results indicate that although THC

significantly affects the slower components of $I_g$ON, the initial fast component was apparently spared from THC action.

Fig. 20 B shows OFF gating current recorded during repolarization to -120 mV after a depolarizing test pulse to 0 mV for 0.4 ms in control (trace *a*) and THC (trace *b*) conditions. $I_g$OFF traces were scaled by matching the plateaus of the integration records. After scaling the two OFF gating current records, THC-induced effects on $I_g$OFF kinetics are not apparent. OFF gating current was integrated over a 3 ms time course. Total gating charge movement was 19 nC/cm$^2$ in control (trace *a*) and 9 nC/cm$^2$ in THC (trace *b*). However, after scaling, the $I_g$OFF integrations are indistinguishable suggesting that the movement of OFF gating charge is relatively insensitive to THC action.

Fig. 20 C shows $Q_{ON}(V_m)$ curves in control (open circles) and after perfusion of 0.1 mM THC (solid circles). The data curves were obtained by plotting the areas under the gating current of this data set as a function of the depolarizing test voltage from a single holding potential of -120 mV. The gating current records were integrated over a 4 ms time course, and the $Q_{ON}(V_m)$ curves presented were not scaled. It is apparent that although there is THC-induced suppression of gating charge movement the voltage reactivity of $Q_{ON}$ movement is not altered by THC exposure.

In summary, the marked slowing action of THC on $I_{Na}$ activation and inactivation kinetics are associated with corresponding effects on gating current. THC significantly alters rates of the intermediate and slow components of $I_g$ON. However, the initial fast component of ON gating current seems insensitive to THC action (Fig. 20 A).

Moreover, integrations of $I_gON$ records reveal THC-induced suppression of total $Q_{ON}$ (~26%) and marked slowing of the intermediate and slow components of ON gating charge movement. On the other hand, the behavior of OFF gating current after THC exposure is strikingly different. The results indicate that THC suppresses total $Q_{OFF}$ ~53%. However, I am unable to detect any kinetic dissimilarities in the scaled records of OFF gating current or the integrations. These observations will be considered further in the Discussion.

Sodium tail current resulting from channel deactivation (''m-gate'' closure) is a rapid process having both fast and slow kinetic components. Fig. 21 shows tail currents recorded at -80 mV after a depolarizing test pulse to 0 mV for 3 ms. The holding potential was -120 mV. Traces *a* were recorded in control and traces *b* were recorded after exposure to 0.5 mM THC. Pulse patterns are presented in the insert of Figs. A and B. I have plotted only the portion of the current traces corresponding to the solid line of the pulse diagram. Both the initial fast and slow kinetic components of the decaying tail current are clearly visible in these records. In Fig. 21 the THC record (trace *b*) was scaled to match the peak tail current in control (trace *a*). It is apparent that the initial fast components of the tail current records overlie exactly with no detectable kinetic dissimilarity in their rates. In Fig. 21 B the THC record (trace *b*) was rescaled to the control record (trace *a*) in an attempt to superimpose the slow components. However, it is apparent that the slow components of the two tail current records do not superimpose, suggesting sensitivity of the slow component to THC action. Because the majority of initial fast component of the tail current is complete

before voltage has settled, its kinetics are highly sensitive to series resistance errors. Changes in $R_s$ were monitored throughout the course of these experiments using peak capacity current as the measured parameter. THC produces a slight decrease in $R_s$ which is associated with a <10% increase in peak capacity current. The magnitude of the capacity currents remained at this level for ~1-2 hr of recording. However, when the magnitude of the leakage currents exceeded criterion levels (see Methods), the experiments were terminated. Therefore, I conclude the slow component of sodium tail current is sensitive to THC action while the kinetics of the initial fast component of ionic tail current were indistinguishable in control and THC conditions.

Oxford (1981) (squid) and Alicata et al. (1990) (crayfish) demonstrated that secondary activation turns on with almost monoexponential kinetics after a depolarizing test pulse has been interrupted by a brief return to holding potential. However, when the duration of the interpulse interval was progressively increased, the kinetics of secondary activation increasingly assumed the sigmoid wave form characteristic of primary activation. The actions of THC on sodium channel ionic and gating currents appear to follow a distinctive pattern. Slower kinetic processes of channel ionic and gating current are sensitive to THC action while the very fast events distinctive of sodium channel ionic and gating currents are apparently spared. Therefore I was interested to see whether the slower sigmoid kinetics of primary activation and the fast monoexponential kinetics of secondary activation would be differentially sensitive to the slowing action of THC. Activation kinetics were analyzed after >90% of fast inactivation was removed by prior treatment with 5 mM ch-T. Fig. 22 A shows control

and THC $I_{Na}$ records obtained from the double pulse protocol with an initial test voltage of -20 mV for 2 ms. Here the dramatic slowing action of THC on primary activation is clearly visible (see primary activation components of the records in Fig. 22 A). The membrane was then repolarized to the holding potential (H.P. -120 mV) for an interpulse interval of 50 μs and depolarized a second time to the test voltage of -20 mV. Here secondary activation turns on with almost monoexponential in both control and THC conditions (see secondary activation kinetics shown in Fig. 22 A and B). Primary activation is markedly slowed by THC. However, the fast kinetics of secondary activation are only slightly slowed. This data suggests that future work may be able to resolve and quantify small effects of THC on the fast kinetics of secondary activation. The results demonstrate that the fast monoexponential kinetics of secondary activation (after a 50 μs interpulse interval) are relatively insensitive to the slowing action of THC. Moreover, when the duration of the interpulse interval was extended to 400 μs, the kinetics and THC sensitivity of secondary activation returned towards those of primary activation (see Fig. 22 C). These observations will be considered further in the Discussion.

Summary

Electrophysiological investigation on squid giant axons (Brady and Carbone, 1973) and on small non-myelinated c-fibers of the vagus nerve of the rabbit (Byck and Ritchie, 1973) demonstrated the ability of the natural marijuana constituent, delta-9-tetrahydrocannabinol (THC), to decrease both the action potential amplitude and its conduction velocity. Strichartz et al. (1978) were the first to investigate the effects of THC on sodium channel conductance mechanisms under voltage-clamp conditions. This work was performed on the excitable membrane at the node of Ranvier of myelinated fibers of the frog sciatic nerve. The authors reported that THC modified channel conductance by slowing the activation kinetics of $I_{Na}$ (lengthening the time-to-peak current, $t_p$) and suppressing ionic conductance ($g_{Na}$) in a voltage-dependent manner. They also noted that channel inactivation processes were not affected by THC action. The authors concluded that the lengthening of $t_p$ and the shift in the voltage-dependence of peak $g_{Na}$ are both related to the relative kinetics of sodium activation and inactivation, and since inactivation was unaffected by THC, alterations of activation alone account for these observed changes.

I have repeated the above observations in crayfish axons, but I can confirm only one of the three results obtained in the previous studies. I find that THC affects both activation and inactivation kinetics.

However, I find that the normalized $F(V_m)$ curves are almost identical indicating no significant shift in surface charge following THC treatment. Furthermore, I find that THC selectively alters only the slower components of ionic and gating current kinetics while sparing the very fast channel processes. These results suggest that fast THC-insensitive processes reflect a THC-insensitive gating mechanism: a "fast m-gate."

# CHAPTER 5

# GENERAL DISCUSSION

The investigation of $D_2O$ and THC substitution presented in this thesis provides critical evidence which strongly supports the recent structural and electrophysiological data suggesting that the sodium channel activation mechanism involves a parallel system of three nonidentical gating particles. I will discuss these current observations and presumptions concerning channel activation and the three alternative modeling systems (see Introduction) which describe activation behavior. Finally, I will examine my data in the context of these recent discoveries.

## Structural evidence

There are three general model types which attempt to describe the sodium channel activation mechanism. The parallel model proposed by Hodgkin and Huxley (1952c) assumed three independent gating particles ("m-gates") with identical voltage-sensitivity. The rate constants $\alpha$ and $\beta$ represent the relative voltage-sensitivity of the forward and backward reactions, respectively. Since the gating particles are identical, the conformational changes of the sodium channel associated with depolarization are determined by the ratio of $n\alpha/n\beta$ and is represented schematically with

a 4-state parallel model (see Scheme 1). However, recent structural and electrophysiological evidence suggests that sodium channel activation involves the behavior of three or four parallel but nonuniform gating particles (S4 segments). The 8-state parallel model does not presume identical kinetics for the S4 segments (see Scheme 2).

The linear sequential model presented by French and Horn (1983) describes the activation process as involving the sequential movement of a single or multiple gating particles with a high degree of electrostatic or allosteric coupling. The gating particles are not necessarily identical. Therefore, different rate constants can be used to describe each of the forward and backward reaction steps (see Scheme 3).

The voltage-gated sodium channel is a membrane protein that modulates the sodium ion permeability of electrically excitable membranes. Catterall (1980) demonstrated that a variety of pharmacological agents, including neurotoxins, affect the function of the sodium channel. The use of binding assays based on the high specificity of such neurotoxins has resulted in the purification of the sodium channel from the electric organ of the eel *Electrophorus electricus* (Agnew et al., 1978; Nakayama et al., 1982; Miller et al., 1983), rat brain (Hartshorne and Catterall, 1981), rat skeletal muscle (Barchi, 1983) and chick cardiac muscle (Lombet and Lazkunski, 1984). It was reported that the *Electrophorus* and chick sodium channels consist of a single polypeptide of ~260 kD. The rat sodium channel contains, in addition to the larger polypeptide two to three smaller peptides of ~37 to 45 kD. The purified eel and rat sodium channel proteins were shown to be functional when incorporated into phospholipid vesicles (Weigele and Barchi, 1982; Tamkun et al., 1984; Rosenberg et al., 1984;

Hanke et al., 1984). Major technical advances have allowed molecular biological manipulation to aid investigators in understanding the molecular dynamics underlying selective ion transport and voltage-dependent gating of the sodium channel. Noda et al. (1984) have successfully sequenced the primary structure of the sodium channel protein of *Electrophorus electricus* electroplax. Using recombinant DNA techniques, the investigators have cloned DNA sequences complementary to the messenger RNA coding for the sodium channel protein. Nucleotide sequence analysis of the cloned cDNA has revealed the complete amino acid sequence of this polypeptide.

Iverson et al. (1988), MacKinnon et al. (1988), Timpe et al. (1988a, b), and Zagotta et al. (1989) have reported that a mRNA transcript coding for only one monomer of the A-type potassium channel was sufficient to generate a functional multimeric voltage-gated channel. A-type potassium channels in *Drosophila* skeletal muscle are coded by the *Shaker* gene, and Modifications of the gene alter transmission at the larval neuromuscular junction and also affect A-type potassium currents in embryonic, larval and adult muscle. Molecular cloning of the *Shaker* gene has revealed that the derived amino acid sequence was homologous with sodium channels from the eel electric organ (Noda et al., 1984), rat brain (Noda et al., 1986; Kayano et al., 1988) and *Drosophila* (Salkhoff et al., 1987). Greatest homology among sodium channels across species lies in the region of the S4 segment. Noda et al. (1984) reported that the S4 segment had a highly conserved sequence of amino acids. A positively charged amino acid was found to be located at every third position with intervening hydrophobic residues.

Translation of the *Shaker* mRNA transcript yields a protein roughly only one fourth as long as in the cloned sodium channels, and the amino acid sequence of the *Shaker* protein corresponds to only one of the sodium channel's four homologous domains. Zagotta and Aldrich (1990) expressed potassium A channels in *Xenopus* oocytes after injection with a single *Shaker*-derived mRNA transcript. Because voltage-dependent gating of the potassium A channels is similar to sodium channels (Neher, 1971), Zagotta and Aldrich (1990) concluded that the A-channel functions as a multimer of identical monomeric subunits. Zagotta and Aldrich (1990) used a linear sequential model to simulate their experimental results. They also suggested that their sequential model was applicable to sodium channels. However, I will explain later in the Discussion that their assumptions are incorrect.

Recent structural evidence revealed that the four S4 segments of the sodium channel are not structurally identical, raising the possibility that they may also be functionally distinct. Stühmer et al. (1989) reported that modification of the S4 segment of repeat domain I markedly altered the effective valence of the sodium channel. The authors expressed functional sodium channels in *Xenopus* oocytes after microinjection of mRNA transcripts derived from rat brain sodium channel complimentary DNA. A single point mutation was introduced to the S4 region of domain I, so as to replace a positively charged amino acid with a neutral or negatively charged residue. The reduction in the net positive charge in the S4 segment of repeat I resulted in a marked decrease in the steepness of the potential dependence of channel activation. Site-directed mutations were also performed on the S4 segments of domains II and III.

However, this procedure had little affect on the voltage-sensitivity of activation. Stühmer et al. (1989) concluded that the positively charged amino acid residues of the S4 segment of domain I were the primary gating charge-carrier (voltage sensing device) for the sodium channel activation process.

Conti and Stühmer (1989) analyzed gating current records from *Xenopus* oocytes injected with mRNA coding for rat-brain-II sodium channels. From these critical studies they determined from holding potentials > -100 mV that the total effective channel valence was ~2.03*e*. The authors also provided evidence from fluctuation analysis studies of gating current suggesting the presence of three separate gating particles. Thus the investigators concluded that the sodium channel activation process may involve three parallel and uniform gating particles each having a valence of ~2.03*e*. However, these conclusions are not consistent with the results reported by Rayner and Starkus (1989) and Ruben et al. (1990) from gating current and ionic current studies, respectively. These investigators determined from $Q_{ON}(V_m)$, $Q_{ON}(V_h)$ (Rayner and Starkus, 1989) and $F(V_m)$ (Ruben et al., 1990) analyses at holding potentials > -100 mV that the sodium channel activation mechanism involved one dominant gating particle with a valence of ~2*e*. Thus, recent investigation of sodium channel activation kinetics from *Xenopus* oocytes and crayfish suggest that the valence of a single gating particle is ~2*e*. However, the current focus of intense scrutiny is to determine if the three parallel gating particles are identical.

## Electrophysiological evidence

The fundamental purpose of kinetic modeling is to discriminate model systems by quantitatively comparing model behavior and experimental results. Hopefully, this would eventually lead to a greater understanding of the sodium channel gating mechanism. Therefore, models under consideration must qualitatively meet a set of criteria established through experimental investigation. A model fails to meet a given criterion behavior when it cannot be fixed by changes in model parameters, without destroying the quality of fit to other aspects of axon performance. So, I will show that the sequential linear, and the parallel identical particle models do not meet experimental criteria. Additionally, the models discussed in this thesis are those which describe axon performance in accordance with two major concepts, (a) Markov kinetics, and (b) the Eyring rate theory. First, a Markov kinetic system describes the movement of gating particles as discrete transitions between closed and open states of the channel. The Markov theory assumes that the rate constant of the transition of a gating particle between channel states is first order (time course has a single exponential), and is independent of how the system reached its final state. For example, tail current kinetics during membrane repolarization to -40 mV are similar whether the transition of gating particles into the closed state is from 0 mV or +20 mV. Second, the Eyring rate theory for an electrical reaction suggests that the characteristic rate constant of the transition of a gating particle between channel states is dependent upon the energy of the electric field, the electrical charge of the gating particle and the energy barrier the

particle must transverse [see Hille, (1984) for a complete discussion of these concepts]. Although other modeling strategies have been considered [e.g., fractal models (Liebovitch, 1989)], accumulated evidence suggests ion channels conform to Markov criteria (Horn and Korn, 1989; McManus et al., 1989).

Parallel and identical particle models

A physical interpretation of the Hodgkin and Huxley model describing the sodium channel activation process suggests that the channel becomes conducting after three "m-gates" undergo independent voltage-sensitive transitions from resting to activating positions. Upon repolarization the channel closes after one "m-gate" moves away from the open position. Since the Hodgkin and Huxley model assumes that the voltage-sensitivity of the sodium channel is derived from the charge-bearing gating particles, then all gating current is a result of their movement. The model predicts that the conducting channel should close as soon as one "m-gate" moves to its resting position, but continue to generate gating current until all three identical "m-gates" have settled into their resting states. Therefore, according to the model, gating current (during repolarization) should last approximately three times longer than the sodium channel ionic tail current (during deactivation). However, Armstrong and Bezanilla (1974) observed that OFF gating current and ionic tail current decayed with almost exactly the same kinetic rates. Thus, the parallel and identical model proposed by Hodgkin and Huxley (1952c) demonstrates a "criterion failure" to the ionic tail current and OFF gating current data of Armstrong and Bezanilla (1974). Hence, the

Hodgkin and Huxley model should be eliminated unless modified to avoid this mismatch. I shall later point out that unequal-valence particle models are suitable in this respect.

Linear sequential models

Oxford (1981) examined reactivation (secondary activation) after return steps to holding potential of differing durations imposed during depolarizing pulses. Brief return steps to holding potential (~100 μs), which should catch channels in closed states adjacent to the open state, demonstrated secondary activation with rapid, almost monoexponential kinetics. He therefore concluded that channel deactivation occurs via reversal of the normal multi-step primary activation pathway. The observations from Oxford's (1981) investigation provided major support for models in which activation is considered as a linear sequential process, and deactivation is considered the reverse of primary activation (French and Horn, 1983; Horn and Vandenberg, 1984; Stimers et al., 1985). However, predictions of linear sequential models are in direct conflict with the data of Schauf and Bullock (1982) and Alicata et al. (1990) who concluded that activation and deactivation must utilize different pathways.

Schauf and Bullock (1979) concluded from their $D_2O$ studies that the sodium channel activation mechanism involved both voltage-sensitive (solvent-insensitive) channel gating and solvent-sensitive (voltage-insensitive) channel opening processes. Schauf and Bullock (1982) demonstrated that ionic tail currents were insensitive to

$D_2O$ substitution. Therefore, the investigators concluded that sodium channel activation involved more than one path leading into the channel conducting state, and that the $D_2O$-insensitive tail current deactivation step could not be the reverse $D_2O$-sensitive channel opening transition. Thus, linear sequential models which describe channel activation as having only one path into the open state are incorrect.

My results from $D_2O$ substitution presented in chapter three of this thesis provides additional support for the major conclusions presented by Schauf and Bullock (1979; 1982). I confirm that activation and fast inactivation of sodium current are both slowed by $D_2O$ (Figs. 10 A and 12) without marked effects on OFF (Fig. 10 B) or ON (Figs. 10 B and 11) gating current kinetics. This observation demonstrates that relatively little gating charge movement (or inherent voltage sensitivity) can be associated with the final channel opening transition. Moreover, I have confirmed Schauf and Bullock's (1982) observation that $D_2O$ does not affect tail current deactivation (Fig. 13). Therefore, a fundamental difference must exist between the channel gating mechanisms responsible for activation and tail current deactivation.

Despite the contradictory conclusions reached by Oxford (1981) and Schauf and Bullock (1982), the secondary activation data of Oxford (1981) and the tail current data of Schauf and Bullock (1982) have been successfully repeated in crayfish axons. I have demonstrated that for short interpulse intervals secondary activation shows rapid, nearly monoexponential, rates (Fig. 16 A). However, $D_2O$ slows the kinetics of primary activation (Fig. 12 and Table 3) without affecting tail current kinetics (Fig. 13). This apparent paradox may be resolved by the experiment shown in (Fig. 17),

which assesses the effect of $D_2O$ on secondary activation. I find that secondary activation, like tail current deactivation, is insensitive to $D_2O$ (see Fig. 17 A). Therefore, I conclude that $D_2O$-insensitive tail current deactivation cannot be the reverse of the $D_2O$-sensitive step responsible for channel opening during primary activation. However, $D_2O$-insensitive secondary activation may well represent reversal of the $D_2O$-insensitive tail current deactivation step. Oxford's (1981) observation can thus be reinterpreted as indicating that the deactivation path, like the primary activation path, involves a multistep reaction sequence. When the interpulse interval is in the order of 50-100 μs, many channels appear to have been caught no further than one reaction step away from the open state. However, these channels may well be following a different $D_2O$-insensitive pathway (just as Schauf and Bullock [1982] concluded). My results appear to rule out the standard linear sequential activation mechanism (Scheme 3). Therefore, no model predicting only one pathway into the channel open state is likely to be correct, and all sequential linear models are wrong.

Zagotta and Aldrich (1990) presented a linear sequential model describing the activation mechanism of voltage-sensitive potassium A channels. Moreover, the authors suggested that their model was applicable to sodium channels. This model was designed to explain their experimental data from single channel and macroscopic measurements. Only one path is shown leading into the channel open state, and the channel deactivation pathway is the reverse of the primary activation step. The unique feature of their linear sequential model is that the gating transitions leading into the channel opening step are voltage-sensitive. However, the final opening transition is

voltage-insensitive. The Zagotta and Aldrich (1990) linear sequential model suggests that the slower voltage-insensitive channel opening transition is allosterically coupled in a linear sequential manner to the faster voltage-sensitive gating process. However, if channel deactivation is the reversal of the channel opening step, then this model suggests that ionic tail currents would also be voltage-insensitive. This prediction is not supported by the voltage-sensitive tail current measurements reported by Bezanilla and Armstrong (1975a,b).

Bezanilla and Armstrong (1975a,b) demonstrated that the time constant of decay for the fast component of ionic tail current and OFF gating current were strongly dependent upon the repolarization potential. The investigators noticed that the time constants of these components were faster at more hyperpolarizing voltages. Thus, this experimental evidence strongly suggests that the sodium channel ionic tail current deactivation step is an inherently voltage-sensitive process. These results are contrary to predictions of the sequential models which assume a voltage-independent final opening step. Therefore, the tail current data of Bezanilla and Armstrong (1975a,b) and the $D_2O$ data of Alicata et al. (1990) critically conflict with the Zagotta and Aldrich (1990) sequential model describing the sodium channel activation system.

Parallel and nonidentical particle models

Zimmerberg et al. (1990) analyzed voltage-sensitive rectifying potassium channels (squid) and observed that hyperosmolar media reduced potassium conductance without

affecting the voltage-sensitivity of the channel. These results were interpreted to show that the channel activation system has both a voltage-sensitive (solvent-insensitive) gating process and a solvent-sensitive (voltage-insensitive) channel opening mechanism. The authors support their hypothesis with two alternative models: (a) a sequential, and (b) a parallel model in which no sequential coupling is postulated between the conformational changes associated with a voltage-sensitive gating mechanism and the osmotic-sensitive conformational changes associated with channel opening. These independent processes were presumed to operate in parallel.

Conti and Stühmer (1989) provided evidence from fluctuation analysis of gating current records suggesting the presence of three separate and uniform gating particles each bearing a valence of ~2.03*e*. However, Stühmer et al. (1989) from site-directed mutagenesis studies reported that the S4 segment of domain I was the dominant voltage sensor involved in channel activation, and the S4 segments of domains II and III were not major contributors to voltage-sensitivity of the channel. Thus, this data could suggest that the voltage-dependent activation mechanism involves three separate and nonuniform gating particles, and only one is the major charge-carrier.

In chapter four of this thesis I demonstrate that THC exposure in crayfish giant axon markedly slows both activation and fast inactivation kinetics of ionic current (Fig. 18) with associated changes to the intermediate and slow components of gating current (Fig. 20) and the slow component of ionic tail current (Fig. 21 B). However, THC appears to spare the fast kinetic components of gating current (Fig. 20) and ionic tail current (Fig. 21 A). A comparative list demonstrating the effects of $D_2O$ and THC

substitution on sodium channel kinetics is shown in Table 6.

It is apparent that THC was able to penetrate the hydrophobic regions of the channel macromolecule, housing the voltage sensor. My evidence suggests that the initial fast kinetics of gating current are associated with the fast component of ionic tail current (during channel deactivation). Moreover, the slower gating current kinetics could be associated with the slower component of tail current. These experimental observations suggest that there is a separate fast gating particle associated with the fast kinetics of gating and ionic current, and this gating particle operates in parallel with two nonuniform gating particles. Thus my results favor of a cyclical (parallel) and nonidentical particle system (see Scheme 2) which demonstrates the paths of three independent and nonuniform gating particles from the resting to the channel open state. The cyclic model provides three paths leading into and out of the channel open position and demonstrates no failure to the experimental data (Ruben et al., 1990).

Summary and conclusions

In chapter three, I present data from the investigation of $D_2O$ substitution on sodium channel kinetics. My results demonstrate that activation and fast inactivation of sodium current are both slowed by $D_2O$ without marked effects on gating current kinetics. This observation demonstrates that relatively little gating charge movement (or inherent voltage sensitivity) can be associated with the final channel opening transition. I also note that $D_2O$ does not affect tail current deactivation or the fast monoexponential kinetics characteristic of secondary activation (after short interpulse

intervals). Therefore, some fundamental difference must exist between the channel gating mechanisms responsible for activation and tail current deactivation. I conclude that $D_2O$-insensitive tail current deactivation cannot be the reverse of the $D_2O$-sensitive primary activation step. However, $D_2O$-insensitive secondary activation may well represent reversal of the $D_2O$-insensitive tail current deactivation step.

In chapter four I demonstrate that THC substitution markedly alters activation and fast inactivation kinetics of $I_{Na}$ and the slow component of ionic tail current with corresponding action on the intermediate and slow components of gating current. Moreover, I note that THC spares the initial fast components of gating current and ionic tail current. My experimental results reveal a separate, distinct and THC-insensitive fast gating particle associated with the fast kinetics of gating and ionic current, and this gating particle operates in parallel with two nonuniform gating particles.

Conti and Stühmer (1989) have recently suggested the presence of three separate and uniform gating particles each having a valence of ~2.03*e*. However, Rayner and Starkus (1989) from gating current measurements and Ruben et al. (1990) from the analysis of macroscopic ionic current have concluded that a single dominant gating particle, having a valence of ~2*e*, operates in parallel with two nonuniform gating particles. In addition, Stühmer et al. (1989) from site-directed mutagenesis studies reported that the S4 segment of domain I was the dominant voltage sensor involved in channel activation, and the S4 segments of domains II and III were not major contributors to voltage-sensitivity of the channel. Therefore, the voltage-dependent activation

mechanism involves three separate and nonuniform gating particles, and only one is the major charge-carrier. Therefore, I conclude from the $D_2O$ and THC substitution investigations that the sodium channel activation mechanism involves a system of three independent and nonuniform gating particles. Although it is possible that each gating particle moves along its path through sequential steps (see Scheme 2), there exist at least three distinct and parallel paths converging into and diverging out from the channel open state.

## TABLE 5

**Effects of THC Across Voltage ($V_m$)**

| $V_m$ | Time to peak $I_{Na}$ $t_p$ (μs) | | Time to 1/2 peak $I_{Na}$ $t_{½}$ (μs) | | Inactivation (Tau) $\tau_h$ (μs) | | Ratio THC / control | | |
|---|---|---|---|---|---|---|---|---|---|
| mV | control | THC | control | THC | control | THC | $t_p$ | $t_{½}$ | $\tau_h$ |
| -60 | 2,000* ±33.9 (2) | 2,240 ±322.0 (3) | 641 ±315.4 (2) | 1,344 ±622.0 (3) | 12.48 ±4.9 (2) | 16.49 ±11.0 (2) | 1.12 | 2.10 | 1.32 |
| -50 | 1,465 ±157.0 (2) | 2,112 ±340.7 (3) | 494 ±246.1 (2) | 842 ±261.6 (3) | 6.71 ±4.4 (2) | 11.77 ±3.5 (3) | 1.44 | 1.70 | 1.75 |
| -40 | 976 ±82.0 (2) | 2,034 ±281.5 (3) | 343 ±134.4 (2) | 673 ±133.3 (3) | 4.53 ±1.2 (2) | 10.18 ±4.1 (3) | 2.08 | 1.96 | 2.25 |
| -30 | 755 ±182.4 (2) | 1,725 ±143.2 (3) | 280 ±90.5 (2) | 586 ±70.5 (3) | 3.88 ±0.6 (2) | 6.77 ±1.8 (3) | 2.29 | 2.10 | 1.74 |
| -20 | 675 ±176.8 (2) | 1,434 ±87.4 (3) | 248 ±79.2 (2) | 506 ±26.0 (3) | 3.13 ±0.8 (2) | 5.59 ±1.9 (3) | 2.13 | 2.04 | 1.79 |
| -10 | 561 ±145.7 (2) | 1,194 ±91.9 (3) | 217 ±66.5 (2) | 418 ±20.2 (3) | 2.38 ±0.7 (2) | 4.72 ±1.5 (3) | 2.13 | 1.93 | 1.98 |
| 0 | 475 ±90.0 (8) | 989 ±68.6 (14) | 192 ±42.3 (8) | 353 ±17.3 (14) | 1.70 ±0.4 (8) | 4.26 ±1.0 (14) | 2.08 | 1.84 | 2.51 |
| 10 | 409 ±94.8 (2) | 829 ±87.6 (3) | 171 ±43.8 (2) | 304 ±24.2 (3) | 1.31 ±0.4 (2) | 3.62 ±0.9 (3) | 2.03 | 1.78 | 2.76 |
| 20 | 357 ±75.0 (2) | 726 ±71.9 (3) | 157 ±35.4 (2) | 270 ±25.5 (3) | 1.12 ±0.4 (2) | 3.31 ±1.1 (3) | 2.03 | 1.72 | 2.96 |
| 30 | 329 ±55.2 (2) | 650 ±91.8 (3) | 148 ±25.5 (2) | 252 ±39.9 (3) | 1.00 ±0.5 (2) | 3.08 ±1.2 (3) | 1.98 | 1.70 | 3.08 |
| 40 | 310 ±31.1 (2) | 588 ±99.0 (2) | 148 ±11.1 (2) | 208 ±00.0 (2) | 0.93 ±0.5 (2) | 3.12 ±1.4 (2) | 1.90 | 1.41 | 3.37 |

* Values presented as mean, ± S.D. and (n).

# TABLE 6

## Comparison of Effects of $D_2O$ and THC on Sodium Channels

| | | $D_2O$ | THC |
|---|---|---|---|
| **Ionic Currents** | | | |
| | activation | + | ++ |
| | inactivation | + | ++ |
| | $2^o$ activation | - | ? |
| Tail Current* | Fast | - | - |
| | Slow | - | + |
| **Gating Currents** | | | |
| $Q_{ON}$ | Fast | - | - |
| | Intermediate | - | + |
| | Slow | - | + |
| $Q_{OFF}$ | Fast | - | - |
| | Slow | - | ? |

*After chloramine-T treatment

**Figure 1** Voltage clamp electrodes and circuit. Schematic diagram of electrode arrangements and voltage clamp circuit. Amplifiers #1, 2 and 3 are voltage recording, #4 is the control amplifier, and #5 is for current recording. Symbols used are: $V_m$, transmembrane potential; $I_m$, membrane current; and $V_h$, holding potential.

Figure from Shrager, P. 1974. Ionic conductance changes in voltage clamped crayfish axons at low pH. *J. Gen. Physiol.* 64:666-690. Figure 1.

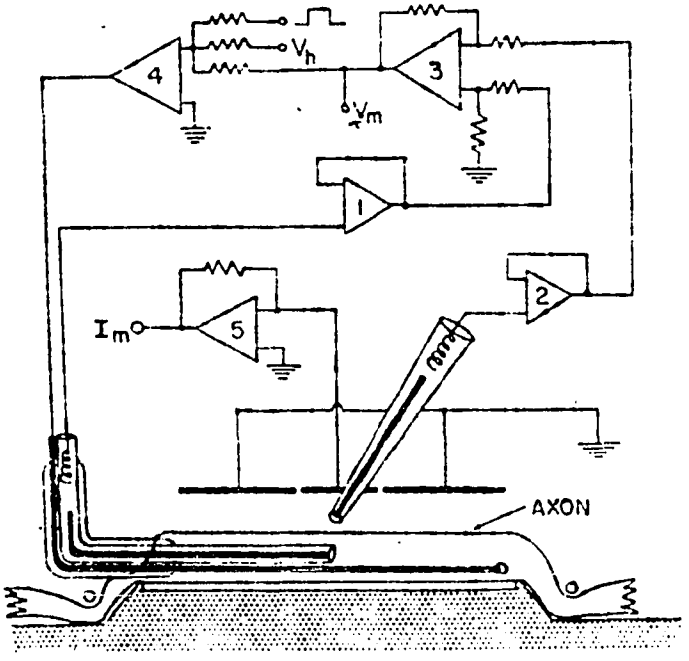

**Figure 2** Location of biological resistors associated with the axon membrane and surrounding Schwann cell layer. The internal and external fluid resistances are not significant contributors to $R_s$. The major source of series resistance lies within the Schwann cell clefts (regions between Schwann cells). The true membrane voltage cannot be directly measured. However, with adequate electronic series resistance compensation, the measured clamp potential closely represents the true membrane voltage.

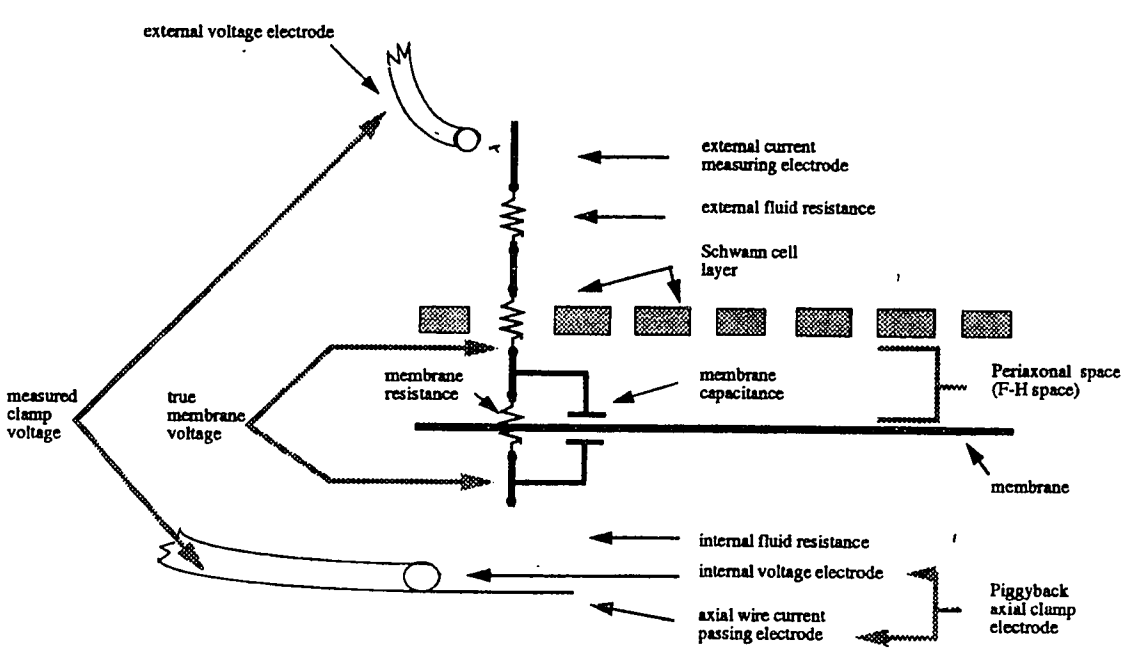

**Figure 3** Simplified structural model of the axon and surrounding Schwann cells. Two patches of axon membrane are shown that are isolated from each other by a resistance owing to the F-H space. The magnitude of this resistance is dependent upon the osmotic gradient across the axon membrane.

Figure from Stimers, J. R., F. Bezanilla, and R. E. Taylor. 1986. Sodium channel gating currents. Origin of the rising phase. *J. Gen. Physiol.* 89:521-540. Figure 6.

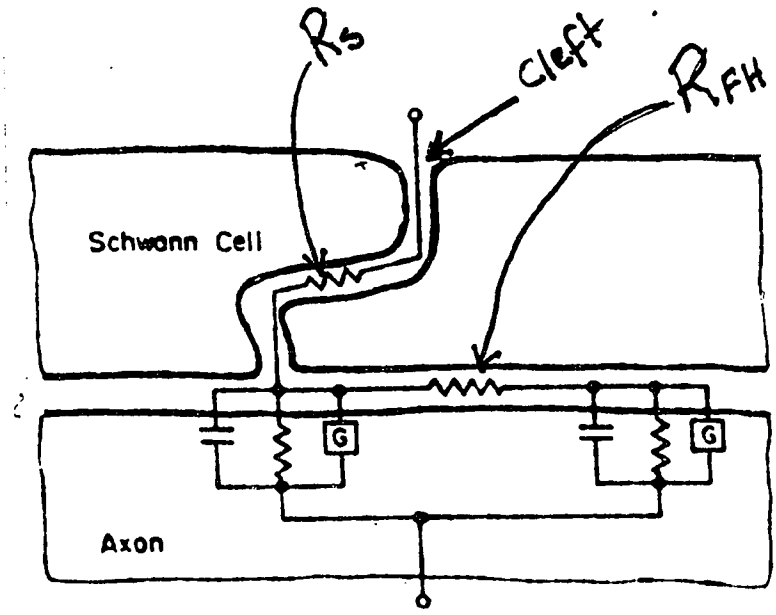

**Figure 4** Changes in series resistance compensation affect gating current, capacity current and clamp rise time.

*Panel A:* Gating currents from the same axon recorded using different levels of $R_s$ compensation. Trace *a*, 10; *b*, 9; *c*, 8; *d*, 7; *e*, 5; *f*, 0 $\Omega.cm^2$. Total gating charge integrated over a 2 ms period was, in trace *a*, 43; *b*, 43; *c*, 44; *d*, 44; *e*, 44 and *f*, 44 $nC/cm^2$. Holding potential was -120 mV; test potential, 0 mV.

*Panel B:* Capacity currents for a 40 mV P/3 control voltage step, recorded at the same $R_s$ compensation levels as in Panel A. Voltage step from -180 to -140 mV; traces labelled as above. The slow capacity current component appears as a plateau at times greater than 60 to 80 µs.

*Panel C:* Integrated fast capacity transients indicate rate of rise of clamp voltage. Slow components were subtracted after integration of the traces from Panel B. Traces were then normalized to facilitate comparison of rates. Errors in maximum charge did not exceed ± 5% prior to normalization. Only traces *a* and *f* are labelled here; intervening traces appear in alphabetical order. Membrane capacitance was calculated as 1.1 $\mu F/cm^2$ in this axon. All data is from axon 871217.

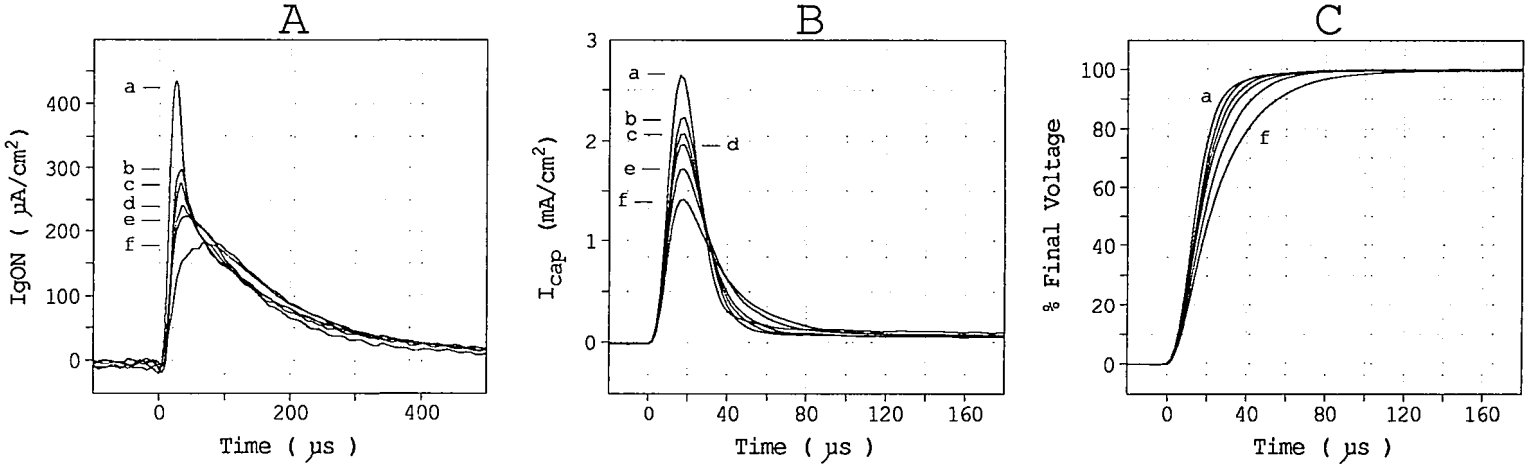

**Figure 5** Absence of kinetic distortion following reduction in sodium current magnitude. Sodium currents were recorded at 0 mV test potential with series resistance compensation set for 10 $\Omega.cm^2$. Reduction in current magnitude (current trace *a*) was achieved in (*A*) by shifting hold from -100 to -85 mV and in (*B*) by lowering external sodium concentration from 50 to 25 mM at a holding potential of -100 mV. Reduced current *a* was scaled (identified as current trace *b*) to permit kinetic comparison with the larger current shown as trace *c*. *(C)* comparison of sodium current kinetics at 0 mV *(a)* and -5 mV *(b)* demonstrates that a 5 mV error from improper series resistance compensation can be readily detected. Currents scaled to the same peak magnitude to illustrate the amount of kinetic distortion that would occur if improper series resistance compensation resulted in an error of 5 mV. *A* and *B*, nonpronased axon 052583: 50 and 25 Na MVH // 230 Cs; *C*, nonpronased axon 042583, 50 Na MVH // 230 Cs 10 Na.

Figure from Starkus, J. G., S. T. Heggeness and M. D. Rayner. 1984. Kinetic analysis of sodium channel block by internal methylene blue in pronased crayfish giant axons. *Biophys. J.* 46:205-218. Figure 1.

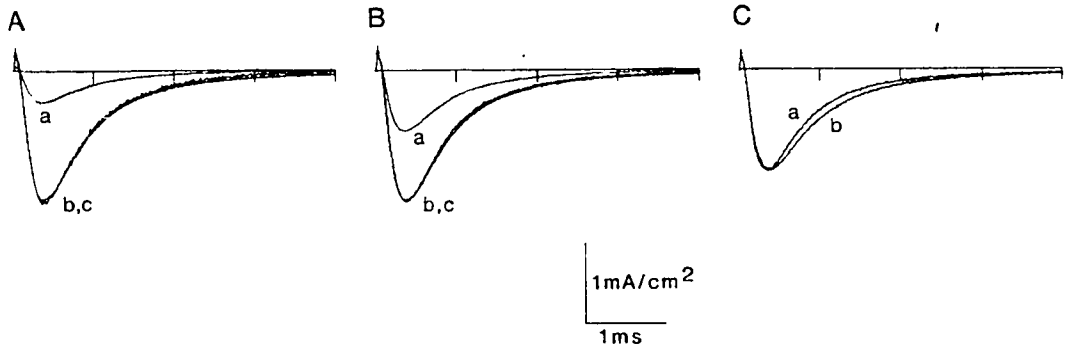

**Figure 6** Invasion artifacts distort ionic current waveform. The inactivation component of $I_{Na}$ is distorted by "notching" as a result of invading current into the space clamp region. The membrane was depolarized to -60 mV. Holding potential was -120 mV. Data from axon 891222, (0 Na // 25 Na).

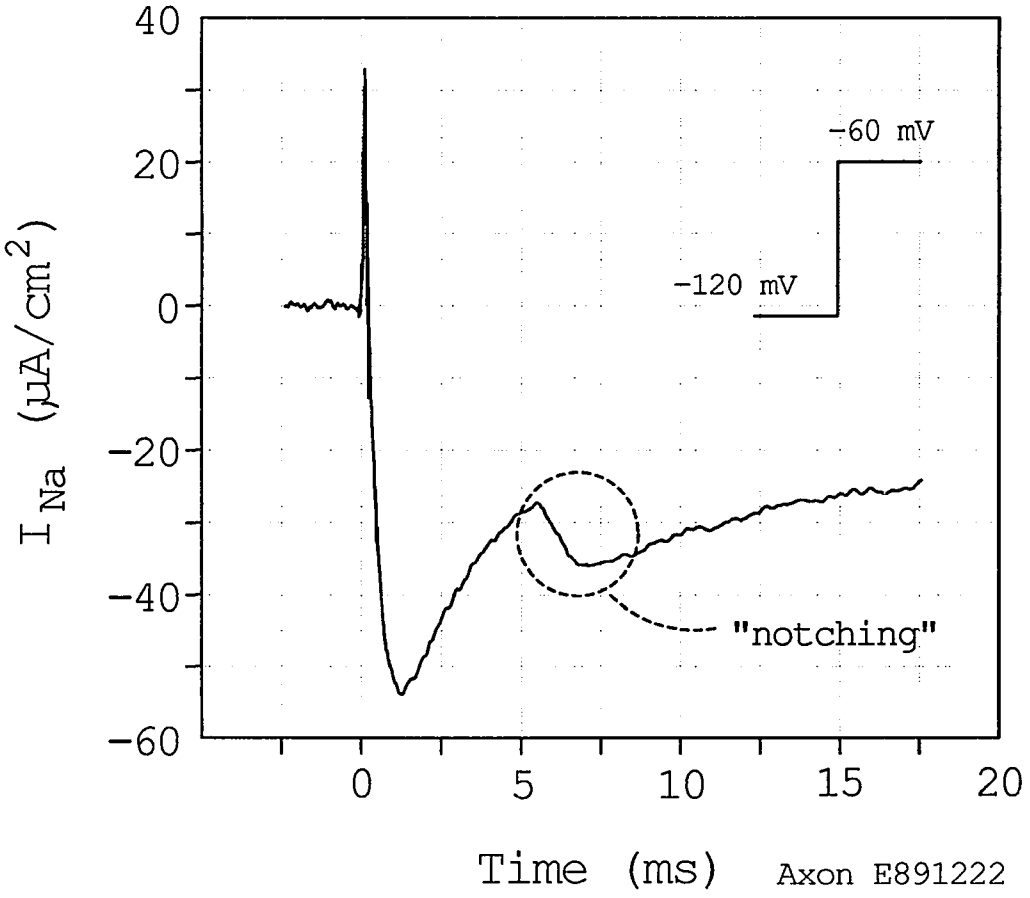

**Figure 7** Direct summation of comparable hyperpolarizing and depolarizing pulses results in complete subtraction of linear capacity and leakage current in crayfish axons. In *A*, membrane currents associated with voltage steps from -200 to -150 mV *(a)* and -150 to -200 mV *(b)*. A slow component of capacity current is identified in these records by the arrow. In *B*, summation of the positive and negative pulses demonstrates the accuracy of the method and linearity of the membrane preparation. Data from axon 022885, (0 Na MVH // 230 TMA).

Figure from Heggeness, S. T., and J. G. Starkus. 1986. Saxitoxin and tetrodotoxin. Electrostatic effects on sodium channel gating current in crayfish axons. *Biophys. J.* 49:629-643. Figure 1.

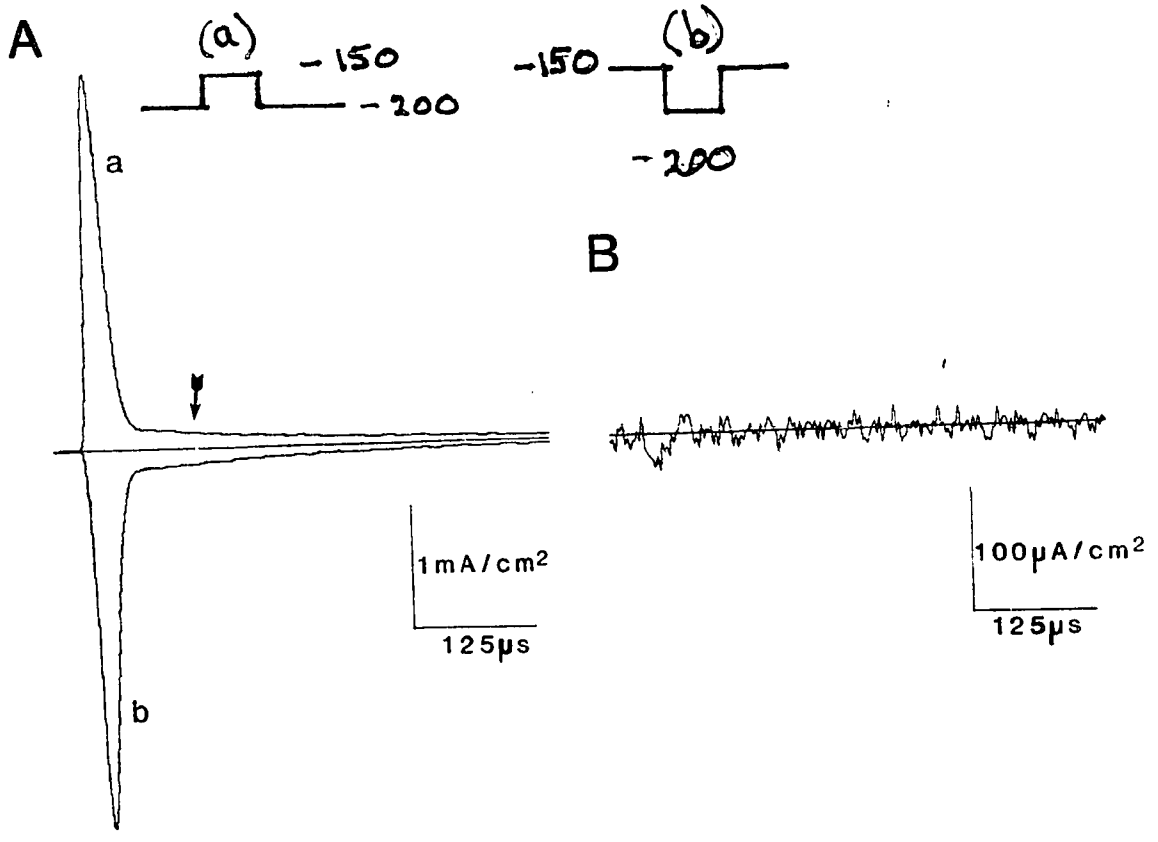

**Figure 8** Signal-averaged capacity currents associated with test depolarizations to 0 mV and control pulses of equal magnitude. *A*, Superimposition of test (P) and control (P/n) capacity currents. *B*, The foot of the falling phase for the capacity current transients. *C*, Asymmetry current obtained by subtracting control current from test current. Data from axon 010881, (0.5 4AP, 1 K // 100 TTX 205 Na), holding potential at -105 mV.

Figure from Starkus, J. G., B. D. Fellmeth, and M. D. Rayner. 1981. Gating currents in the intact crayfish giant axon. *Biophys. J.* 35:521-533. Figure 4.

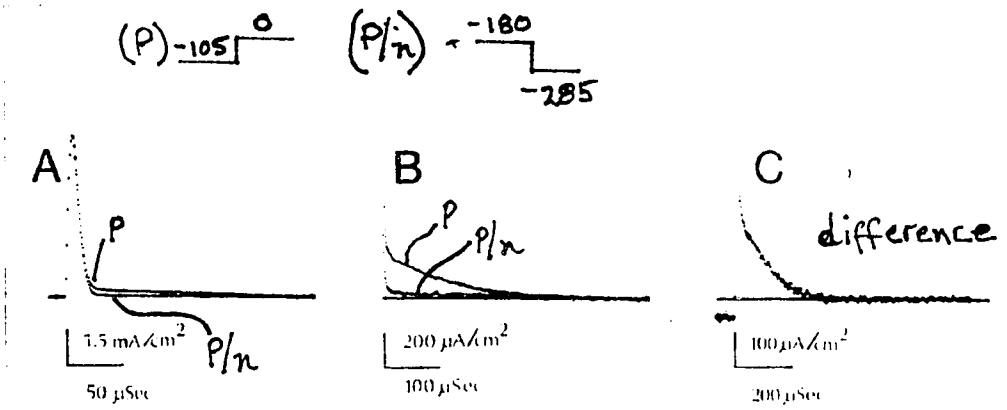

**Figure 9** Molecular structure of delta-9-tetrahydrocannabinol. $C_{21}$ $H_{30}$ $O_2$. M. W. 314.45.

Figure from Razdan, Raj K. 1986. Structure-activity relationships in cannabinoids. *The American Society for Pharmacology and Experimental Therapeutics*. Figure 1.

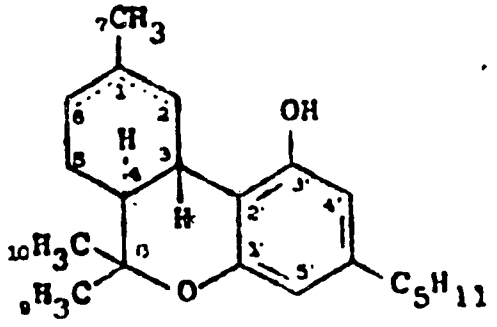

**FIGURE 10** $D_2O$ slows $I_{Na}$ activation without affecting tail current or gating current. (A) Activation (at −20 mV) and deactivation (at −80 mV) of sodium currents before (trace *a*), during (trace *b*), and after (trace *c*) internal $D_2O$ perfusion. Traces in $D_2O$ are scaled to match peak $I_{Na}$ in $H_2O$ for comparison of kinetic changes. Holding potential was −120 mV. Data from axon 890726, ($D_2O$, 20 Na // $H_2O$, 50 Na). (B) ON and OFF gating current at −20 mV before (trace *a*) and during (trace *b*) external $D_2O$ perfusion. Holding potential, −120 mV. Data from axon 881115, (0 Na // $D_2O$, TTX, 0 Na).

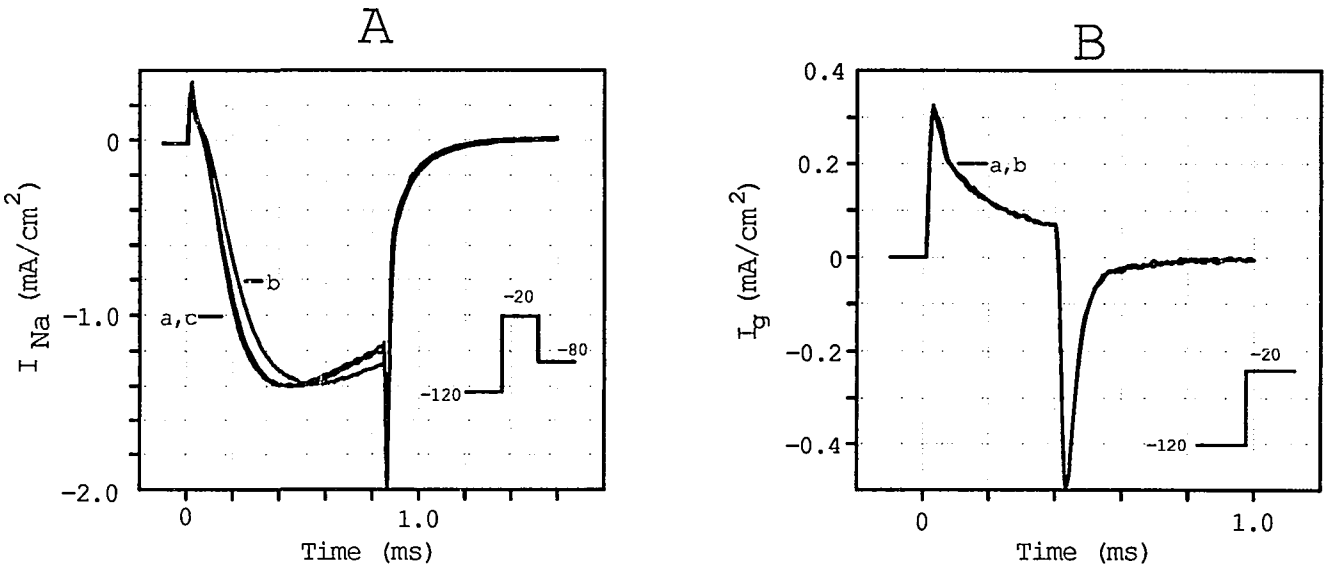

**FIGURE 11** Gating currents are relatively insensitive to $D_2O$. Gating currents and corresponding integrations at 0 mV before (traces *a*) and during (traces *b*) internal (panel A) and external (panel B) $D_2O$ perfusion. Integration of these gating current traces over a 2 ms period gives the following total gating charge movements: panel A, trace *a*, 38; *b*, 37 $nC/cm^2$, and panel B, trace *a*, 31; *b*, 32 $nC/cm^2$. Holding potential, −120 mV. Data represented are from axons 890726, ($D_2O$, 20 Na // TTX, 50 Na), panel A, and 881118, (0 Na // $D_2O$, TTX, 0 Na), panel B.

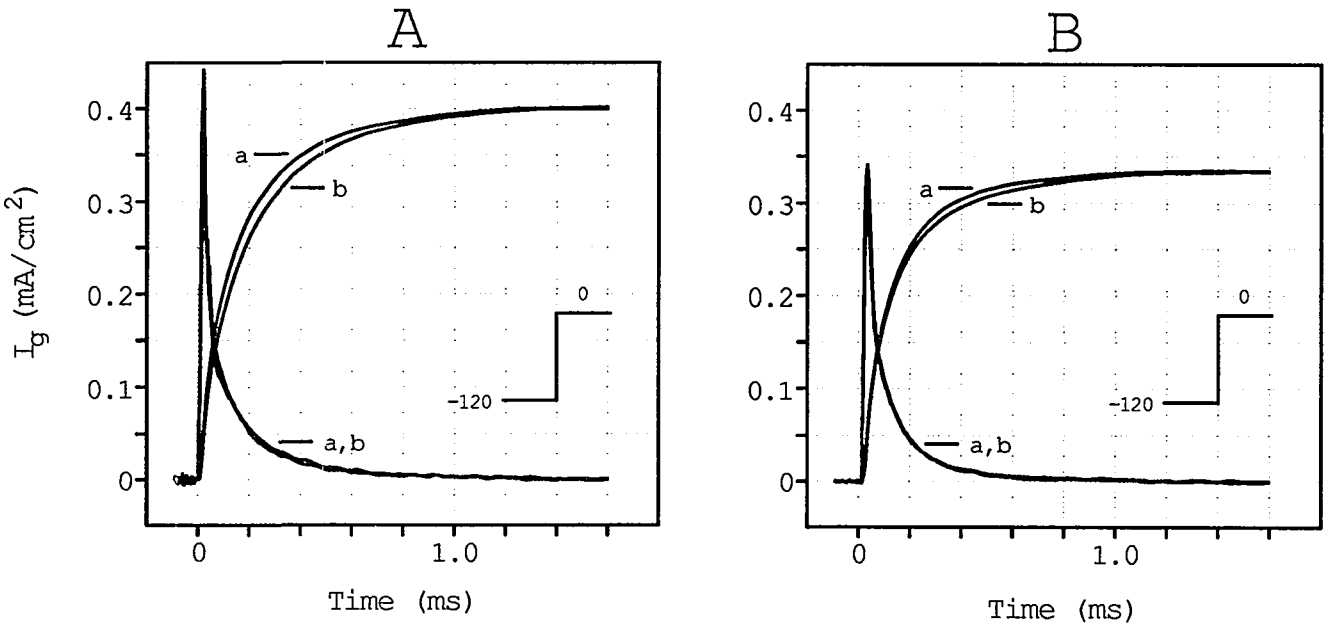

**FIGURE 12** $I_{Na}$ activation and inactivation kinetics are slowed by $D_2O$. Ionic currents before (traces *a*) and during external $D_2O$ perfusion (traces *b*) are compared for voltages of −20 mV (panel A), 0 mV (panel B) and +20 mV (panel C). $D_2O$ records (traces *b*) have been recorded with a higher external sodium concentration and then scaled to account for reduction in peak current magnitude. Holding potential, −120 mV. All data are from axon 881122, (0 Na // 50 Na) in $H_2O$ and (0 Na // $D_2O$, 100 Na) in $D_2O$.

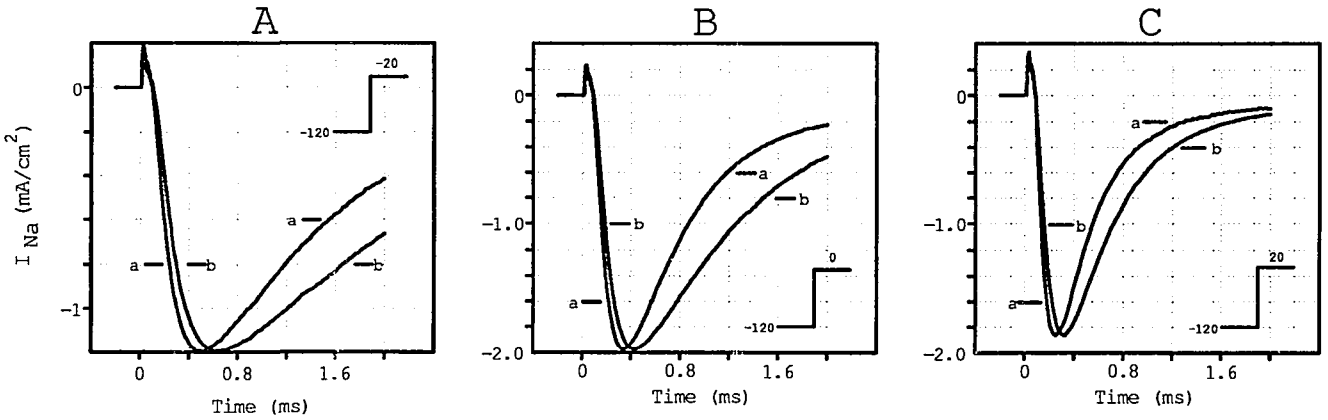

**FIGURE 13** The rates of the fast and slow components of sodium channel tail current are not affected by $D_2O$. Tail currents at −80 mV following a depolarizing pulse of +20 mV for 1 ms are shown before (traces *a*) and during external $D_2O$ perfusion (traces *b*). Data traces correspond to the continuous line of the pulse pattern insert shown in panel A. (A) $D_2O$ trace has been scaled, such that the slow components overlie, to aid visual comparison of the rates. (B) Records from panel A were rescaled to the same peak tail current magnitude to compare the rates of the fast components. Holding potential, −120 mV. All data are from axon 881122, (0 Na // 50 Na) in $H_2O$ and (0 Na // $D_2O$, 100 Na) in $D_2O$.

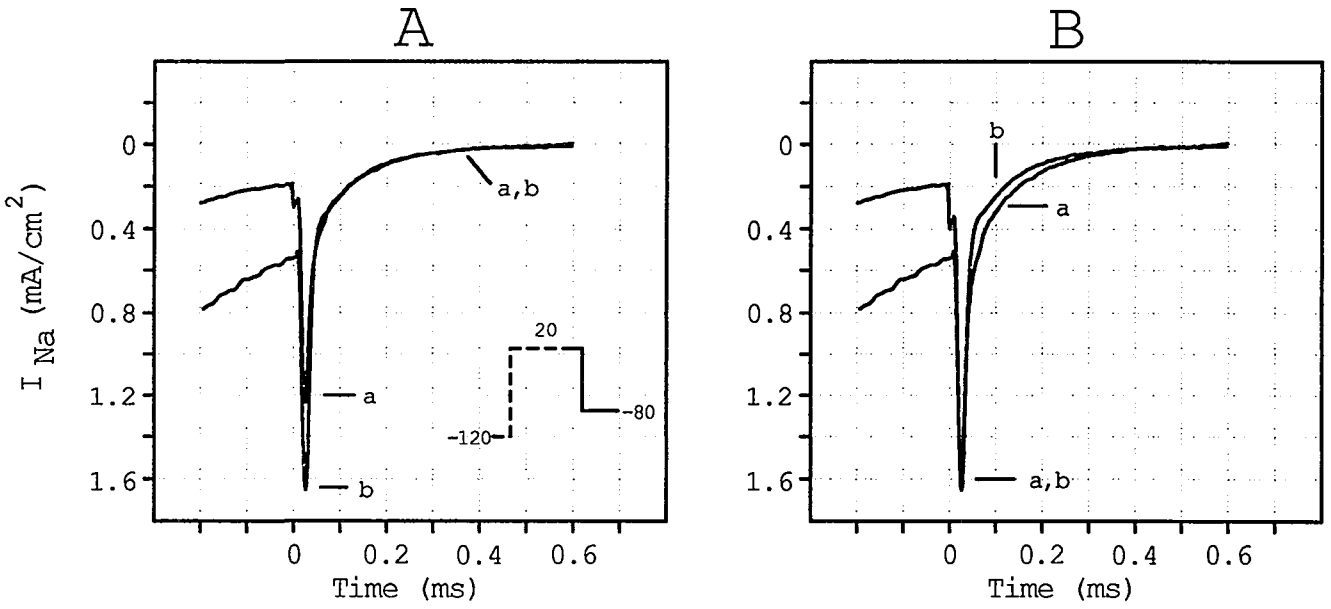

**FIGURE 14** $D_2O$ does not affect the relative magnitude of the prepulse-induced "Cole-Moore-type" shifts in channel activation. (A) Ionic current at 0 mV in $H_2O$ and $D_2O$. Traces were not scaled to illustrate the $D_2O$-induced slowing of activation and inactivation kinetics and the decrease in sodium conductance. Holding potential, −120 mV. Ionic current at 0 mV in $H_2O$ (panel B) and $D_2O$ (panel C) following a single pulse (traces *a*) and a 5 ms prepulse to −65 mV (traces *b*). Current records resulting from the prepulse (traces *b*) were scaled to peak current magnitude of the single pulse record (traces *a*) for comparison of the "Cole-Moore-type" shifts in channel activation. The "Cole-Moore-type" shifts are 20 μs for $H_2O$ in (B) and 32 μs for $D_2O$ in (C), but the ratio $\Delta t_{1/2} / t_{1/2}$ (single pulse) is not altered by solvent substitution (see Table 4). All data are from axon 880928b, (20 Na // 80 Na) in $H_2O$ and (20 Na // $D_2O$, 100 Na) in $D_2O$.

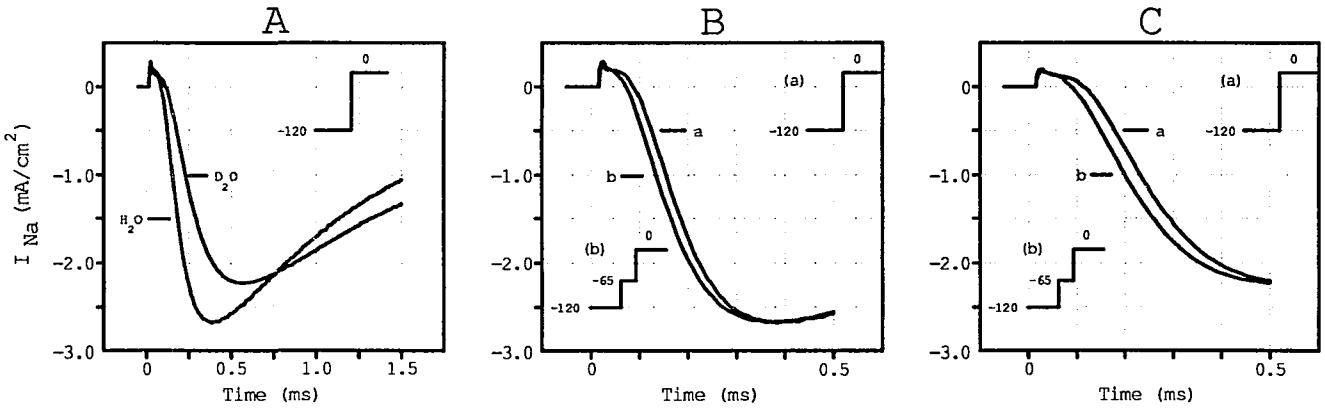

**FIGURE 15** $D_2O$ slows sodium channel activation kinetics after removal of fast inactivation by 10 mM chloramine-T. Ionic current with inactivation intact at 0 mV before (trace *a*) and during internal $D_2O$ perfusion (trace *b*). Holding potential, −120 mV. Ionic current at 0 mV before (trace *c*) and during internal $D_2O$ perfusion (trace *d*) after < 90% of fast inactivation was removed by prior treatment with 10 mM chloramine-T. Holding potential, −90 mV. All records were scaled to approximately 1 mA/cm$^2$ current magnitude for comparison of activation kinetics. All data from axon 890608, ($D_2O$, 20 Na // 75 Na).

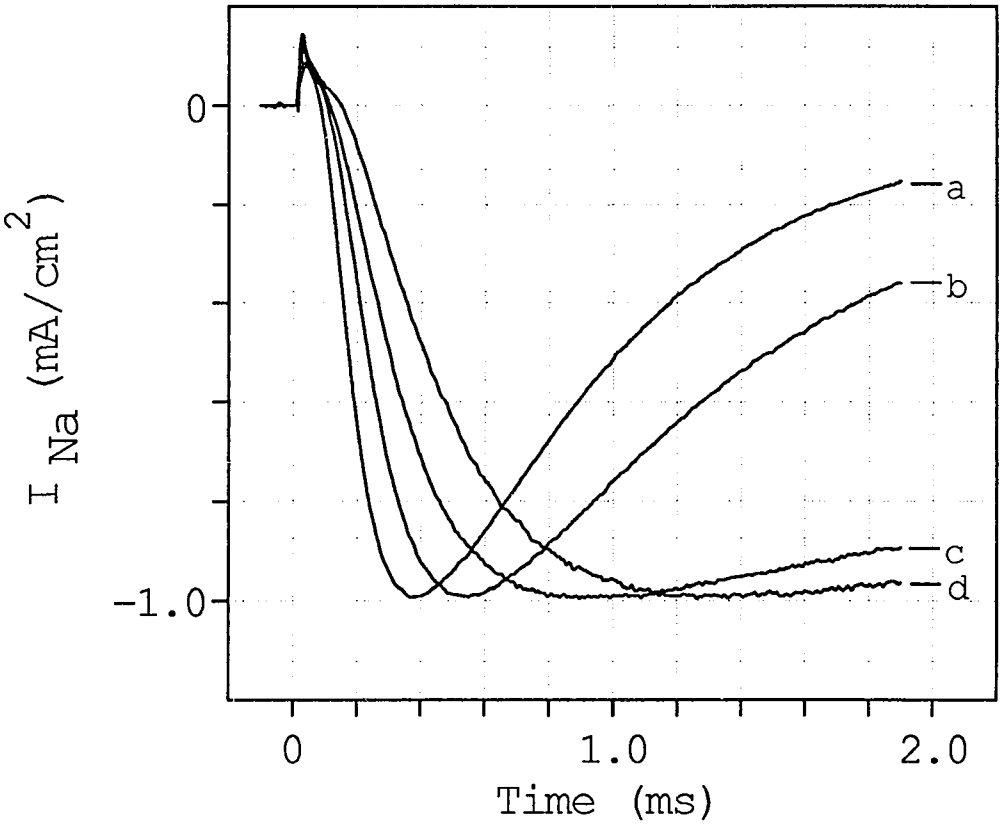

**FIGURE 16** Double pulse protocol (Oxford, 1981) reveals a component of activation which turns on very rapidly with almost monoexponential kinetics. (A) Ionic current at 0 mV following a control single pulse (trace *a*) and a double pulse interrupted by a 50 μs return to holding potential (trace *b*). (B) Ionic current at 0 mV following a control single pulse (trace *a*) and a double pulse interrupted by a 400 μs interpulse interval (trace *b*). For comparison of activation kinetics the single pulse (traces *a*, A and B) is superimposed on the $I_{Na}$ record associated with the second pulse of a double pulse protocol (traces *b*, A and B). See pulse insert. Holding potential, −90 mV. Records were obtained following treatment with 10 mM chloramine-T. All data from axon 890608, ($D_2O$, 20 Na // 75 Na).

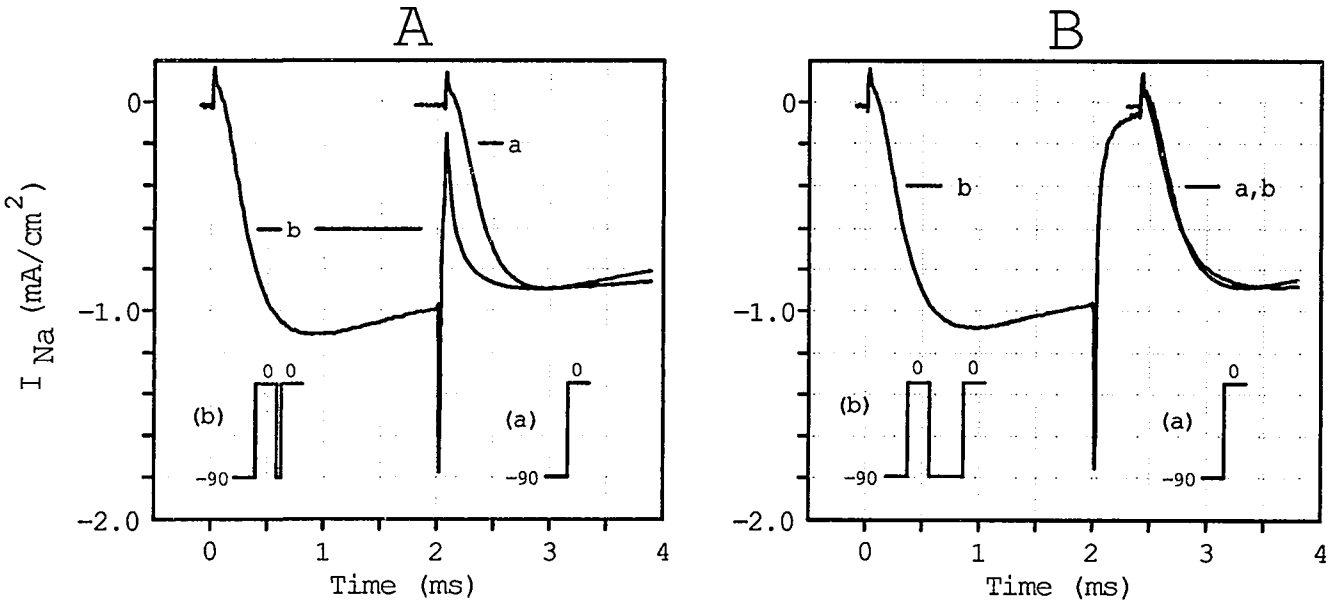

**FIGURE 17** secondary activation is insensitive to the slowing effects of $D_2O$. Ionic current at 0 mV before and during internal $D_2O$ perfusion are shown following a double pulse protocol with interpulse intervals of 50 μs (panel A) and 400 μs (panel B). Traces in $H_2O$ and $D_2O$ are superimposed in Panels A and B to facilitate comparison of activation kinetics. Holding potential, –90 mV. Records were obtained following treatment with 10 mM chloramine-T. All data from axon 890608, ($D_2O$, 20 Na // 75 Na).

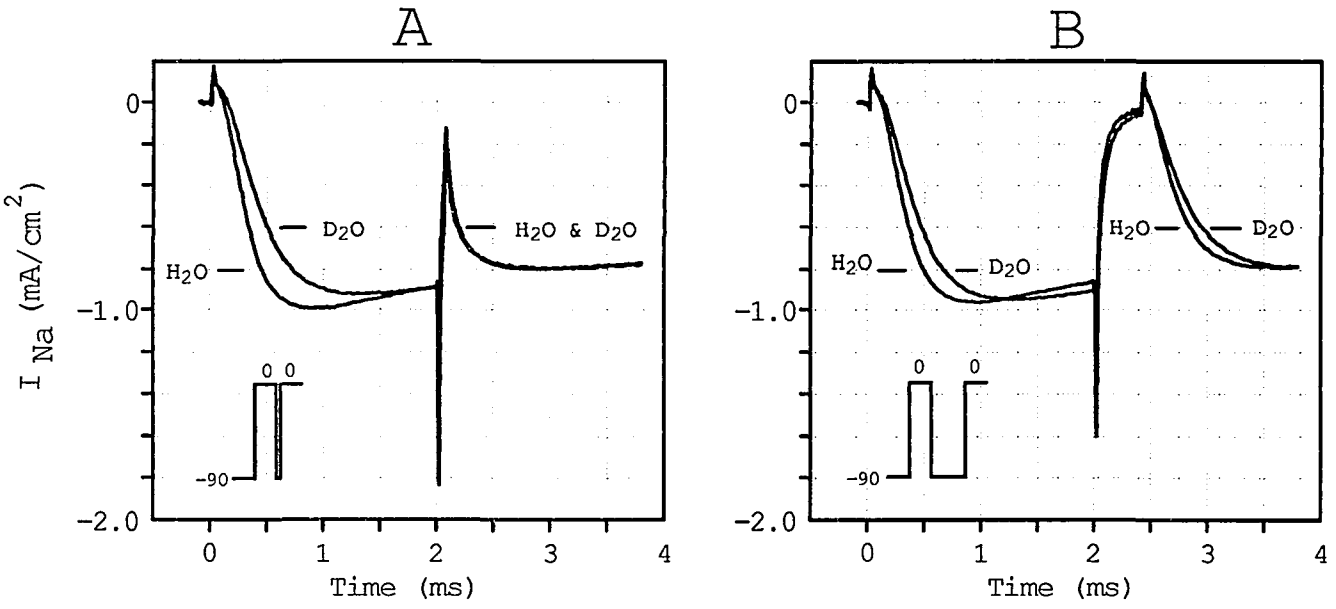

**Figure 18** $I_{Na}$ activation and inactivation kinetics are slowed by THC. Ionic currents before (traces *a*) and after internal (1 mM) THC perfusion (traces *b*) are compared for voltages of -20 mV (*A*), 0 mV (*B*), and +20 mV (*C*). THC records (traces *b*) have been recorded with a higher external sodium concentration and then scaled to account for reduction in peak current magnitude. Holding potential, -120 mV. All data are from axon 900105b, (0 Na // 100 Na) in control and (0 Na // 1 THC, 200 Na) in THC.

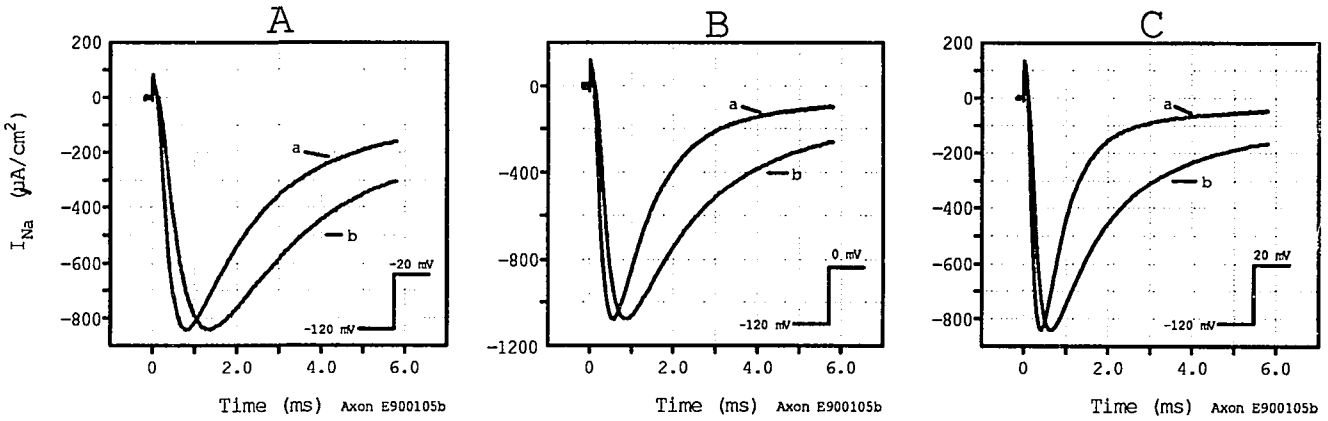

**Figure 19** THC exposure produces no obvious shift in voltage dependence. (*A*) Peak inward current before (open circles) and after (solid circles) THC perfusion. Peak inward current is reduced by THC, and the maximum occurs at 0 mV for both control and THC curves. (*B*) Peak sodium conductance before (open circles) and after (solid circles) THC perfusion. The THC curve has been rescaled to coincide with the control curve. (*C*) Slope factors before (open circles) and after THC perfusion (solid circles) measured as the natural log (ln) of the $t_{1/2}$-activation versus the membrane potential. Holding potential, -120 mV. Data presented in panels *A* and *B* are from axon 900105b, (0 Na // 100 Na) in control and (0 Na // 1 THC, 200 Na) in THC. Data in panel *C* from axon 900104, (0 Na // 50 Na) in control and (0 Na // 1 THC, 200 Na) in THC.

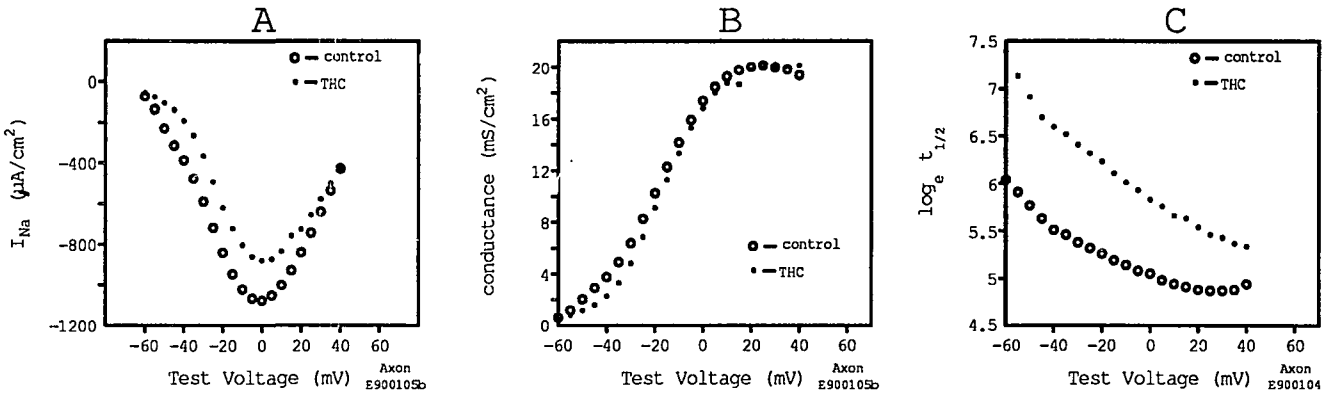

**Figure 20** Gating currents are sensitive to THC. Panel *A* ON gating currents and corresponding integrations at 0 mV before (traces *a*) and after (traces *b*) THC perfusion. Panel *B* OFF gating currents and corresponding integrations at 0 mV before (traces *a*) and after (traces *b*) THC perfusion. Gating current records after THC exposure (traces *b* in panels *A* and *B*) have been scaled to control (traces *a*) by matching the peak amplitudes of the integration records. Integration of these gating current traces over a 4-ms period gives the following total gating charge movements: (*A*) trace *a*, 27; *b*, 20 nC/cm$^2$, (*B*) trace *a*, 19; *b*, 9 nC/cm$^2$. Panel *C* $Q_{ON}(V_m)$ curves before (open circles) and after (solid circles) THC exposure. Holding potential, -120 mV. Data represented are from axons 900131, (0 Na // 0 Na, TTX) in control and (0 Na // 0 Na, 0.5 THC, TTX) in THC, panels *A* and *B*, and axon 900126 (0 Na // 0 Na, STX) in control and (0 Na // 0 Na, 0.1 THC, STX) in THC, panel *C*.

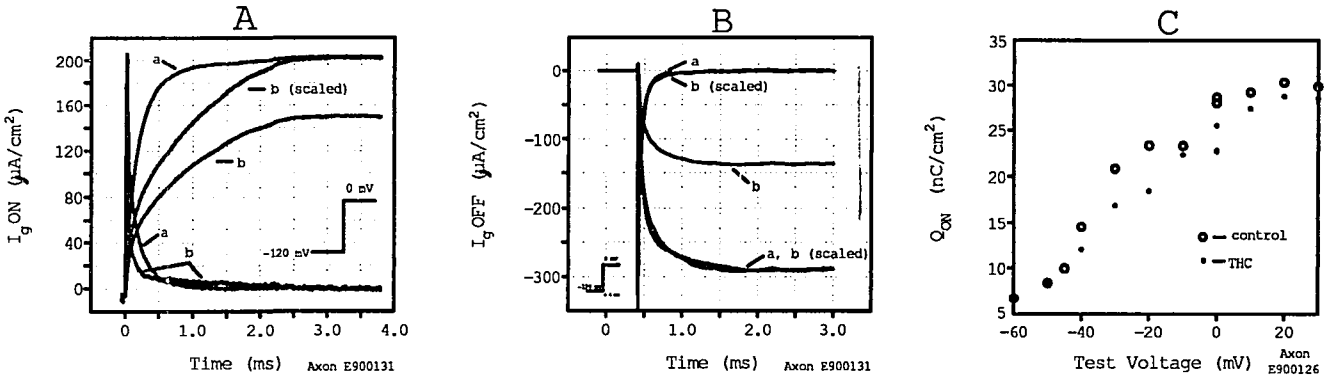

**Figure 21** The rates of the fast and slow components of sodium channel tail current are differentially affected by THC. Tail currents at -80 mV after a depolarizing pulse of 0 mV for 3 ms are shown before (traces *a*) and after THC perfusion (traces *b*). Data traces correspond to the continuous line of the pulse pattern insert shown in each panel. (*A*) Records were scaled to the same peak tail current magnitude to compare the rates of the fast components. (*B*) THC trace has been scaled, in an attempt to overlie the slow components, to aid visual comparison of the rates. Holding potential, -120 mV. Records were obtained after treatment with 10 mM chloramine-T. All data are from axon 900130, (0 Na // 50 Na) in control and (0 Na // 100 Na, 0.5 THC) in THC.

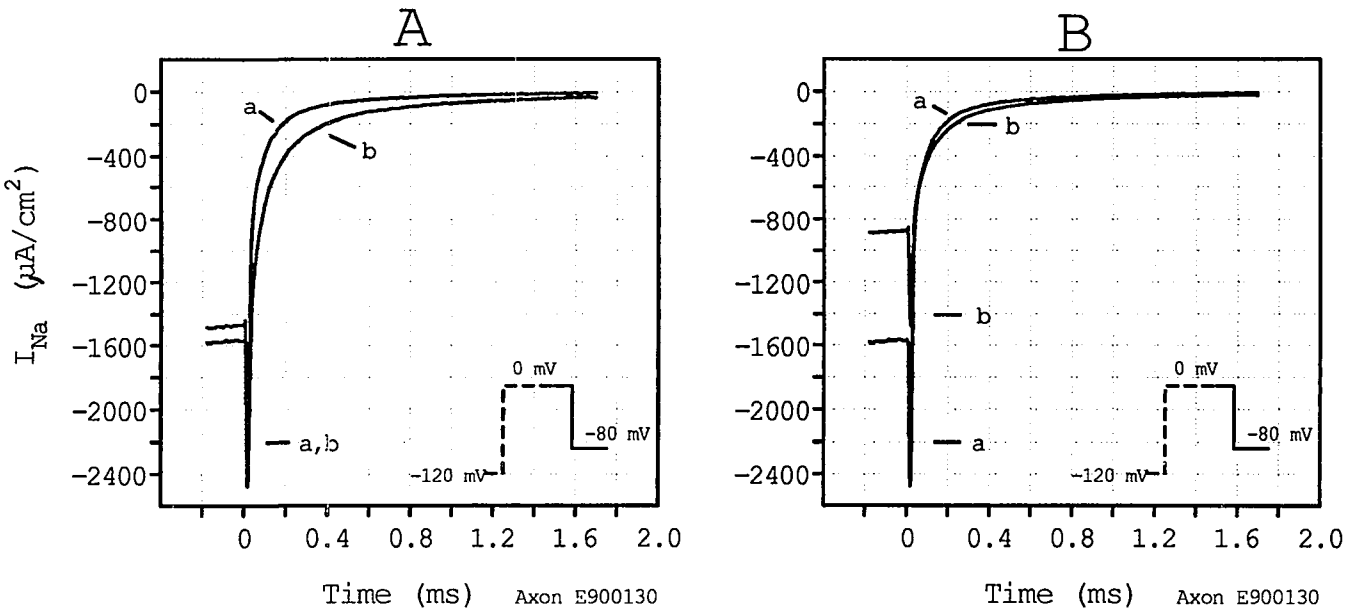

**Figure 22** Is secondary activation affected by THC? Ionic current at -20 mV before and after internal THC perfusion are shown after a double-pulse protocol with interpulse intervals of 50 µs (*A* and *B*) and 400 µs (*C*). Traces in control and THC are superimposed in *A*, *B* and *C* to facilitate comparison of activation kinetics. *B* Records from *A* are rescaled to permit comparison of the rates of secondary activation. Data traces in *B* correspond to the continuous line of the pulse pattern shown in the insert. Holding potential, -120 mV. Records were obtained after treatment with 5 mM chloramine-T. All data from axon 900117, (0 Na // 50 Na) in control and (0 Na // 50 Na, 1 THC) in THC.

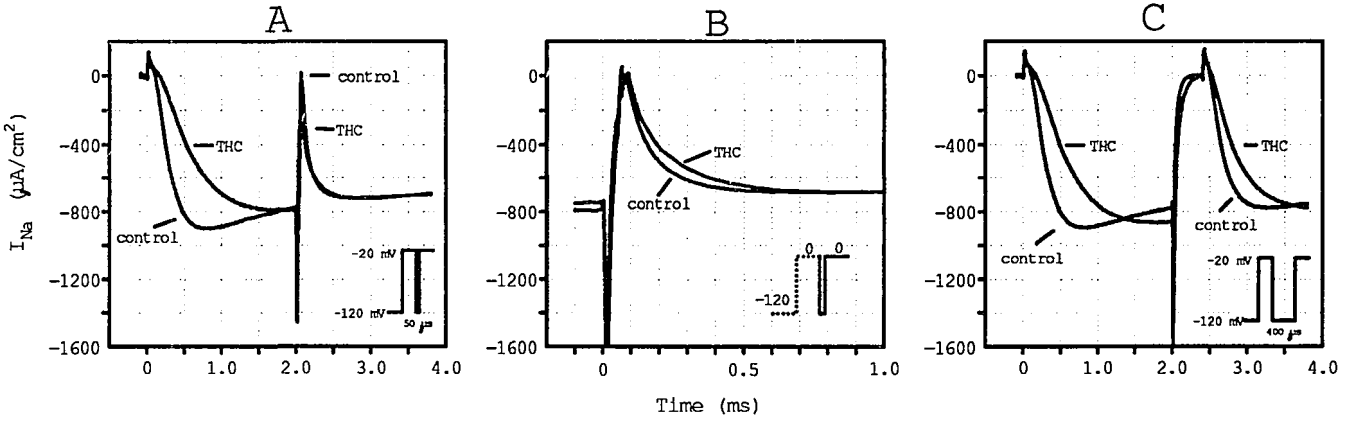

# REFERENCES

Adelman, W. J., J. Moses and R. V. Rice. 1977. An anatomical basis for the resistance in series with the excitable membrane of the squid axon. *J. Neurocytol.* 6:621-646.

Aldrich, R. W., and C. F. Stevens. 1984. Inactivation of open and closed sodium channels determined separately. *Cold Spring Harbor Symp. Quant. Biol.* 48:147-154.

Alicata, D. A., M. D. Rayner, and J. G. Starkus. 1989. Osmotic and pharmacological effects of formamide on capacity current, gating current, and sodium current in crayfish giant axons. *Biophys. J.* 55:347-353.

Alicata, D. A., M. D. Rayner, and J. G. Starkus. 1990. Sodium channel activation mechanisms: Insights from deuterium oxide substitution. *Biophys. J.* 57:745-758.

Almers, W. 1978. Gating currents and charge movements in excitable membranes. *Rev. Physiol. Biochem. Pharmacol.* 82:96-190.

Armstrong, C. M. 1981. Sodium channels and gating currents. *Physiol. Rev.* 61:644-683.

Armstrong, C. M., F. Bezanilla, and E. Rojas. 1973. Destruction of sodium conductance inactivation in squid axons perfused with pronase. *J. Gen. Physiol.* 62:375-391.

Armstrong, C. M., and F. Bezanilla. 1973. Currents related to the movement of gating particles of the sodium channels. *Nature (Lond.).* 242:459-461.

Armstrong, C. M., and F. Bezanilla. 1974. Charge movement associated with the opening and closing of the activation gates of the Na channels. *J. Gen. Physiol.* 63:533-552.

Armstrong, C.M., and F. Bezanilla. 1975. Currents associated with the ionic gating structures in nerve membrane. *Ann. N.Y. Acad. Sci.* 264:265-277.

Armstrong, C.M., and F. Bezanilla. 1977. Inactivation of the sodium channel II: Gating current experiments. *J. Gen. Physiol.* 70:567-590.

Armstrong, C. M., and L. Binstock. 1965. Anomalous rectification in the squid giant axon injected with tetraethylammonium chloride. *J. Gen. Physiol.* 48-859-872.

Armstrong, C. M., and W. F. Gilly. 1979. Fast and slow steps in the activation of sodium channels. *J. Gen. Physiol.* 74:691-711.

Auld, V, J. Marshall, A. Goldin, A. Dowsett, W. Catteral, N. Davidson, and R. Dunn. 1985. Cloning and characterization of the gene for alpha-subunit of the mammalian voltage-gated sodium channel. *Journal of General Physiology.* 86 (6):10A-11A.

Barchi, R. L. 1983. Protein components of the purified sodium channel from rat skeletal muscle sarcolemma. *J. Neurochem.* 40:1377-1385.

Bekkers, J. M., N. G. Greeff, R. D. Keynes, and B. Neumcke. 1984. The effect of local anaesthetics on the components of the asymmetry current in the squid giant axon. *J. Physiol. (Lond.).* 352:653-668.

Bezanilla, F. 1982. Gating charge movements and kinetics of excitable membrane proteins. *Proteins in the Nervous System: Structure and Function.* Alan R. Liss, Inc., 150 Fifth Avenue, New York, NY 10011. p. 3-16.

Bezanilla, F., and C. M. Armstrong. 1975a. Kinetic properties and inactivation of the currents of sodium channels in squid axons. *Philos. Trans. R. Soc. Lond. B Biol. Sci.* 270:449-458.

Bezanilla, F., and C. M. Armstrong. 1975b. Properties of the sodium channel gating current. *Cold Spring Harbor Symposia in Quant. Biol.* 40:297-304.

Bezanilla, F., and C. M. Armstrong. 1977. Inactivation of the sodium channel I. Sodium current experiments. *J. Gen. Physiol.* 70:549-566.

Bezanilla, F., R. E. Taylor and J. M. Fernandez. 1982. Distribution and kinetics of membrane dielectric polarization. 1. Long-term inactivation of gating currents. *J. Gen. Physiol.* 79:21-40.

Brady, R. O., and E. Carbone. 1973. Comparison of the effects of delta-9-tetrahydrocannabinol, 11-hydroxy-delta-9-tetrahydrocannabinol, and ethanol on the electrophysiological activity of the giant axon of the squid. *Neuropharmacology.* 12:601-605.

Briggs, G. E. 1930. The accumulation of electrolytes in plant cells-a suggested mechanism. *Proc. Roy. Soc. B.* 107:248-269.

Byck, R. and J. M. Ritchie. 1973. Delta-9-tetrahydrocannabinol: Effects on mammalian nonmyelinated nerve fibers. *Science (Washington).* 180:84-85.

Bullock, J. O., and C. L. Schauf. 1978. Combined voltage-clamp and dialysis of *Myxicola* axons: behavior of membrane asymmetry currents. *J. Physiol. (Lond)* 278:309-324.

Cahalan, M. D. 1975. Modification of sodium channel gating in frog myelinated nerve fibers by *Centruroides sculpturatus* scorpion venom. *J. Physiol. (Lond.)* 244:511-534.

Catterall, W. A. 1980. Neurotoxins that act on voltage-sensitive sodium channels in excitable membranes. *Annu. Rev. Pharmacol. Toxicol.* 20:15-43.

Catterall, W. A. 1986. Voltage-dependent gating of sodium channels: correlating structure and function. *TINS.* 9:7-10.

Cole, K. S. 1949. Dynamic electrical characteristics of the squid axon membrane. *Arch. Sci. Physiol.* 3:253.

Cole, K. S. 1968. *Membrane, Ions and Impulses*. Berkeley California: University of California Press.

Conti, F. 1986. The relationship between electrophysiological data and thermodynamics of ion channel conformations. *Neurol. Neurobiol.* 20:25-41.

Conti, F., and W. Stühmer. 1989. Quantal charge redistributions accompanying the structural transitions of sodium channels. *Eur. Biophys. J.* 17:53-59.

Cota, G. and C. M. Armstrong. 1989. Sodium channel gating in clonal pituitary cells the inactivation step is not voltage dependent. *J. Gen. Physiol.* 94:213-232.

Dodge, F. A. and B. Frankenhaeuser. 1959. Sodium currents in the myelinated nerve fiber of *Zenopus laevis* investigated with the voltage clamp technique. *J. Physiol. (Lond)* 148:188-200.

Fishman, H. M. 1973. Low impedance capillary electrode for wide band recording of membrane potential in large axons. *IEEE Trans. Bio-Med. Eng.* BME-20:380.

Frankenhaeuser, B., and A. L. Hodgkin. 1956. The after-effects of impulses in the giant nerve fibers of *Loligo*. *J. Physiol. (Lond.)* 131:341-376.

French, Robert J., and Richard Horn. 1983. Sodium channel gating: models, mimics, and modifiers. *Ann. Rev. Biophys. Bioeng.* 12:319-356.

Gillespie, J. I. and H. Meves. 1980. The time course of sodium inactivation in squid giant axons. *J. Physiol.(Lond.)* 299:289-307.

Gilly, W. F., R. P. Swenson, and C. M. Armstrong. 1981. Sodium channel activation in pronased squid axons: the slow last step. *Proc. VII Int. Biophys. Congress. Mexico City.* 330.

Goldman, D. E. 1943. Potential, impedance, and rectification in membranes. *J. Gen. Physiol.* 27:37-60.

Goldman, L. 1976. Kinetics of channel gating in excitable membranes. *Q. Rev. Biophys.* 9:491-526.

Goldman, L., and J. L. Kenyon. 1982. Delays in inactivation development and activation kinetics in *Myxicola* giant axons. *J. Gen. Physiol.* 80:83-102.

Goldman, L., and C. L. Schauf. 1972. Inactivation of the sodium current in *Myxicola* giant axons. Evidence of coupling to the activation process. *J. Gen. Physiol.* 59:659-675.

Greeff, N. G., R. D. Keynes, and D. F. VanHelden. 1982. Fractionation of the asymmetry current in the squid giant axon into inactivating and non-inactivating components. *Proceedings of the Royal Society of London, Series B.* 215:375-389.

Greenblatt, R. E., Y. Blatt, and M. Montal. 1985. The structure of the voltage-sensitive sodium channel. Inferences derived from computer-aided analysis of the *Electrophorus electricus* channel primary structure. *Federation of Experimental Biology Society Letters*. 193:125-134.

Guy, H. R., and Seetharamulu, P. 1986. Molecular model of the action potential sodium channel. *Proc. Natl. Acad. Sci. USA*. 83:508:512.

Hagiwara, S., and N. Saito. 1959. Voltage-current relations in nerve cell membrane of *Onchidium verruculatum*. *J. Physiol. (Lond.)* 148:161-179.

Hahin, Richard. 1988. Removal of inactivation causes time-invariant sodium current decays. *J. Gen. Physiol.* 92:331-350.

Hahin, R., and L. Goldman. 1978. Initial conditions and the kinetics of the sodium conductance in *Myxicola* giant axons. I. Effects on the time course of the sodium conductance. *J. Gen. Physiol.* 72:863-878.

Hamill, O. P., and F. Sakmann. 1981. A cell-free method for recording single channel currents from biological membranes. *J. Physiol. (Lond.)*. 312:41-42P.

Hille, B. 1984. Ionic channels of excitable membranes. Sinauer Associates, Inc., Sunderland, Mass. 01375.

Hodgkin, A. L., A. F. Huxley, and B. Katz. 1952. Measurement of current-voltage relations in the membrane of the giant axon of *Loligo*. *J. Physiol. (Lond.)*. 116:424-448.

Hodgkin, A. L., and A. F. Huxley. 1952a. Currents carried by sodium and potassium ions through the membrane of the giant axon of *Loligo*. *J. Physiol. (Lond.)*. 116:449-472.

Hodgkin, A. L., and A. F. Huxley. 1952b. The components of membrane conductance in the giant axon of *Loligo*. *J. Physiol. (Lond.)*. 116:473-496.

Hodgkin, A. L., and A. F. Huxley. 1952c. The dual effect of membrane potential on sodium conductance in the giant axon of *Loligo*. *J. Physiol. (Lond.)*. 116:497-506.

Hodgkin, A. L., and A. F. Huxley. 1952d. A quantitative description of membrane current and its application to conductance and excitation in nerve. *J. Physiol. (Lond.)*. 117:500-544.

Hodgkin, A. L., and B. Katz. 1949. The effect of sodium ions on the electrical activity of the giant axon of the squid. *J. Physiol. (Lond.)* 108:37-77.

Horn, R. and S. J. Korn. 1989. Model selection: reliability and bias. *Biophys. J.* 55:379-381.

Horn, R. and J. B. Patlak. 1980. Single channel currents from excised patches of muscle membrane. *Proc. Natl. Acad. Sci. USA*. 77:6930-6934.

Horn, R., J. Patlak and C. F. Stevens. 1981. Sodium channels need not open before they inactivate. *Nature (Lond.)* 291:426-427.

Horn, R., and C. A. Vandenberg. 1984. Statistical properties of single sodium channels. *J. Gen. Physiol.* 84:505-534.

Huang, J. M., J. Tanguy, and J. Z. Yeh. 1987. Removal of sodium inactivation and block of sodium channels by chloramine-T in crayfish and squid giant axons. *Biophys. J.* 52:155-163.

Iverson, L. E., M. A. Tanouye, H. A. lester, N. Davidson, and B. Rudy. 1988. A-type potassium channels expressed from Shaker locus cDNA. *Proceedings of the National Academy of Sciences*. 85:5723-5727.

Julian, F. J., J. W. Moore and D. E. Goldman. 1962. Current-voltage relations in the lobster giant axon membrane under voltage clamp conditions. *J. Gen. Physiol.* 45:1217-1238.

Kayano, T., M. Noda, V. Flockerzi, H. Takahashi, and S. Numa. 1988. Primary structure of rat brain sodium channel III deduced from the cDNA sequence. *Federation of Experimental Biology Society Letters*. 228:187-194.

Keynes, R. D. 1983. The Croonian Lecture. Voltage gated ion channels in the nerve membrane. *Proc. R. Soc. Lond. B.* 220-1-30.

Keynes, R. D. 1985. Sodium channels from squid to electric eel *Electrophorus-Electricus. Anais Da Academia Brasileira De Ciencias.* 57:239-248.

Keynes, R. D. 1986. Properties of the sodium gating current in the squid giant axon. *Ann. N. Y. Acad. Sci.* 479:431-438.

Keynes, R. D., and E. Rojas. 1973. Characteristics of the sodium gating current in the squid giant axon. *J. Physiol. (Lond.)* 233:28P-30P.

Keynes, R. D., and E. Rojas. 1974. Kinetics and steady state properties of the charged system controlling sodium conductance in the squid giant axon. *J. Physiol. (Lond).* 239:393-434.

Liebovitch, L. S. 1989. Testing fractal and Markov models of ion channel kinetics. *Biophys. J.* 55:373-377.

Keynes, R. D., and E. Rojas. 1976. The temporal and steady state relationships between activation of the sodium conductance and movement of the gating particles in the squid giant axon. *J. Physiol. (Lond.)* 255:157-189.

Levis, R. 1979. Temporal control of potential in a giant axon voltage clamp. *Biophys. J.* 25:306a.

Kraner, S. D., J. C. Tanaka, and R. L. Barchi. 1985 Purification and functional reconstruction of the voltage-sensitive sodium channel from rabbit t-tubular membranes. *J. Biol. Chem.* 260:6341-6347.

MacKinnon, R., P. H. Reinhart, and M. M. White. 1988. Charybdotoxin block of Shaker $K^+$ channel suggests that different types of $K^+$ share common structural features. *Neuron.* 1:997-1001.

Marmont, G. 1949. Studies on the axon membrane. *J. cell. comp. Physiol.* 34:351-382.

McManus, O. B., C. E. Spivak, A. L. Blatz, D. S. Weiss, and K. L. Magleby. 1989. Fractal models, Markov models, and channel kinetics. *Biophys. J.* 55:383-385.

Messner D. J., and W. A. Catterall. 1985. The sodium channel from rat brain separation and characterization of subunits. *J. Biol. Chem.* 260:10597-10604.

Meves, H. 1974. The effect of holding potential on the asymmetry currents in squid giant axons. *J. Physiol. (Lond)* 243:847-867.

Meves, H. 1978. Inactivation of the sodium permeability in squid giant nerve fibers. *Prog. Biophys. Mol. Biol.* 33:207-230.

Meves, H., and W. Vogel. 1977a. Inactivation of the asymmetrical displacement current in giant axons of *Loligo forbesi*. *J. Physiol. (Lond.).* 267:377-393.

Meves, H., and W. Vogel. 1977b. Slow recovery of sodium current and gating current from inactivation. *J. Physiol. (Lond.).* 267:395-410.

Miller, J. A., W. S. Agnew and S. R. Levinson. 1983. Principal glycopeptide of the tetrodotoxin/saxitoxin binding protein from *Electrophorus electricus*: Isolation and partial chemical and physical characterization. *Biochemistry* 22:462-470.

Moore, J. W., and W. J. Adelman Jr. 1961. Electronic measurement of the intracellular concentration and net flux of sodium in the squid axon. *J. Gen. Physiol.* 45:77-92.

Moore, J. W., and K. S. Cole. 1963. Voltage clamp techniques. *Physical Techniques in Biological Research.* ed. W. L. Nastuk, Academic Press, New York. p. 263-321.

Moore, J. W., and T. Narahashi. 1967. Tetrodotoxin's highly selective blockage of an ionic channel. *Fed. Proc.* 26:1655-1663.

Mozhayeva, G. N., A. P. Naumov, Y. A. Negulyaev, and E. D. Nosyreva. 1977. Permeability of aconitine-modified sodium channels to univalent cations in myelinated nerve. *Biochim. Biophys. Acta* 466:461-473.

Mullins, L. J., and K. Noda. 1963. The influence of sodium-free solutions on the membrane potential of frog muscle fibers. *J. Gen. Physiol.* 47:117-132.

Narahashi, T., J. W. Moore, and W. R. Scott. 1964. Tetrodotoxin blockage of sodium conductance increase in lobster giant axons. *J. Gen. Physiol.* 47:965-974.

Neher, E. 1971. Two fast transient current components during voltage clamp on snail neurons. *Journal of General Physiology.* 58:36-53.

Neher, E. 1981. Unit conductance studies in biological membranes. In: Baker P. F. (ed), Techniques in cellular physiology. Elseveir/NorthHolland, Amsterdam.

Neher, E., and B. Sakmann. 1976. Single channel currents recorded from membrane of denervated frog muscle fibres. *Nature.* 260:799-802.

Neher, E., B. Sakmann, and J. H. Steinbach. 1978. The extracellular patch clamp: A method of resolving currents through individual open channels in biological membranes. *Pflügers Arch.* 375:219-228.

Neumcke, B., W. Nonner, and R. Stämpfli. 1976. Asymmetrical displacement current and its relation with activation of the sodium current in the membrane of frog myelinated nerve. *Pflügers Arch.* 363:193-203.

Noda, M., S. Shimizu, T. Tanabe, T. Takai, T. Kayano, T. Ikeda, H. Takahashi, H. Nakayama, Y. Kanaoka, N. Minamino, K. Kangawa, H. Matsuo, M. A. Raftery, T. Hirose, S. Inayama, H. Hayashida, T. Miyata, and S. Numa. 1984. Primary structure of *Electrophorus electricus* sodium channel deduced from cDNA sequence. *Nature Lond.* 312:121-127.

Noda, M., T. Ikeda, T. Kayano, H. Suzuki, H. Takeshima, M. Kurasaki, H. Takahashi, and S. Numa. 1986. Existence of distinct sodium channel messenger RNAs in rat brain. *Nature.* 320:188-192.

Noda, M., T. Ikeda, H. Suzuki, H. Takeshima, M. Kuno, and S. Numa. 1986. Expression of functional sodium channels from cloned cDNA. *Nature.* 322:826-828.

Oxford, Gerry S. 1981. Some kinetic and steady-state properties of sodium channels after removal of inactivation. *J. Gen. Physiol.* 77:1-22.

Patlak, C. S. 1960. Derivation of an equation for the diffusion potential. *Nature. (Lond)* 188:944-945.

Patlak, J., and R. Horn. 1982. Effect of N-bromoacetamide on single sodium channel currents in excised membrane patches. *J. Gen. Physiol.* 79:333-351.

Quandt, F. N. (1987). Burst kinetics of sodium channels which lack fast inactivation in mouse neuroblastoma cells. *J. Physiol. (Lond.)* 392:563-585.

Rayner, M. D. and J. G. Starkus. 1989. The steady state distribution of gating charge in crayfish giant axons. *Biophys. J.* 55:1-19.

Razdan, R. K. 1986. Structure-activity relationships in cannabinoids. *The American Society for Pharmacology and Experimental Therapeutics.* 38(2):75-149.

Rojas, E., R. E. Taylor, I. Atwater and F. Bezanilla. 1969. Analysis of the effects of calcium or magnesium on voltage-clamp currents in perfused squid axons bathed in solutions of high potassium. *J. Gen. Physiol.* 54:532-552.

Ruben, Peter C., John G. Starkus and Martin D. Rayner. 1990. Holding potential modifies the voltage dependence of sodium current activation in crayfish giant axons. *Biohphys. J.* : .

Salkhoff, L., A. Butler, A. Wei, N. Scavarda, K. Giffen, C. Ifune, R. Goodman, and G. Mandel. 1987. Genomic organization and deduced amino acid sequence of a putative sodium channel gene in *Drosophila. Science.* 237:744-749.

Schauf, C. L. 1983. Insensitivity of activation delays in potassium and sodium channels to heavy water in *Myxicola* giant axons. *J. Physiol. (Lond)* 337:173-182.

Schauf, C. L., and J. O. Bullock. 1979. Modifications of sodium channel gating in *Myxicola* giant axons by deuterium oxide, temperature, and internal cations. *Biophys. J.* 27:193-208.

Schauf, C. L., and J. O. Bullock. 1980. Solvent substitution as a probe of channel gating in *Myxicola.* Differential effects of $D_2O$ on some components of membrane conductance. *Biophys. J.* 30:295-306.

Schauf, C. L., and J. O. Bullock. 1982. Solvent substitution as a probe of channel gating in *Myxicola*. Effects of $D_2O$ on kinetic properties of drugs that occlude channels. *Biophys. J.* 37:441-452.

Schauf, C. L., and M. A. Chuman. 1986. Mechanisms of sodium channel gating revealed by solvent substitution. In Neural Membranes. Alan R. Liss, Inc., New York. 3-23.

Schneider, M. F., and W. K. Chandler. 1973. Voltage-dependent charge movement in skeletal muscle: A possible step in excitation-contraction coupling. *Nature (Lond.)* 242:244-246.

Shrager, P. 1974. Ionic conductance changes in voltage clamped crayfish axons at low pH. *J. Gen. Physiol.* 64:666-690.

Shrager, P., J. G. Starkus, M-V. C. Lo and C. Peracchia. 1983. The periaxonal space of crayfish giant axons. *J. Gen. Physiol.* 82:221-244.

Sigworth, F J., and E. Neher. 1980. Single $Na^+$ channel currents observed in cultured rat muscle cells. *Nature.* 287:447-449.

Starkus, J. G. and M. D. Rayner. 1987. Immobilizable and non-immobilizable components of gating charge in crayfish giant axon. *Biophys. J.* 51:434a. (Abstr.)

Starkus, J. G. and P. Shrager. 1978. Modification of slow sodium inactivation in nerve after internal perfusion with trypsin. *Am. J. Physiol.* 4:C238-244.

Starkus, J. G., B. D. Fellmeth, and M. D. Rayner. 1981. Gating currents in the intact crayfish giant axon. *Biophys. J.* 35:521-533.

Starkus, J. G., S. T. Heggeness and M. D. Rayner. 1984. Kinetic analysis of sodium channel block by internal methylene blue in pronased crayfish giant axons. *Biophys. J.* 46:205-218.

Stimers, J. R., F. Bezanilla and R. E. Taylor. 1985. Sodium channel activation in the squid giant axon. Steady state properties. *J. Gen. Physiol.* 85:65-82.

Stimers, J. R., F. Bezanilla and R. E. Taylor. 1987. Sodium channel gating currents. Origin of the rising phase. *J. Gen. Physiol.* 89:521-540.

Strichartz, G. R., S. Y. Chiu, and J. M. Ritchie. 1978. The effect of delta-9-tetrahydrocannabinol on the activation of sodium conductance in node of Ranier. *J. Pharm. and Exp. Ther.* 207:801-809.

Stühmer, W., C. Methfessel, B. Sakmann, M. Noda, and S. Numa. 1987. Patch clamp characterization of sodium channels expressed from rat brain cDNA. *Eur. Biophys. J.* 14:131-138.

Stühmer, W., F. Conti, H. Suzuki, X. Wang, M. Noda, N. Yahagi, H. Kubo, and S. Numa. 1989. Structural parts involved in activation and inactivation of the sodium channel. *Nature Lond.* 339:597-603.

Swain, C. G., and D. F. Evans. 1966. Conductances of ions in light and heavy water at 25 °C. *J. Am. Chem. Soc.* 88:383-390.

Taylor, R. E., and F. Bezanilla. 1983. Sodium and gating current time shifts resulting from changes in initial conditions. *J. Gen. Physiol.* 81:773-784.

Timpe, L. C., Y. N. Jan, and L. Y. Jan. 1988a. Four cDNA clones from the Shaker locus of *Drosophila* induce kinetically distinct A-type potassium currents in *Zenopus* oocytes. Neuron. 1:659-667.

Timpe, L. C., T. L. Schwarz, B. L. Tempel, D. M. Papazian, Y. N. Jan, and L. Y. Jan. 1988b. Expression of functional potassium channels from Shaker cDNA in *Zenopus* oocytes. Nature. (Lond.) 331:143-145.

Van Harreveld, A. 1936. A physiological solution for fresh water crustaceans. *Proc. Soc. Exp. Biol. Med.* 34:428-432.

Wang, G. K., M. S. Brodwick, and D. C. Eaton. 1985. Removal of sodium channel inactivation in squid axon by the oxidant chloramine-T. *J. Gen. Physiol.* 86:289-302.

Zagotta, William N., and Richard W. Aldrich. 1990. Voltage-dependent gating of shaker A-type potassium channels in *Drosophila* muscle. *J. Gen. Physiol.* 95:29-60.

Zagotta, W. N., T. Hoshi, and R. W. Aldrich. 1989. Gating of single Shaker potassium channels in *Drosophila* muscle and in *Zenopus* oocytes injected with Shaker mRNA. *Proceedings of the National Academy of Sciences*. 86:7243-7247.

Zimmerberg, Joshua, Francisco Bezanilla, and V. Adrian Parsegian. 1990. Solute inaccessible aqueous volume changes during opening of the potassium channel of the squid giant axon. *Biophys. J.* 57:1049-1064.